REVIEWS OF MODERN PHYSICS, VOLUME 77, JANUARY 2005

Structural properties of nanoclusters: Energetic, thermodynamic, and kinetic effects

Francesca Baletto* and Riccardo Ferrando†

INFM and Dipartimento di Fisica, Università di Genova, via Dodecaneso 33, 16146 Genova, Italy

(Published 24 May 2005)

The structural properties of free nanoclusters are reviewed. Special attention is paid to the interplay of energetic, thermodynamic, and kinetic factors in the explanation of cluster structures that are actually observed in experiments. The review starts with a brief summary of the experimental methods for the production of free nanoclusters and then considers theoretical and simulation issues, always discussed in close connection with the experimental results. The energetic properties are treated first, along with methods for modeling elementary constituent interactions and for global optimization on the cluster potential-energy surface. After that, a section on cluster thermodynamics follows. The discussion includes the analysis of solid-solid structural transitions and of melting, with its size dependence. The last section is devoted to the growth kinetics of free nanoclusters and treats the growth of isolated clusters and their coalescence. Several specific systems are analyzed.

CONTENTS

I. INTRODUCTION

In the last decade, we have seen the explosive development of a new field, now commonly known as nanoscience (Nalwa, 2004). This field extends through physics, chemistry, and engineering and addresses a huge number of important issues, ranging from basic science to a variety of technological applications (in the latter case, the word nanotechnology is often employed). The purpose of nanoscience and nanotechnology is to under-

---

*Present address: The Abdus Salam International Center for Theoretical Physics, Strada Costiera 11, I34014 Trieste, Italy. Electronic address: baletto@ictp.trieste.it

†Electronic address: ferrando@fisica.unige.it

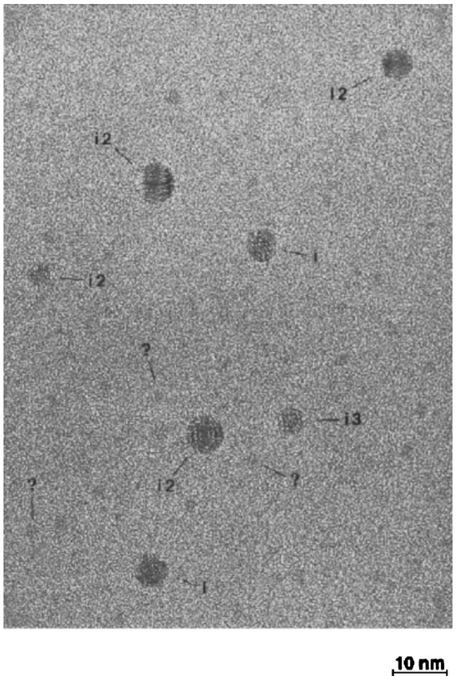

FIG. 1. High-resolution electron microscopy image of Ag clusters deposited on an inert substrate after being produced in an inert-gas aggregation experiment. The clusters indicated by arrows are identified as being icosahedra. Adapted from Reinhard, Hall, Ugarte, and Monot, 1997.

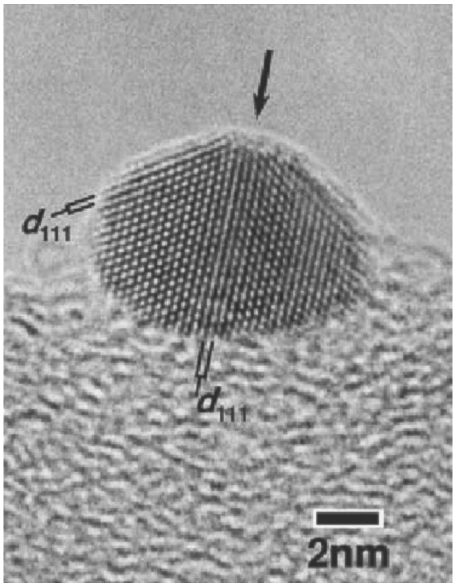

FIG. 2. High-resolution electron microscopy image of a $8.6 \times 6.3\text{-nm}^2$ truncated decahedral gold particle deposited on amorphous carbon. The particle was produced in an inert-gas aggregation experiment and then deposited and observed. Adapted from Koga and Sugawara, 2003.

stand, control, and manipulate objects of a few nanometers in size (say, 1–100 nm). These nano-objects are thus intermediate between single atoms and molecules and bulk matter. Their properties are often peculiar, being qualitatively different from those of their constituent parts (either atoms or molecules) and from those of macroscopic pieces of matter. In particular, nano-objects can present properties that vary dramatically with size. This opens the possibility of controlling these properties by controlling precisely their formation process.

Among nano-objects, *nanoclusters* occupy a very important place, since they are the building blocks of nanoscience. Nanoclusters are aggregates of atoms or molecules of nanometric size, containing a number of constituent particles ranging from ~ 10 to 10^6 (Castleman and Bowen, 1996; Johnston, 2002; Wales, 2003).

In contrast to molecules, nanoclusters do not have a fixed size or composition. For example, the water molecule contains one oxygen and two hydrogen atoms, which are placed at a well-defined angle to each other. On the other hand, silver, gold (see Figs. 1 and 2), or even water clusters may contain any number of constituent particles and, for a given size, present a variety of morphologies. There are borderline cases that are not easily classifiable unambiguously either as clusters or molecules, the fullerene buckyball (C_{60}) being an example. In the following, we shall classify C_{60} as a molecule, since clusters and solids of buckyballs have been produced in which each C_{60} constituent preserves its individuality. Clusters can be homogeneous, that is, composed of only one type of atom or molecule, or heterogeneous. They may be neutral or charged. They may be held together by very different kinds of forces: strong attraction between oppositely charged ions (as in NaCl clusters), van der Waals attraction (as in He and Ar clusters), covalent chemical bonds (as in Si clusters), or a metallic bond (as in Na and Cu clusters). Small clusters of metal atoms are held together by forces more like those of covalent bonds than like the forces exerted by the nearly free electrons of bulk metals.

Clusters containing no more than a few hundred particles (diameters of 1–3 nm) are expected to have strongly size-dependent properties (for example, geometric and electronic structure, binding energy, melting temperature). Larger clusters, with many thousands of atoms and diameters in the range of 10 nm and more, have a smoothly varying behavior, which tends to the bulk limit as size increases.

Nanoclusters have peculiar properties because they are finite small objects. To finite objects, the constraint of translational invariance on a lattice does not apply. For this reason, clusters can present noncrystalline structures, icosahedra and decahedra being the best known. Of course, it is possible also to build up crystalline clusters, which are simply pieces of bulk matter. An important issue in cluster science is to understand whether crystalline or noncrystalline structures prevail for a given size and composition. Being small objects, nanoclusters have a very high surface/volume ratio. Thus the surface energy contribution (including terms from facets, edges, and vertices) is not negligible and usually strongly size dependent.

Nanoclusters are well suited for several applications, whose number is rapidly increasing. There has been a traditional interest in applications to catalysis (see, for example, Henry, 1998), because of the very favorable surface/volume ratio of nanoclusters. More recently, there have been developments towards biological uses. For example, gold nanoparticles studded with short segments of DNA (Alivisatos *et al.*, 1996; Mirkin *et al.*, 1996) could form the basis of an easy-to-read test to single out genetic sequences (Alivisatos, 2001). Some applications of nanoclusters have a much older history. It has been recently discovered (Borgia *et al.*, 2002; Padeletti and Fermo, 2003) that the Renaissance masters in Umbria, Italy, used nanoparticles in the decoration of majolicas with lustre. Lustre consists of a thin film containing silver and copper clusters with diameters up to a few tens of nanometers, often of noncrystalline structure. Due to the inclusion of these nanoparticles, lustre gives beautiful iridescent reflections of different colors.

The starting point for an understanding of cluster properties is the study of their structure. With this goal in mind, the first question to answer is the following: Given size and composition, what is the most stable cluster structure from an energetic point of view? To answer to this question we need to find the global minimum on the *potential-energy surface* (PES) of the cluster (Wales, 2003). The PES is the product of the elementary interactions among the cluster constituents.

Once the answer to this first question is given, a second one arises: What is the effect of raising the temperature on the structural properties of a cluster? The study of this question introduces us to a fascinating field, the thermodynamics of finite systems.

Finally, the experimental time scales of cluster production are often short with respect to the time scales of morphology transitions. This leads to a third important question: What are the kinetic effects in the formation of nanoclusters? To answer to this question, the cluster growth process must be analyzed.

In this review, we try to summarize and discuss the present knowledge about these three points and, to the best of our ability, to answer the above questions concerning the behavior of free clusters. Two general results can, however, be anticipated.

First, what clearly emerges from the comparison of experimental and theoretical results is that all three factors, energetics, thermodynamics, and growth kinetics of nanoclusters, must be taken into account when analyzing realistic situations. Second, interactions among the constituent particles must be understood in terms of the basic concepts of range and type. The interaction range rules the behavior of systems with pair potentials (see, for example, Wales, 2003). In systems characterized by interactions with strong many-body character, metals, for example, other factors come into play together with the interaction range, namely, the bond-order/bond-length correlation and the directionality of the interactions.

The focus of this review article is on theoretical and simulation issues in free-cluster science. We remark that cluster science is a field in which the interplay among experiments, theory, and simulations is very active: in fact, the analysis of an experiment is very often carried out by some kind of simulation. In the words of Marks (1994) "small particle structures cannot be understood purely from experimental data, and it is necessary to simultaneously use theoretical or other modeling." The discussion of theoretical and simulation results will make frequent reference to the experiments.

We cannot pretend to be exhaustive on the subjects of our review, since thousands of articles about nanoclusters have been produced in the last decade. Some fascinating fields, for example, the field of binary clusters and nanoalloys, whose properties depend crucially not only on size but also on composition, are completely left out for space reasons. But even on the topics that we explicitly treat we do not claim to be exhaustive. If some contributions have been left out, we apologize in advance.

The review is structured as follows. In Sec. II we give a brief description of the methods for free-cluster production. In Sec. III we deal with the energetics of free nanoclusters, describing general trends, modeling the elementary interactions, and finding the global minima of the PES. In Sec. IV we consider the thermodynamics of nanoclusters, focusing on the possibility of solid-solid transitions at finite temperature and on the melting transition. Finally Sec. V treats the growth kinetics of nanoclusters, which may take place either in the liquid or in the solid state, and the coalescence of nanoclusters. In each part, specific systems are treated in details.

II. EXPERIMENTAL METHODS FOR FREE-NANOCLUSTER PRODUCTION

The experimental methods for producing free nanoclusters have been reviewed by de Heer (1993) and more recently by Milani and Iannotta (1999) and Binns (2001). Here we present a brief summary, focusing on those aspects (such as the time scale of free-nanocluster growth) most closely related to the subjects treated below.

Sources producing free beams of nanoscale clusters were made available about 30 years ago for the production of noble-gas clusters (Raoult and Farges, 1973) and more than 20 years ago for producing metallic clusters (Sattler *et al.*, 1980; Dietz *et al.*, 1981); more recent developments have made available sources that are ultrahigh vacuum compatible, that can produce binary clusters (Rousset *et al.*, 1996; Cottancin *et al.*, 2000), and that incorporate extremely efficient mass-selection techniques (see Binns, 2001, and references therein).

In most cases, the heart of a cluster source is a region where a supersaturated vapor of the material forming the clusters is produced. The first step in cluster production is the heating of the material to obtain a hot vapor. This can be done in different ways, for example, by heating up a piece of bulk material in a crucible (as in seeded supersonic nozzle and inert-gas aggregation sources), or by hitting a target with a laser pulse or an ion beam (laser evaporation and ion sputtering sources). To obtain supersaturation, the hot vapor must be cooled down. There are essentially two ways to achieve this. The first is by means of a supersonic expansion (as in seeded supersonic nozzle sources, where the material is mixed with a high-pressure inert gas and then expanded), which causes an adiabatic cooling (Anderson and Fenn, 1985). Hot clusters are usually produced at temperatures close to the evaporation limit (Bjørnholm *et al.*, 1991). In the second way, the hot vapor is mixed with a cold inert-gas flow, which acts as a collisional thermostat. This method is used in inert-gas aggregation sources to produce very cold metallic clusters. Here, due to the low temperature of the inert gas, cluster production proceeds mainly by the addition of single atoms, and reevaporation is negligible (de Heer, 1993). When growth ceases, the clusters can be further reheated or cooled down by subsequent stages of contact with gas at different temperatures.

What are the typical time scales of nanocluster production? This question is extremely important, because, as we see in the following, the finite lifetime of free clusters in flight may cause their trapping into metastable structures. Let us consider an inert-gas aggregation source for noble-metal clusters (Reinhard, Hall, Ugarte, and Monot, 1997; Reinhard *et al.*, 1998; Koga and Sugawara, 2003). There, the typical metal vapor temperature T_v and pressure p_v are of the order of 1000–1500 K and 1–10 mbar, respectively. Consider now a growing nanocluster, say with a radius R of 1 nm, which can correspond to 100–200 atoms. If we assume a spherical cluster, the kinetic theory of gases gives for the atomic flux Φ_v (i.e., the number of metal atoms per second hitting the cluster surface)

$$\Phi_v = \frac{p_v A_{eff}}{\sqrt{2\pi m_v k_B T_v}}, \tag{1}$$

where $A_{eff}=4\pi R^2$, and m_v is the mass of the atoms. This gives $\Phi_v \sim 10^7$ s^{-1}, corresponding to an interval between depositions $\tau_{dep}=\Phi_v^{-1} \sim 10^2$ ns. Thus a cluster of 10^3 atoms is grown on a time scale of a fraction of a millisecond.

Once clusters are produced, they have to be detected in some way, possibly while they are still in their beam. Indeed, the detection of slow neutral clusters is a difficult task; however, the cluster structures can be investigated by diffraction methods. They can then be ionized for an efficient mass-selective detection and finally deposited and observed by several microscopy techniques (Henry, 1998; José-Yacamán, Ascencio, *et al.*, 2001).

In a diffraction experiment, a well-collimated electron beam with an energy of 30 to 50 keV crosses a cluster beam. The fast electrons are scattered from the cluster atoms, and the diffraction pattern is recorded. A series of diffraction rings around the position of the primary electron beam is recorded. The interpretation of diffraction profiles is not straightforward (Hall *et al.*, 1991; Reinhard, Hall, Berthoud, *et al.*, 1997, 1998; Reinhard, Hall, Ugarte, and Monot, 1997), being based on a fit to a theoretical profile whose construction assumes the presence of some selected cluster structures. However, information on the geometry, the average size, and the temperature of the clusters in the beam can be extracted as follows. Remembering that the scattered intensity is the squared modulus of the Fourier transform of the scatterers with respect to the momentum transfer $\mathbf{q}$, one builds a theoretical diffraction pattern by weighting contributions from clusters of different structures. In fact, one can expect that, for example, an icosahedron has a different Fourier transform than a part of an fcc lattice. The geometry is obtained directly by fitting the weights of the different structures to the experimental data. On the other hand, information on the size can be obtained from the width of the diffraction rings, because the larger the cluster, the narrower the diffraction rings. The more scatterers add their contributions coherently, the sharper the resulting pattern. Finally, information about the cluster temperature is contained in the temperature dependence of the scattered intensity

$$I(T) = I_{(T=0)} e^{-2W}. \tag{2}$$

Here W is the Debye-Waller factor,

$$W = \frac{1}{3}\langle u^2\rangle q^2, \tag{3}$$

where $\langle u^2\rangle$ is the mean-square vibrational amplitude of the cluster atoms. For harmonic vibrations, $\langle u^2\rangle \propto T$.

III. ENERGETICS OF FREE NANOCLUSTERS

At low temperatures, the most favored structure of a cluster of N particles is the one that minimizes its total energy. For example, in atomic clusters, the most favored structure is the global minimum of the potential energy as a function of the coordinates of the atomic cores (the potential-energy surface or PES). Traditionally, great effort has been devoted to finding reliable methods for calculating the total energy, and searching for local and global minima. This task implies the following two steps:

(a) Construction of a model for the interactions between the elementary constituents of the cluster; this can be accomplished either by trying to solve directly the Schrödinger equation (*ab initio* methods) or by constructing semiempirical interparticle potentials (see Sec. III.C).

(b) A search for the most favored isomers by some global optimization algorithm (see Sec. III.D).

Depending on material and size, both (a) and (b) may present enormous difficulties. Therefore, as a preliminary step, it is extremely important to find general trends that help to single out sequences of favorable structures in different size ranges. This can be done either on the basis of geometric considerations, as in Sec. III.A (where the construction of families of highly symmetric structures, the *structural motifs*, is treated), or based on electronic shell effects, as in Sec. III.B. The sizes of the most energetically stable structures are often called *magic sizes*. Magic sizes may (tentatively) correspond either to the completion of a geometrically perfect structure (geometric magic sizes) or to the closing of an electronic shell (electronic magic sizes).

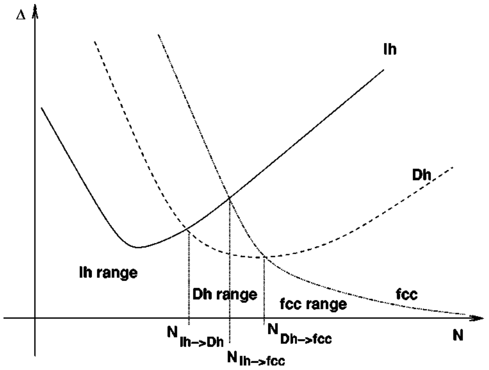

FIG. 3. Qualitative behavior of Δ [Eq. (5)] for crystalline, icosahedron, and decahedron clusters.

Section III.E is devoted to the study of selected systems of special interest.

A. Geometric shells: Structural motifs and general trends in energetics

In general, the binding energy E_b of a cluster of size N with a given structure can be written in the form[1]

$$E_b = aN + bN^{2/3} + cN^{1/3} + d, \tag{4}$$

where the first term corresponds to a volume contribution, while the others represent surface contributions from facets, edges, and vertices. Volume and surface contributions are in competition. Clusters with low surface energy must have quasispherical shapes (thus optimizing the surface/volume ratio), and close-packed facets. On the other hand, it is not possible to build up clusters of spherical shape without internal strain, which gives a volume contribution.

A useful parameter for comparing the stability of clusters in different size ranges is $\Delta(N)$,

$$\Delta(N) = \frac{E_b(N) - N\varepsilon_{coh}}{N^{2/3}}, \tag{5}$$

where ε_{coh} is the cohesive energy per particle in the bulk solid and Δ is the excess energy (that is, the energy in excess with respect to N atoms in a perfect bulk crystal) divided approximately by the number of surface atoms. Other indicators of structural stability are the binding energy per atom, $E_b(N)/N$, and the first and second differences $\Delta_1(N)$ and $\Delta_2(N)$ in the binding energy,

$$\Delta_1(N) = E_b(N-1) - E_b(N),$$

$$\Delta_2(N) = E_b(N-1) + E_b(N+1) - 2E_b(N). \tag{6}$$

Δ_1 and Δ_2 measure the relative stability of clusters of nearby sizes. Peaks in $\Delta_2(N)$ were found to be well correlated to peaks in the mass spectra (Clemenger, 1985).

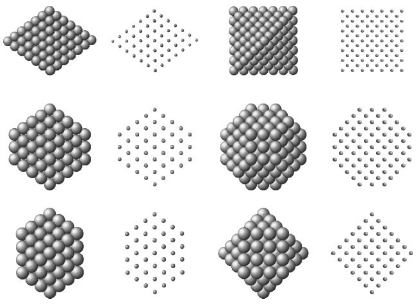

FIG. 4. Face-centered-cubic clusters: (a) octahedron; (b) truncated octadedron; (c) cuboctahedron. Each cluster is shown in four views. (a) An octahedron is made up of two square pyramids sharing a common basis. Its surface consists of eight triangular close-packed (111) facets, but the structure has a high surface/volume ratio. Polyhedra with a lower surface/volume ratio, are obtained by truncating symmetrically the six vertices of an octahedron, thus obtaining square and hexagonal (or triangular, see below) facets. A truncated octahedron can be characterized by two indexes: n_l is the length of the edges of the complete octahedron; n_{cut} is the number of layers cut at each vertex. In the figure, for the octahedron in (a) $(n_l,N_{cut}) = (7,0)$, the truncated octahedron in (b) $(n_l,N_{cut}) = (7,2)$, and the cuboctahedron in (c) $(n_l,N_{cut}) = (7,3)$. A perfect truncated octahedron has thus a number of atoms, $N_{TO}(n_l,n_{cut}) = \frac{1}{3}(2n_l^3 + n_l) - 2n_{cut}^3 - 3n_{cut}^2 - n_{cut}$. This equation defines the series of magic numbers for truncated octahedron structures. The square facets have a (100) symmetry and edges of $n_{cut}+1$ atoms. The (111) facets are not in general regular hexagons. In fact, three edges of the hexagons are in common with square facets, thus having $n_{cut}+1$ atoms, while the remaining three edges have $n_l - 2n_{cut}$ atoms. Regular hexagons are thus possible if $n_l = 3n_{cut}+1$; truncated octahedra with regular hexagonal facets are referred to as regular truncated octahedra. When $n_l = 2n_{cut}+1$ the hexagonal facets degenerate to triangles and the cuboctahedron is obtained, which is usually not energetically favored because of its large (100) facets.

Let us now build up structural motifs by trying to optimize either volume or surface energy contributions. The easiest way to minimize volume contributions is to cut a piece of bulk matter so that interparticle distances inside the cluster are automatically optimized. For such clusters of *crystalline* structure the parameter a in Eq. (4) is simply ε_{coh}, so that $\lim_{N\to\infty} \Delta = b$. As we shall see in the following, nanoclusters can be also of *noncrystalline* structures; for these clusters a is larger than ε_{coh}, and Δ diverges at large sizes (see Fig. 3).

Consider now fcc crystalline structures. Try to cut a cluster from a bulk fcc crystal in such a way that its surface has only close-packed facets. A possible resulting shape is the octahedron (see Fig. 4), that is, two square pyramids that share a basis. Even if the whole surface of the octahedron is close packed, its shape does not optimize the surface energy because of its high surface/volume ratio. Clusters with more spherical shapes are obtained by cutting the vertices, thus producing a *truncated octahedron*. Its surface has eight close-packed (111) and six square (100) facets; the latter have a higher surface energy in most materials. A deeper cut

---

[1] See, for example, Hill (1964), Northby *et al.* (1989), Xie *et al.* (1989), Cleveland and Landman (1991), Jortner (1992), Uppenbrink and Wales (1992), Baletto, Ferrando, *et al.* (2002).

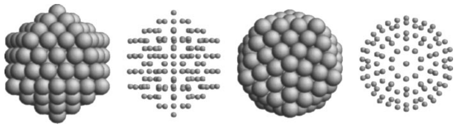

FIG. 5. Icosahedral clusters. The Mackay icosahedron is a noncrystalline structure organized in shells. An icosahedron with k shells has $N_{Ih}(k)=\frac{10}{3}k^3-5k^2+\frac{1}{3}k-1$ atoms (so that the series of magic numbers is 1, 13, 55, 147,…). The icosahedron in the figure has $k=4$ shells. An icosahedron with k shells has the same number of particles as a cuboctahedron with $n_{cut}=k-1$. An icosahedron has 20 triangular facets of side k and 12 vertices. Each pair of opposite vertices lie along a fivefold symmetry axis. An icosahedron can be thought of as composed of 20 fcc tetrahedra sharing a common vertex (in the central site). When 20 regular tetrahedra are packed around a common vertex, large interstices remain. To fill these spaces the tetrahedra must be distorted, thus generating a huge strain on the structure. Intershell distances are compressed, while intrashell distances are expanded. The facets of an icosahedron are of distorted (111) symmetry. Adatoms deposited on the facets of a Mackay icosahedron can be placed either on sites of fcc or hcp stacking. Islands of fcc stacking are part of the next Mackay shell, while islands of hcp stacking form a so-called anti-Mackay overlayer.

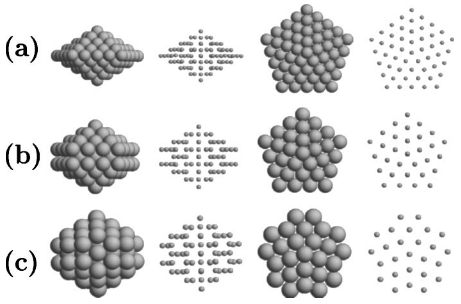

FIG. 6. Decahedral clusters: (a) regular decahedra; (b) Ino truncated decahedra (Ino, 1969); (c) Marks truncated decahedra. A decahedron is made up of two pentagonal pyramids sharing a common basis. It has a single fivefold axis and is formed by five tetrahedra sharing a common edge along the fivefold axis. When five regular tetrahedra are packed, gaps remain, but they are smaller than in the case of the icosahedra. These gaps are filled by distorting the tetrahedra, thus introducing some strain. Regular decahedra (first row) are limited by ten close-packed (111)-like facets, but have a large surface/volume ratio, which can be lowered by truncating the edges around the common basis, thus obtaining the Ino decahedron with five (100)-like facets. An even better structure is the Marks decahedron (Marks, 1984), obtained by introducing reentrances that separate the (100)-like facets (see the third row). A decahedron is characterized by three integer indices (m,n,p), where m and n are the lengths of the sides of the (100) facets, perpendicular and parallel to the axis, respectively; p is the depth of the Marks reentrance. A regular decahedron has indices of the form $(m,1,1)$ [the (5,1,1) decahedron is shown in the top row]; Ino decahedra have indices $(m,n,1)$, with $n>1$ [the (4,2,1) Ino decahedron is shown in the second row], and Marks decahedra have (m,n,p) with $n,p>1$ [the (2,2,2) Marks decahedron is shown in the third row]. A Marks decahedron has $h=m+n+2p-3$ atoms along its symmetry axis and a total number of atoms given by $N_{M-Dh}=(30p^3-135p^2+207p-102)/6+\{5m^3+(30p-45)m^2+[60(p^2-3p)+136]m\}/6+\{n[15m^2+(60p-75)m+3(10p^2-30p)+66]\}/6-1$. From this formula it follows that a Ino decahedron has $N_{Ino}=[5m^3-15m^2+16m+n(15m^2-15m+6)]/6-1$ atoms. For $n=m$ and $p=1$ [square (100)-like facets] a decahadron has thus the same number of atoms as an icosahedron of m shells and as a cuboctahedron with $n_{cut}=m-1$. Finally, a regular decahedron has $N_{Dh}=(5m^3+m)/6$ atoms.

gives a more compact shape having, however, larger square facets. If size is sufficiently large, the optimal cut is given by the Wulff construction. This was developed to find the equilibrium shape of macroscopic crystals by minimizing the surface energy at fixed volume (see, for example, Pimpinelli and Villain, 1998). From the Wulff construction, the best truncated octahedron structure should fulfill the condition

$$\frac{\gamma_{(100)}}{\gamma_{(111)}}=\frac{d_{(100)}}{d_{(111)}}, \tag{7}$$

where $\gamma_{(100)}$ and $\gamma_{(111)}$ are the (100) and (111) surface energies, respectively, whereas $d_{(100)}$ and $d_{(111)}$ are the distances of the facets from the center of the cluster. At large size, the introduction of higher-order facets can make fcc clusters more spherical (see, for example, Raoult *et al.*, 1989a). Different groups (Cleveland and Landman, 1991; Valkealahti and Manninen, 1998; Baletto, Ferrando, *et al.*, 2002) have shown that the Wulff construction is a reliable tool for identifying the best crystalline clusters for nanometric sizes. In any case, even the optimal Wulff shapes are quite far from being spherical and are expected to be the most favorable clusters at large sizes.

A better solution to the problem of building up compact quasispherical shapes was found by Mackay (1962; see also Martin, 1996), who constructed the *Mackay icosahedron* (see Fig. 5). This is a noncrystalline structure, with fivefold rotational axes. Icosahedral clusters are limited by (111)-like close-packed facets only, thus optimizing the surface energy well. However, this is obtained at the expense of a volume contribution, since interatomic distances are not the ideal ones: radial (intershell) bonds are compressed, while intrashell bonds are expanded. Therefore Mackay icosahedra are highly strained structures, and their Δ is proportional to $N^{1/3}$ as $N\rightarrow\infty$. This indicates that icosahedra could be expected to be the most favorable structures only at small sizes.

Icosahedra are not the only possible noncrystalline structures. Another noncrystalline motif is represented by the decahedra (see Fig. 6). A decahedron is formed by two pentagonal pyramids with a shared base; its surface has only close-packed facets, but its shape is very far from being spherical, so that truncations are advantageous also in this case. Ino (1969) proposed a truncation in which the five edges limiting the common basis of the pyramids are cut to expose (100)-like facets. This improves the surface/volume ratio, but usually does not produce the best possible decahedra in a given size range (see, for example, Baletto, Ferrando, *et al.*, 2002) because it creates large (100)-like facets. Marks (1984, 1994) proposed a more efficient truncation scheme, with reentrances exposing further close-packed facets which separate neighboring (100)-like facets. Marks decahedra can achieve a better optimization of the surface energy than truncated octahedron structures. On the other hand, decahedra are also strained structures, with a volume contribution to the excess energy giving $\Delta \propto N^{1/3}$ at large N. The strain, however, is much smaller than for icosahedra.

In summary, the icosahedral motif should be the most favored at small sizes, while truncated octahedron clusters are expected for large sizes; truncated decahedra could be favored in intermediate ranges. This trend has been verified in experiments. Farges *et al.* (1986) found a transition from icosahedron to close-packed [not necessarily fcc, see van de Waal *et al.* (2000)] structures at $N \sim 750$ in Ar clusters obtained in a free-jet expansion; Reinhard, Hall, Berthoud, *et al.* (1997, 1998) were able to identify small icosahedra, intermediate-size decahedra, and large fcc clusters in inert-gas aggregation experiments on Cu. Several systems have been investigated theoretically, showing that the icosahedral → decahedral and decahedral → fcc crossover sizes are strongly material dependent.[2]

Doye *et al.* (1995) proposed a quite simple principle for a qualitative understanding of crossover sizes. This principle states that *soft interactions*, with wide potential wells, stabilize strained structures, while *sticky interactions*, with narrow potential wells, cannot easily accommodate the strain and thus favor crystalline structures. Doye *et al.* (1995) considered a pair potential and decomposed the cluster energy into three parts,

$$E_b = - n_{NN}\varepsilon_{NN} + E_{strain} + E_{NNN}, \tag{8}$$

where n_{NN} is the number of nearest-neighbor pairs, ε_{NN} is their bond strength at the optimal distance, E_{strain} is the strain contribution due to the fact that some nearest-neighbor pairs can be at nonoptimal distances, and E_{NNN} is the contribution from further neighbors, which is, to a first approximation, negligible. The usual competition is between the first and the second term in Eq. (8); icosahedral structures, which have the largest number of nearest-neighbor bonds, optimize the first term at the expense of the second, while the opposite holds for fcc clusters. The relative weights of these two terms depend on the range of the potential. Decreasing the range has the effect of destabilizing strained structures, because the potential wells narrow so that the distortion of the nearest-neighbor distance with respect to its ideal value becomes more costly. In the case of a Morse (1929) interaction potential, Doye *et al.* (1995) were able to construct a structural phase diagram. The Morse potential U_M can be written as

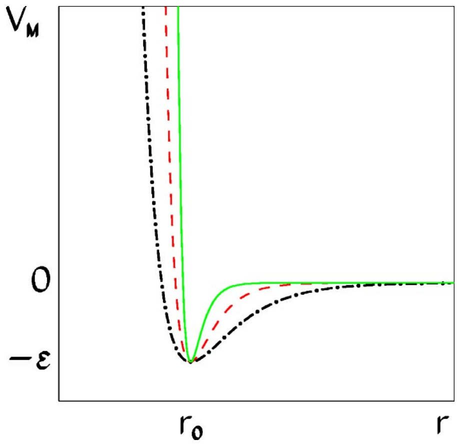

FIG. 7. (Color in online edition) Morse potential for ρ_0 values: dash-dotted line, sodium atoms; dashed line, Lennard-Jones molecules; and solid line, C_{60} molecules. The last is a very sticky interaction.

$$U_M = \epsilon \sum_{i<j} e^{\rho_0(1-r_{ij}/r_0)}[e^{\rho_0(1-r_{ij}/r_0)} - 2], \tag{9}$$

where the r_{ij} are the interatomic distances, r_0 is the equilibrium separation, and ϵ is the well depth. Thus by varying the parameter ρ_0 one can adjust the width of the potential well without changing the position or depth of the minimum. Large values of ρ_0 give short-ranged attractions with a steep repulsive part, that is, a narrow well and a sticky interaction (see Fig. 7). Small ρ_0 correspond to soft potentials. As can be seen in Fig. 8, the most favored structure changes from icosahedral at small ρ_0 to decahedral in the intermediate range, and finally to close-packed clusters at high values of ρ_0. A qualitative idea of the trends among different materials can be obtained by fitting the parameters of the Morse potential. This fit gives large values of ρ_0 for the interaction potentials between fullerene molecules [$\rho_0 = 13.62$ and 11.92 for Girifalco (1992) and Pacheco and Prates-

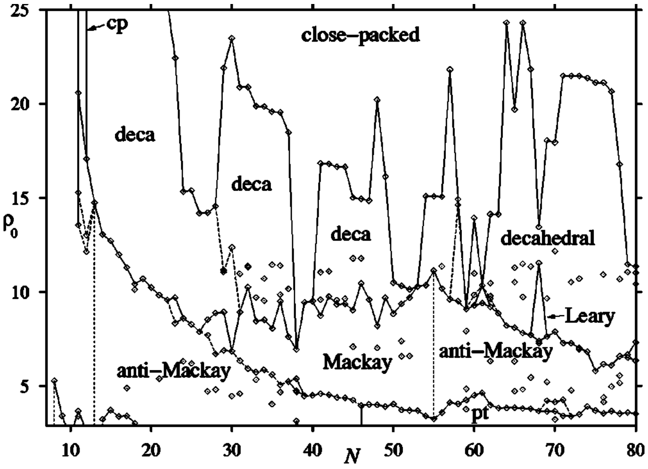

FIG. 8. Phase diagram for Morse clusters: The lines separate domains pertaining to different structural motifs. Figure courtesy of Jonathan Doye.

---

[2] See Raoult *et al.* (1989b), Cleveland and Landman (1991), Uppenbrink and Wales (1992), Turner *et al.* (2000), Doye *et al.* (2001), Baletto, Ferrando, *et al.* (2002), Doye and Hendy (2003) and Sec. III.E for details on some specific systems.

Ramalho (1997) potentials, respectively], $\rho_0=6$ for a Lennard-Jones crystal, $\rho_0=3.96$ for Ni (Stave and DePristo, 1992), and even smaller values for alkali metals [$\rho_0=3.15$ and 3.17 for sodium and potassium (Girifalco and Weizer, 1959)].

Baletto, Ferrando, *et al.* (2002) applied a similar criterion, based on the stickiness of the interactions, to discuss crossover sizes in noble-metal and quasi-noble-metal clusters modeled by many-body semiempirical potentials. This point is discussed in detail in Sec. III.E.3, where it is shown that there are other factors, besides the interaction range, that determine the structure of metallic clusters (Soler *et al.*, 2000). These factors arise from the many-body character of the metallic interactions, which causes a strong correlation between bond order and bond length, whose effects tend to make icosahedral structures less stable than what follows from the analysis of the interaction range. Moreover, bond directionality effects can be important. Finally, the presence of multiple minima or of secondary maxima in the two-body part of the interaction (Doye and Wales, 2001; Doye, 2003) can have strong effects on the preferred cluster structures.

B. Electronic shells

Electronic shell closing has been extremely successful in explaining the observed experimental abundances of alkali-metal clusters, like those found in the seminal experiments of Knight *et al.* (1984) on sodium clusters. In this framework, a cluster is modeled as a super-atom; valence electrons are delocalized in the cluster volume and fill discrete energy levels. There are several degrees of sophistication of this model. Detailed accounts can be found in the reviews by Brack (1993) and de Heer (1993); a simple and very clear discussion is found in Johnston (2002). Here we briefly sketch only the spherical jellium model.

The spherical jellium model assumes a uniform background of positive charge, in which electrons move and are subjected to an external potential. The simplest forms of the potential are the infinitely deep spherical well and the harmonic well. The solution of the single-electron Schrödinger equation for the spherical well gives the following series of magic numbers: 2, 8, 18, 20, 34, 40, 58,…, etc. On the other hand, the harmonic well gives the series: 2, 8, 20, 40, 70,…, etc. The experimental spectra of Knight *et al.* (1984) reveal high peaks at 8, 20, 40 in agreement with both models. There are, however, less evident peaks at 18 and 58, which appear only in the spherical well. Experiments on larger sodium clusters have revealed electronic shells in these clusters, up to about 2000 atoms (Martin *et al.*, 1991a; Martin, 1996, 2000), and in other metals; see, for example, Johnston (2002).

Candidates for observing electronic shell effects are the metals with weakly bound valence electrons, primarily the alkali and then the noble metals. It seems also that the temperature T, which determines whether the cluster is solid or liquid depending on N (see Sec. IV.B.3), plays a crucial role. The major evidence for electronic shell closing is for small alkali-metal clusters (Knight *et al.*, 1984; Bjørnholm *et al.*, 1990; Nishioka *et al.*, 1990). For these systems, several calculations (Röthlisberger and Andreoni, 1991; Spiegelman *et al.*, 1998; Solov'yov *et al.*, 2002) indicate that electronic shell closing is a better criterion than atomic packing for determining the most stable clusters. For larger alkali clusters the situation is more complicated. In fact, Martin *et al.* (1991a) and Martin (1996, 2000) have shown that Na clusters, after presenting electronic magic numbers up to 2000 atoms, reveal a series of geometric magic numbers at larger sizes (see Fig. 9). This would correspond to a transition from liquid to solid clusters at increasing size. Moreover, when solid Na clusters are heated and melted, geometric magic numbers disappear to the advantage of electronic magic numbers. The same kind of behavior was also found for aluminum clusters (Martin *et al.*, 1992; Baguenard *et al.*, 1994). Therefore the indication is that electronic shells are seen when hot liquid clusters are produced, while geometric shells are exhibited by cold, solid clusters (Johnston, 2002). In small clusters, both electronic and geometric effects can play important roles, as Zhao *et al.* (2001) have shown in their tight-binding global optimization study of Ag clusters at $N\leqslant 20$. In conclusion, the interplay of electronic and geometric shell effects, depending on material and size, remains to be fully understood.

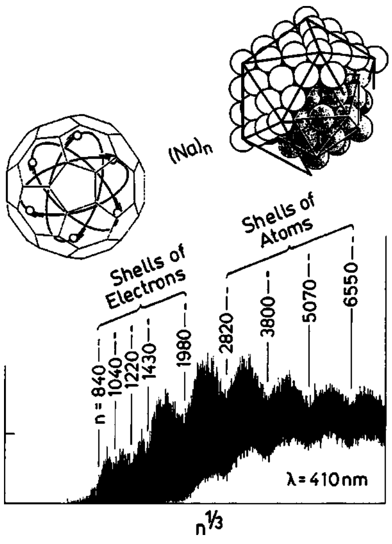

FIG. 9. Mass spectrum of Na$_n$ clusters of size n, photoionized with 3.02-eV photons. Closed-shell clusters are more difficult to ionize, so that they correspond to minima in the spectrum. Two sequences of minima appear in the spectrum. These sequences are at equally spaced $n^{1/3}$ intervals on the size scale and correspond to an electronic shell sequence and a structural shell sequence. Adapted from Martin, 2000.

C. Calculation of the total energy of nanoclusters

A key point in the theoretical study of clusters is the choice of an appropriate energetic model. This depends on the material and the size of the cluster, as well as on the physical and chemical properties one wishes to investigate. To cover and illustrate in detail all the methods used in theoretical cluster science would require an entire book, and it is well beyond the scope of our review. Here we mention only the main methods, trying to give an idea of their underlying philosophy and range of applicability.

As pointed out in the review by Bonacić-Koutecký *et al.* (1991), even clusters of a few atoms are very complicated systems. Indeed, the complexity of quantum mechanics forces one to employ approximate methods.

The *ab initio* methods of quantum chemistry [Hartree-Fock and post Hartree-Fock; see Bonacić-Koutecký *et al.* (1991), and references therein] were extensively applied to the study of small clusters about 20 years ago. For example, small-size ($2 \leqslant N \leqslant 9$) Li and Na clusters contain relatively few electrons, so that all-electron calculations were possible (Boustani *et al.*, 1987). When either the size of the cluster or the nuclearity of the atoms increase, these methods become cumbersome, and at present they are less commonly employed than in the past.

Methods based on density-functional theory (Hohenberg and Kohn, 1964; Kohn and Sham, 1965), when adequately tested, can be of very high accuracy and less cumbersome from the computational point of view, making it possible to treat a wide variety of systems and somewhat larger sizes. Calculations on metals up to a few hundred atoms are present in the literature, even for difficult systems such as the transition and noble metals (see, for example, Häberlen *et al.*, 1996; Jennison *et al.*, 1997; Garzón, Michaelian, *et al.*, 1998; Fortunelli and Aprà, 2003; Nava *et al.*, 2003). The weak point in density-functional calculations is often the exchange and correlation term, which is treated in an approximate way. The validity of the treatment depends on the systems and has to be checked each time. The simplest approximation is the local-density approximation; more sophisticated approaches include gradient corrections (very important in transition and noble metals), which are often called the *generalized gradient approximation*. At this level, different exchange and correlation functionals are available (see Perdew and Wang, 1986; Becke, 1988, 1996; Perdew *et al.*, 1992, 1996). In order to check the validity of gradient-corrected density-functional calculations, Mitás *et al.* (2000) performed quantum Monte Carlo simulations (Ceperley, 1994) on small-size silicon clusters. In quantum Monte Carlo, which is computationally very demanding, many-body correlations are directly taken into account by an explicit correlation in the trial wave function. It turned out that there were significant discrepancies between the density-functional (with different types of exchange and correlation functionals) and the quantum Monte Carlo results. Mitás *et al.* (2000) confirmed the already known bias of density-functional calculations towards compact structures; this bias is very strong at the level of the local-density approximation, and considerably reduced if gradient corrections are included. There are some functionals that give the same qualitative results as the quantum Monte Carlo calculations in ordering the different isomers of the Si_{20} cluster, even though there are still some quantitative differences.

Density-functional calculations can be inserted into a molecular-dynamics procedure to give the *ab initio* molecular dynamics. The best known example is the Car-Parrinello method (Car and Parrinello, 1985), which could be well suited to the investigation of thermodynamic and kinetic properties at $T>0$ K.

Even though density-functional methods are nowadays reliable and efficient for a large variety of systems, there is still a great interest in developing methods requiring a smaller computational effort. In fact, global optimization (see Sec. III.D) of clusters in the framework of *ab initio* calculations is not feasible at present except for a few systems and at very small sizes. Moreover, *ab initio* molecular dynamics is limited to small systems on short time scales, so that both the accurate sampling of thermodynamic properties and the simulation of kinetic processes (diffusion, structural transformations, growth) are far beyond present capabilities.

Therefore several approximate energetic models for clusters have been developed, often on semiempirical grounds. At an intermediate degree of computational effort, there is the tight-binding model for semiconductors (Ho *et al.*, 1998) and metals (Barreteau, Guirado-Lopez, *et al.*, 2000; Bobadova-Parvanova *et al.*, 2002). This allows global optimization searches for clusters of a few tens of atoms, and molecular-dynamics simulations even for clusters of 10^2 atoms (Yu *et al.*, 2002), even though on rather short time scales.

Larger sizes and longer time scales can be now treated by classical atom-atom (or even molecule-molecule) potentials, which are built up on the basis of approximate quantum models. These potentials contain parameters fitted to experimental material properties (semiempirical potentials) or to density-functional calculations [*ab-initio*-based potentials (Kallinteris *et al.*, 1997; Garzón, Kaplan, *et al.*, 1998)]. For metallic systems, several atom-atom potentials have been developed, such as embedded-atom (Daw and Baskes, 1984; Voter, 1993), glue (Ercolessi *et al.*, 1988), second-moment tight-binding (Gupta, 1981; Rosato *et al.*, 1989), Sutton-Chen (Sutton and Chen, 1990), and effective-medium (Jacobsen *et al.*, 1987) potentials. A discussion of the criteria for fitting the parameters in Gupta (1981) potentials is found in López and Jellinek (1999). For metals, these potentials must contain a many-body term, which is responsible for the correct surface relaxations (Desjonqueres and Spanjaard, 1998). The advantage of this approach is that it allows full global optimization to sizes of the order of ~ 200 atoms, local relaxation of clusters of $\sim 10^5$ atoms, and molecular-dynamics simulations on time scales of 10 μs and more for clusters of 10^2 atoms, quite close to the growth time scales of free clusters in inert-gas aggregation sources. The disadvantage is that even the qualitative accuracy of these potentials is often questionable, and they must be tested carefully before being used (see, for example, Ala-Nissila *et al.*, 2002). As we shall see in the following, there are several systems for which reliable potentials have been developed. In any case, the use of semiempirical potentials is in practice a necessary tool for the study of medium- or large-size clusters. In contrast to bulk materials and crystal surfaces, where one usually knows where to place the atoms, the best structures of clusters are not known in principle, so that a semiempirical modeling is the starting point for more sophisticated approaches. For example, in the work of Garzón, Michaelian, *et al.* (1998), global optimization by a semiempirical potential selects the most promising candidates for a further relaxation study by *ab initio* methods.

Semiempirical interaction potentials for molecular clusters have been built up too. Here we note the Girifalco (1992) and Pacheco and Prates-Ramalho (1997) potentials for fullerene molecules. Finally we mention the oldest semiempirical potentials, Lennard-Jones and Morse potentials, which are the usual benchmarks for testing new theoretical tools. The Lennard-Jones potential is also a popular model for noble gases.

D. Global optimization methods

Given the potential-energy surface of the cluster, that is, the potential energy $U(\{\mathbf{r}\})$ [where $\{\mathbf{r}\}=(\mathbf{r_1},\mathbf{r_2},\ldots,\mathbf{r_N})$] as obtained by methods like those of the previous section, one is confronted with the formidable task of finding its deepest minimum. Indeed, Wille and Vennik (1985) demonstrated that this problem is NP-hard by a mapping to the traveling-salesman problem.[3] The number of minima increases more than polynomially with the size [there are indications of a proportionality to $\exp(N)$]: a Lennard-Jones cluster of 13 atoms has about 10^3 local minima (Hoare and McInnes, 1976; Tsai and Jordan, 1993), but this number is at least 10^{12} for a 55-atom cluster (Doye and Wales, 1995). Clearly, a complete sampling of all these minima would be simply impossible, and the ability of a given system to reach its energy global minimum (or at least one of the usually few good local minima) should reside in some special features of its PES. This point has also been extensively debated in the field of protein folding (Wales, 2003), since proteins efficiently fold to their native state (which may not coincide with the lowest minimum in the PES) even if their PES presents a huge number of local minima. A good search algorithm should exploit the features of the PES to ensure a fast convergence to low-lying minima. However, as we show below, depending on the interaction potential, size, and composition of the cluster, there are easy potential-energy surfaces where most algorithms converge fast to some good *putative* global minima, and others where there are low-lying minima (often of very high symmetry) that are extremely difficult to reach, so that most algorithms get stuck in some less favorable configuration. A remark is necessary at this stage: no global optimization technique can warrant that the lowest minimum is really reached; the only way to reach the global minimum with probability one is to sample all minima, compare them, and choose the lowest one. This can be done only in essentially infinite time in cases of practical interest. For example, while good putative global minima for Lennard-Jones clusters have been obtained at sizes well above 100 atoms, only for much smaller sizes have these minima proven to be global (Maranas and Floudas, 1992).

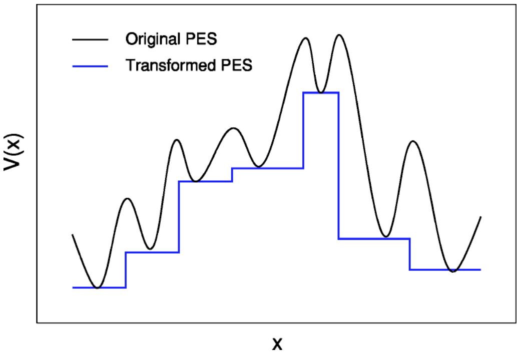

FIG. 10. (Color in online edition) Transformation of the potential-energy surface (PES) to a staircase. Figure courtesy of Giulia Rossi.

Let us now analyze the good features of a PES which allows fast convergence to its global minimum and correspondingly how an efficient global optimization algorithm must be constructed to exploit these features (Doye, 2004). To this end, a few definitions are needed in the framework of what was proposed by Stillinger and Weber (1982) introducing the inherent structure of liquids. Here below we follow the very clear exposition of Becker and Karplus (1997). A thorough account is given in the excellent book by Wales (2003).

We introduce a mapping from the continuum configurational space of the cluster into the discrete set of its local minima. The mapping associates each point $\{\mathbf{r}\}$ with its closest minimum, i.e., the one reached by a steepest-descent (or a quenching) minimization starting at $\{\mathbf{r}\}$. This amounts effectively to the following transformation of the PES (see Fig. 10):

$$\tilde{U}(\{\mathbf{r}\}) = \min[U(\{\mathbf{r}\})], \tag{10}$$

where min means that the minimization is started from $\{\mathbf{r}\}$. $\tilde{U}(\{\mathbf{r}\})$ is a multidimensional staircase potential (Li and Scheraga, 1987; Doye and Wales, 1998a).

The set of all points associated with a minimum s constitutes its *basin*. All points of a given basin are connected by definition. This mapping is a partition of the $(3N-6)$-dimensional space of the internal coordinates of the cluster into disjoint sets, which are indeed the attraction basins of the different minima. The boundaries between the basins constitute a network of $3N-7$ dimensions, where the mapping is not defined. Nearby basins (usually of the same structural family) can be grouped into *metabasins*, at different level of complexity. A very

---

[3] NP stands for nonpolynomial. The computational complexity of this optimization increases more than polynomially with cluster size.

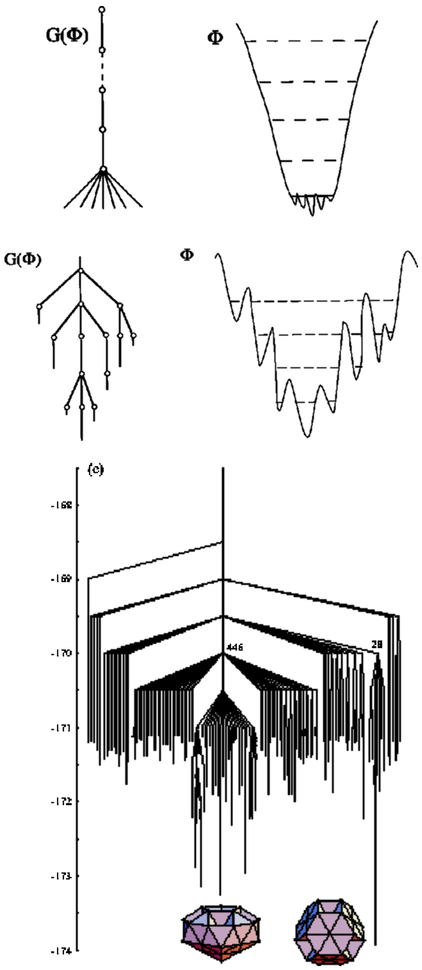

FIG. 11. (Color in online edition) Disconnectivity diagrams: Top panel, schematic of a single-minimum potential-energy surface (PES) with weak noise; center panel, a single-funnel PES. The disconnectivity diagrams of these two panels show at which energetic level the different local minima of a PES can be considered connected. Adapted from Becker and Karplus, 1997. The lowest panel gives the disconnectivity diagram for the complete double-funnel PES of the Lennard-Jones cluster of size 38. Figure courtesy of Jonathan Doye.

convenient representation of the connections between basins, metabasins, etc. is given by the *disconnectivity diagram* (see Fig. 11), which allows one to understand pictorially which basins are connected at different values of the total energy of the cluster (two basins are connected when the highest point on the minimum-energy path between them lies below that total energy).

Portions of the PES can be classified into three different types according to the features of the connections among the basins that they contain: rough PES, single-minimum PES with weak noise, and funnel-like PES (see Fig. 11). It can be easily understood that the absolute minimum is reached quickly in both a single-minimum or a steep funnel-like portion of the PES, while a rough PES will resist global minimization. Therefore we expect that in systems whose entire PES is given by a single minimum with weak noise or by a single funnel the global minimum can be found quickly. Correspondingly, such systems are much easier to attack by good global optimization algorithms than those with rough PES or with multiple-funnel PES. As an example, for a cluster of given size, icosahedral structures are usually grouped in a wide metabasin with a funnel structure, which is easily accessible from liquidlike configurations (Doye and Wales, 1998a), because the latter have in common with the icosahedra a pronounced polytetrahedral character (Nelson and Spaepen, 1989; Doye and Wales, 1996a), being formed by tetrahedral units packed together. In contrast, decahedral and truncated octahedral funnels are much narrower, so that global minima pertaining to these motifs are not easily reached from liquidlike configurations. The best-known example of this kind is the Lennard-Jones cluster of 38 atoms, which presents a double-funnel PES (see Fig. 11), with a wide icosahedral funnel and a narrower but deeper close-packed funnel, so that the trapping of search algorithms in the former is very likely. Moreover, one can expect that systems with short-range (sticky) potentials will present a larger number of minima and a rougher PES than systems with soft potentials (Wales *et al.*, 2000; Doye, 2004). Multicomponent systems will be harder to optimize because of their much smaller number of equivalent permutational isomers with respect to pure systems (Darby *et al.*, 2002).

From the above considerations, it is clear that an efficient search algorithm must be able to perform and integrate the following tasks:

(a) From any given point on the PES, to find the local minimum with which it is associated; this is simply what is needed to construct the above-described mapping, or equivalently to transform the PES into a multidimensional staircase.

(b) To make transitions possible from a given basin to another and, more important, from one metabasin to another. In this way, the algorithm would also be able to explore a multiple-funnel PES.

The search by global optimization algorithms can be *unbiased* when the starting configuration is randomly chosen, or *seeded* when a set of (supposedly) good structures is used to begin the optimization procedure. Seeded searches are often faster, since they use prior knowledge about the system under study, but they have the disadvantage of making difficult the finding of unexpected low-lying minima. Almost every algorithm mentioned below can be used either for unbiased or for seeded searches; obviously, when comparing different algorithms, the unbiased search is more significant.

Genetic algorithms have applications in a large variety of fields; they are based on the analogy of evolution through natural (fitness-based) selection. The fitness is the parameter to be optimized, here the potential energy. The coordinates of each cluster are encoded in a string of bits, called the chromosome. At each step, from the present generation of clusters, a new generation is built up. Sons are built up by mixing the chromosomes of parent clusters, or simply by inserting some mutation in the present chromosomes. The individuals of the old generation are compared to the sons via their fitness, and a new generation is formed from the old individuals and the sons, by some rule, which always includes the best-fit individual in the new generation. Very often, several populations are evolved in parallel, and individuals are exchanged between them from time to time. In a genetic algorithm, task (b) is accomplished by chromosome mixing and mutations and by exchanges of individuals between subpopulations, while task (a) corresponds to comparing the fitness of the individuals after a local minimization on them, i.e., comparing $\tilde{U}$(sons) to $\tilde{U}$(parents). Recent developments include similarity checking among cluster structures to keep the diversity of the population as the genetic optimization goes on, as in Cheng *et al.* (2004). The use of genetic algorithms in cluster optimization was pioneered by Hartke (1993) and by Xiao and Williams (1993), who made applications to Si_4 and various molecular clusters, respectively. Their work was followed by applications to a wide variety of systems. Michaelian *et al.* (1999) optimized transition and noble-metal clusters by a symbiotic variant of a genetic algorithm (Michaelian, 1998). Hartke (2000, 2003) also treated water clusters; Deaven and Ho (1995), Deaven *et al.* (1996), and Ho *et al.* (1998) optimized Lennard-Jones and silicon clusters; Rata *et al.* (2000) and Bobadova-Parvanova *et al.* (2002) considered silicon and iron clusters; Darby *et al.* (2002), Massen *et al.* (2002), Bailey *et al.* (2003), and Lloyd *et al.* (2004) optimized Pd-Pt, Au-Cu, and Al-Ni nanoalloy clusters; finally Rossi *et al.* (2004) searched for the global minima of Ag-Cu, Ag-Ni, and Ag-Pd clusters. Recent reviews are those of Hartke (2002) and Johnston (2003).

The *basin-hopping algorithm* (Li and Scheraga, 1987; Doye and Wales, 1998a; Doye, 2004) differs from genetic algorithms because it accomplishes task (b) simply by a canonical Monte Carlo simulation at constant T on the transformed PES. In this framework, the transformation of the PES amounts to lowering the barriers between basins to the maximum possible extent, while keeping the levels of the minima unchanged. Starting from a given basin, a move with random displacements is tried, and the energy difference between the new and the old position $\Delta\tilde{U}$ is calculated. If $\Delta\tilde{U}<0$ the move is accepted with probability 1, otherwise with probability $\exp[-\Delta\tilde{U}/(k_BT)]$. On $\tilde{U}$, transitions can occur in any direction, not only through saddle points, and transitions to lower-lying minima are always accepted. Basin hopping has been applied successfully to the optimization of a large variety of systems, from Lennard-Jones clusters (Wales and Doye, 1997) to clusters of fullerene molecules (Doye *et al.*, 2001), of transition and noble metals (Doye and Wales, 1998b), and of aluminum (Doye, 2003). Basin hopping was able to find the difficult putative global minima in Lennard-Jones clusters at sizes 38, 75, 76, 77, and 98, starting from random initial conditions. Recently, Lai *et al.* (2002) optimized sodium clusters by both genetic and basin-hopping algorithms, finding the same set of minima. This could indicate that both algorithms have comparable efficiency.

Another popular algorithm is *simulated annealing* (Kirkpatrick *et al.*, 1983; Biswas and Hamann, 1986; Freeman and Doll, 1996). In thermal simulated annealing, the system is evolved at constant high T on the untransformed PES by either Monte Carlo or molecular dynamics, then slowly cooled down. Simulated annealing has the advantage of being pretty much physical: one tries to mimic the procedure of cooling a sample which hopefully will reach its most stable configuration if cooling is sufficiently slow. This algorithm is easily incorporated into standard Monte Carlo and molecular-dynamics codes (including *ab initio* molecular dynamics), and the analysis of its output is easy and intuitive. For these reasons, this algorithm has been used for a large variety of systems.[4] There is, however, a major drawback to simulated annealing: it utilizes effectively a single local optimization, and if the system fails to be confined to the basin of attraction of the global minimum as the temperature is decreased, the algorithm may fail, even if it passed through the basin of the global minimum when T was high. As a result, simulated annealing is less efficient than genetic and basin-hopping algorithms (Hartke, 1993; Zeiri, 1995). To avoid trapping in a single basin, one can make long high-T Monte Carlo or molecular-dynamics runs, collecting a large quantity of different snapshots and quenching them down (Sebetci and Güvenc, 2003; Baletto *et al.*, 2004), monitoring the short-term average of kinetic energy (Jellinek and Garzón, 1991; Garzón and Posada-Amarillas, 1996). T must be chosen carefully. If it is too high, the probability of catching the global minimum is very small; if T is too low, the cluster is likely to remain trapped in the basin it starts from.

Another family of annealing algorithms is known as *quantum annealing* (Amara *et al.*, 1993; Finnila *et al.*, 1994; Freeman and Doll, 1996). In quantum annealing, the system is first collapsed into its quantum ground state by using diffusion or Green's-function Monte Carlo techniques (Ceperley, 1994) and then quantum mechanics is slowly turned off. This algorithm utilizes delocalization and tunneling as the primary means for avoiding trapping in metastable states. Amara *et al.* (1993) and Finnila *et al.* (1994) applied quantum annealing to Lennard-Jones clusters up to $N=19$. Lee and Berne (2000) coupled quantum and thermal annealing, being thus able to find the fcc global minimum of the Lennard-Jones cluster of size 38, but this approach failed for other difficult cases at larger size, such as the Marks decahedron at $N=75$. Recently, Liu and Berne (2003) have developed a new quantum annealing procedure, based on quantum staging of path-integral Monte Carlo sampling and local minimization of individual imaginary time slices. This method is able to locate all Lennard-

---

[4] To cite but a few, Jones (1991), Kumar and Car (1991), Röthlisberger and Andreoni (1991), Jones and Seifert (1992), Stave and DePristo (1992), Vlachos *et al.* (1992), Cheng *et al.* (1993), Christensen and Cohen (1993), Jones (1993), Ma and Straub (1994), Ahlrichs and Elliott (1999), Bacelo *et al.* (1999).

Jones minima for $N \leqslant 100$ except at $N=76,77,98$, being thus comparable to basin-hopping and genetic algorithms. This form of quantum annealing uses local minimization to accomplish task (a), and mutations (in which coordinates of randomly selected atoms are reset) to facilitate task (b).

An algorithm that tries to combine the advantages of simulated-annealing, genetic, and basin-hopping approaches has been recently developed by Lee *et al.* (2003). Their algorithm was able to optimize Lennard-Jones clusters up to size 201.

Finally, a very recent proposal is to search for global minima by means of a growth procedure. Solov'yov *et al.* (2003, 2004) applied this method to Lennard-Jones clusters, starting from a tetrahedron, and adding one atom at a time according to different procedures (adding an atom on the surface, inside the surface, or at the center of mass of the cluster). After adding a new atom, the cluster is quenched down to search for the closest local minimum, and the results of the different addition procedures are compared to select the best minimum. This procedure exploits the fact that clusters of similar sizes are likely to have global minima with some resemblance, and in this respect it is a seeded algorithm. Solov'yov *et al.* (2004) were able to find all global minima up to $N=150$. Again, their procedure works on $\tilde{U}$, since clusters are compared for selection after local minimization.

This last observation lead us to a summarizing comment. The most successful algorithms make extensive use of local minimization, comparing the structures for selection *after* having performed that minimization. This amounts effectively to working on $\tilde{U}$. To use the words of Doye (2004), "the method for searching $\tilde{U}$ is of secondary importance to the use of the transformation itself." The searching method may be based on thermal Monte Carlo, quantum tunneling, or genetic operations, but in the end the efficiencies are comparable, given that the algorithms are well constructed.

Doye and Wales (1998a) have shown that the transformation to $\tilde{U}$ modifies the thermodynamics of the system in such a way that the temperature range in which transitions among different funnels are possible is enlarged, and the probability of occupying the basin of the global minimum is increased. This can be understood by analyzing the occupation probability of a minimum s. For an untransformed PES within the harmonic approximation (see Sec. IV) $p_s \propto \exp(-\beta E_s)/\Omega_s^{3N-6}$, where E_s is the potential energy of minimum s, Ω_s is the geometric mean vibrational frequency, and $\beta=(k_B T)^{-1}$, with k_B the Boltzmann constant. For a transformed PES, $p_s \propto A_s \exp(-\beta E_s)$, where A_s is the hyperarea of the basin of attraction of minimum s. The differences between these expressions, the vibrational frequency and hyperarea terms, have opposite effects on the thermodynamics. The higher energy minima are generally less rigid and have a favorable vibrational entropy, so that the transitions are pushed down to lower temperature and sharpened. By contrast, the hyperarea of the minima decreases with increasing potential energy, thus stabilizing the lower energy states and broadening the thermodynamics. The transformation to a staircase PES is not the only useful transformation. Other possibilities have been suggested by Pillardy and Piela (1995), Locatelli and Schoen (2003), and Shao *et al.* (2004).

What are the maximum sizes presently tractable by global optimization? This answer depends on the system under study and on the degree of sophistication of the interaction potential. In the Cambridge Cluster Database (see www-wales.ch.cam.ac.uk/CCD.html), putative global minima for several systems are reported, ranging from Lennard-Jones to Morse, metallic, and water clusters. Even for the simplest potentials, the largest sizes are up to $N=190$ [for Al (Doye, 2003) and Pb clusters (Doye and Hendy, 2003) modeled by the glue potential (Lim *et al.*, 1992)], and sizes decrease for more complex interactions. Very recent seeded optimizations of Lennard-Jones clusters (Shao *et al.*, 2004) reached $N=330$. In order to treat large sizes, Krivov (2002) has proposed a hierarchical method for optimizing quasiseparable systems. In these systems, distant parts are independent, so that a perturbation to the coordinates of a given part has very little influence on distant atoms. According to Krivov (2002), one can exploit this property to build up a hierarchical procedure that can treat Lennard-Jones clusters of several hundreds of atoms. More complex systems such as water clusters have been optimized up to $N \simeq 30$ (Wales and Hodges, 1998; Hartke, 2003). Ahlrichs and Elliott (1999) optimized aluminum clusters within a density-functional approach up to $N=15$ by simulated annealing. Tekin and Hartke (2004) optimized Si clusters by a combination of an empirical global search and density-functional local optimization up to $N=16$. In the case of tight-binding modeling of the interactions, the sizes amenable by global optimization approaches extend to a few tens of atoms. See, for example, Zhao *et al.* (2001), who optimized Ag clusters up to $N=20$ by a genetic algorithm.

How do the best algorithms scale with cluster size? This might be an ill-posed question, since there is no demonstration that the minima found by the different algorithms are really global. However, Liu and Berne (2003) find that their quantum annealing algorithm scales as $N^{3.2}$ for Lennard-Jones clusters in the size range 11–55, and Hartke (1999) finds that his genetic algorithm scales approximately as N^3, again for Lennard-Jones clusters up to $N=150$.

E. Studies of selected systems

In this section we review the energetics of atomic clusters of some selected materials, chosen both for their importance from the point of view of basic science (for example, noble-gas and alkali-metal clusters, which have been the benchmark for testing theoretical models) and for their practical applications (silicon clusters, transition and noble-metal clusters). Finally, we treat a specific kind of molecular cluster, those of fullerene molecules, whose interpretation in energetic terms has been a longstanding puzzle.

1. Noble-gas clusters

Noble-gas clusters have been thoroughly studied since the early 1980s. Excellent accounts of their properties are those of Haberland (1994) and Johnston (2002). Here we briefly review their energetics, focusing on the transition sizes among structural motifs and comparing theory with experiment. A special place among noble-gas clusters is occupied by He clusters, which are the best known example of quantum clusters. Recently there has been a noticeable experimental interest in He clusters, which can be formed by ^{4}He, ^{3}He, or a mixture of the two.[5] In the following, we treat "classical" clusters first and then He clusters.

In a classical series of electron-diffraction experiments, Farges *et al.* (1983, 1986) investigated the structure of neutral Ar clusters produced in a free-jet expansion. They compared the experimental diffraction patterns with those obtained by freezing Lennard-Jones droplets of different sizes in molecular-dynamics simulations and were thus able to identify the experimental products up to $N \sim 10^3$ atoms. Harris *et al.* (1984) measured the mass spectra of charged Ar clusters at $N < 100$. At $20 < N < 50$, both experiments found polyicosahedral structures, composed by interpenetrating 13-atom icosahedra. From $N = 50$ to $N \sim 750$ multishell structures based on the Mackay icosahedron were found. Farges *et al.* (1986) were also able to single out features from diffraction by fcc planes in their spectra of clusters with $N > 600$ atoms. Thus they came to the conclusion that the icosahedron→fcc transition is placed at $N \sim 750$. However, in a more recent analysis, van de Waal *et al.* (2000) have shown that the transition is to a mixture of fcc, hcp, and random close-packed regions, with no significant preference for the fcc bulk structure.

Let us see how the energetics calculations compare with these experimental results. Most of the calculations are based on the use of the Lennard-Jones potential, which is a very popular model for noble-gas systems even though not completely accurate. Several global optimization studies have shown that the icosahedron motif is dominant at small sizes,[6] with few exceptions. Polyicosahedral clusters are formed at sizes 19, 23, and 26 (Farges *et al.*, 1988; Ikeshoji *et al.*, 1996). Indeed, Wales and Doye (1997) found that there are only seven exceptions in the range $13 \leqslant N \leqslant 150$: at $N = 38$ the global minimum is a truncated octahedron; at $N = 75$, 76, 77 and $N = 102$, 103, 104 the best structures are based on the (2,2,2) and (2,3,2) Marks decahedra, respectively. Later on, Leary and Doye (1999) discovered that the global minimum at $N = 98$ is tetrathedral. Romero *et al.* (1999) optimized clusters in the range $148 \leqslant N \leqslant 309$ on icosahedral and decahedral lattices, finding again a prevalence of icosahedron putative global minima with only 11 decahedron exceptions.

At larger sizes, Raoult *et al.* (1989b) compared perfect icosahedron and decahedron structures and concluded that Marks decahedra finally prevail over icosahedra at $N > 1600$. Concerning the transition to fcc structures, Xie *et al.* (1989) compared icosahedral and cuboctahedral clusters, finding a crossover at $N \sim 10^4$. However, cuboctahedra are not the most favorable fcc clusters. Therefore the crossover should be at much lower sizes (Raoult *et al.*, 1989a; van de Waal, 1989), comparable to the crossover size with Marks decahedra.

The combination of these energy-minimization results gives a reasonable interpretation of the experiments, even though there are some points that probably cannot be explained in terms of the energetics alone. At small sizes, the agreement between the global optimization calculations and the experiments is good, even though the decahedron global minima are not yet observed. This may indicate the presence of entropic effects, of the kind discussed in Sec. IV.A, or that even at small sizes some kind of kinetic trapping is taking place (see Sec. V.A). At larger sizes, the comparison of theory and experiment is much more difficult, and there has been considerable debate in the interpretation of the diffraction data in terms of known structures (van de Waal, 1996). For example, fcc clusters with twin faults give electron diffraction patterns very similar to those of Marks decahedra. In any case, a coarse-grained picture is in agreement with the general trend of a transition from the icosahedron motif to other structures. A more detailed analysis reveals that several kinds of clusters can be present in the same size range, so that structural transitions are not really sharp. Quantitative agreement on the transition size between the Lennard-Jones calculations and the experiments has not been reached, probably due to the limited accuracy of the Lennard-Jones potential for Ar. At present, it is very difficult to ascertain whether the diffraction data from large clusters support the existence of either entropic or kinetic effects. Some interesting results addressing this point (Ikeshoji *et al.*, 2001) are discussed in Sec. V.A.

Let us now consider ^{4}He clusters. While the dimer is stable but very weakly bound (Luo *et al.*, 1993; Grisenti *et al.*, 2000), the trimer [which should have a noticeable contribution from linear configurations according to the calculations by Lewerenz (1996)] and larger clusters are much more stable (Toennies and Vilesov, 1998). Chin and Krotscheck (1992) calculated the ground-state properties of various ^{4}He clusters modeled by the Aziz *et al.* (1987) potential, considering several sizes up to $N = 112$, by diffusion Monte Carlo simulations. They found evidence of density oscillations indicating a possible shell structure. Chin and Krotscheck (1995) confirmed the existence of these oscillations for larger clusters, as well,

---

[5] Recent discussions of He clusters are those of Whaley (1994), Toennies and Vilesov (1998), Scoles and Lehmann (2000), Callegari *et al.* (2001), Northby (2001), Johnston (2002), Jortner (2003).

[6] See Hoare and Pal (1975), Farges *et al.* (1985), Freeman and Doll (1985), Northby (1987), Wille (1987), Coleman and Shalloway (1994), Xue (1994), Pillardy and Piela (1995), Deaven *et al.* (1996), Wales and Doye (1997), Romero *et al.* (1999).

and were also able to recover the bulk limit of the excitation spectrum. In a very recent experiment Brühl *et al.* (2004) observed magic sizes at $N=10$, 11, 14, 22, 26, 27, and 44 atoms, in ^{4}He clusters produced in a free-jet expansion. By comparing the experimental results with diffusion Monte Carlo calculations, Brühl *et al.* (2004) showed that these magic sizes are not related to enhanced binding energies at specific values of N, but to the sizes at which excited levels cross the chemical-potential curve and become stabilized.

Clusters of ^{3}He are much less stable, because the constituent atoms are fermions, so that the minimum number of atoms N_{min} needed to form a stable cluster is relatively large. A configuration-interaction calculation based on a phenomenological density functional gave $N_{min}=29$ (Barranco *et al.*, 1997), while subsequent variational Monte Carlo calculations with the Aziz potential gave 34–35 as an upper bound to N_{min} (Guardiola, 2000; Guardiola and Navarro, 2000). The same kind of calculations (Guardiola and Navarro, 2002) have recently been applied to mixed ^{4}He-^{3}He clusters, finding that their stability has a nontrivial dependence on size and composition.

2. Alkali-metal clusters

The structural properties of small Li and Na clusters have been the subject of extensive theoretical activity, following the seminal experiments of Knight *et al.* (1984). Bonacić-Koutecký *et al.* (1991) gave an excellent account of the earlier developments, which are very briefly summarized here. Systematic *ab initio* configuration-interaction studies on Li and Na clusters (Boustani *et al.*, 1987; Bonacić-Koutecký *et al.*, 1988) for $N\leqslant 9$ have shown a complete analogy between the two elements. The lowest isomers are planar up to the pentamer; at $N=6$ a pentagonal pyramid and a triangular planar structure are in very close competition; larger clusters are 3D. In agreement with the experimental magic numbers and with the electronic shell closing arguments, the cluster of 8 atoms, of tetrahedral symmetry (Jellinek *et al.*, 1994), is especially stable compared to neighboring sizes. Röthlisberger and Andreoni (1991) and Röthlisberger *et al.* (1992) performed Car-Parrinello calculations on Na at slightly larger sizes. At $N=13$, they found that the most stable isomer is neither an icosahedron nor a cuboctahedron, but a capped pentagonal bipyramid. At $N=18$ the most stable isomer was the double icosahedron minus one vertex, and at $N=20$ the isomers based on pentagonal symmetries (which are closely related to the double icosahedron) were found to be more stable than structures with tetrahedral symmetry. On the other hand, Bonacić-Koutecký *et al.* (1991) found that two tetrahedron structures are the lowest in energy for Li_{20} and Na_{20} (Bonacić-Koutecký, Fantucci, *et al.*, 1993). Spiegelman *et al.* (1998) found results in reasonable agreement with the previous calculations by a tight-binding approach.

Recent developments are discussed by Ishikawa *et al.* (2001), Solov'yov *et al.* (2002), and Matveentsev *et al.* (2003). Ishikawa *et al.* (2001) reanalyze the problem of Li_6, in which planar and 3D structures were found to be in competition, by a global optimization procedure employing the *replica exchange method* (Swendsen and Wang, 1986) applied to *ab initio* calculations. They find a 3D structure of D_{4h} symmetry group, which is slightly lower in energy than the planar triangle and the pentagonal pyramid. Poteau and Spiegelmann (1993) performed a search for the best Na isomers up to $N=34$ by a growth Monte Carlo algorithm in the framework of a distance-dependent tight-binding (Hückel) model. They found that at $N=34$ the best isomer is the double icosahedron surrounded by a ring of 15 atoms. Sung *et al.* (1994) optimized Li clusters up to $N=147$ by simulated annealing within the local spin-density approximation to the density-functional theory, finding that for $55\leqslant N\leqslant 147$ the structures based on the Mackay icosahedron are the lowest in energy. This has been recently confirmed by Reyes-Nava *et al.* (2002), who performed a global genetic optimization of sodium modeled by Gupta (1981) potentials. A thorough global optimization study (by both genetic and basin-hopping algorithms) of Na, K, Rb, and Cs clusters in the framework of the Gupta potential (as developed by Li *et al.*, 1998) has been performed by Lai *et al.* (2002) up to $N=56$. They found a sequence based on icosahedron clusters except for $N=36$ and $N=38$. At $N=38$ the global minimum is a truncated octahedron, with distorted facets in the cases of Na and Cs; at $N=36$ the structure is a distorted incomplete truncated octahedron.

The transition from electronic to geometric magic numbers in Na clusters has already been discussed in Sec. III.B. Here we simply recall that for $2000<N<20\,000$, there is experimental evidence (Martin *et al.*, 1991a; Martin, 1996, 2000) of peaks in the abundances of Na clusters at sizes corresponding to the completion of perfect icosahedron, Ino decahedron (Ino, 1969), or cuboctahedron structures, which have exactly the same magic numbers. From these magic numbers, one cannot directly infer the actual cluster structures. However, there is at least one indirect argument in favor of icosahedral structures: in fact, while complete icosahedra are surely more favorable than incomplete ones, Ino decahedra are not usually the best decahedral structures, nor are cuboctahedra the best among the possible truncated octahedron clusters.

3. Noble-metal and quasi-noble-metal clusters

Here we treat the energetics of pure clusters of the elements of the last two columns of the transition series: Ni, Cu, Pd, Ag, Pt, and Au. We restrict our treatment to neutral clusters unless otherwise specified.

a. Gold clusters

Small Au clusters ($N\leqslant 10$) have been thoroughly treated by *ab initio* methods. Bravo-Pérez *et al.* (1999a) studied sizes $3\leqslant N\leqslant 6$, finding that the best structures are planar (Bravo-Pérez *et al.*, 1999b). These results have

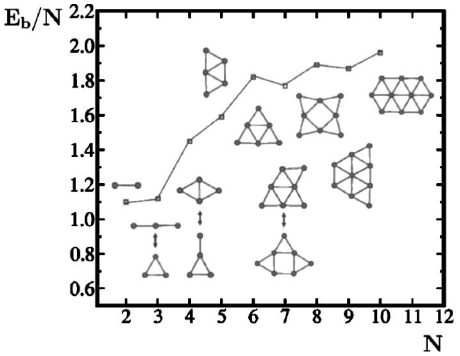

FIG. 12. Lowest-energy isomers of Au clusters according to Bonacić-Koutecký *et al.* (2002). All clusters are planar up to $N=10$ at least. The binding energy per atom E_b/N (in eV) is also shown. For isomers with energy difference smaller than 0.1 eV, both competing structures are shown (see sizes 3, 4, and 7). From Bonacić-Koutecký *et al.*, 2002.

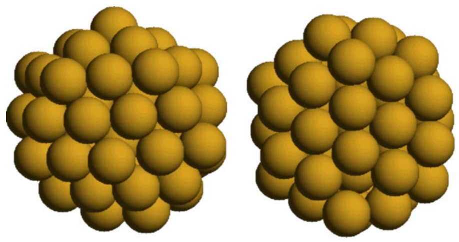

FIG. 13. (Color in online edition) Two views of the lowest-energy isomer of Au at $N=55$ as found by Garzón, Michaelian, *et al.* (1998). This cluster is a strongly rearranged and distorted 55-atom icosahedron, similar to the double-rosette structure discussed in the case of Pt_{55} in Sec. V.A.4. Figure courtesy of Ignacio Garzón.

been confirmed and extended by others.[7] Au clusters are planar up to $N=10$ at least, according to Bonacić-Koutecký *et al.* (2002; see Fig. 12), and only to $N=6$ according to Wang *et al.* (2002), who however found that flat (but nonplanar) structures are the lowest in energy up to $N=14$. In the experiments on Au cations by Gilb *et al.* (2002) there is evidence for planar clusters at least up to $N=7$. The physical origin of the preference for planar structures is discussed in Sec. III.E.4. On the other hand, Li *et al.* (2003) found experimental and computational evidence that Au_{20} is a tetrahedron, well separated from higher isomers. This finding has been confirmed by the calculations of Wang, Wang, and Zhao (2003).

Global optimization methods (Wilson and Johnston, 2000) have been applied to larger clusters modeled by semiempirical potentials. Garzón and co-workers (Garzón, Michaelian, *et al.*, 1998; Garzón, Beltrán, *et al.*, 2003) and Michaelian *et al.* (1999) modeled Au by the Gupta (1981) potential and searched the best isomers by a genetic algorithm, to use them as the starting point of a local relaxation by the density-functional method. They found that Au presents low-symmetry structures at some geometric magic numbers, such as $N=38$ and 55, which therefore are not true magic numbers for Au clusters. These structures are often called "amorphous" in the literature, even though the most appropriate terminology is *low-symmetry structures*. The low-symmetry cluster at $N=55$ is a strongly rearranged and distorted icosahedron, which conserves some fivefold vertexes (see Fig. 13). Low-symmetry structures are found in several semiempirical calculations,[8] the only exception being the Murrell-Mottram potential (Cox *et al.*, 1999), which gives high-symmetry clusters. All these results indicate that high- and low-symmetry structures are in close competition, and the global minimum is sensitive to the fine details of the potential parametrization. An argument in favor of the low-symmetry structures follows from the density-functional relaxation at $N=75$ seen by Michaelian *et al.* (1999), who found that a low-symmetry structure is lower in energy than the (2,2,2) Marks decahedron, in contrast with all semiempirical results. The physical origin of low-symmetry structures is discussed in Sec. III.E.4.

For larger sizes, Cleveland *et al.* (1997) and Baletto, Ferrando, *et al.* (2002) performed semiempirical calculations to compare structures of the different motifs, finding that Marks decahedra are the most favorable, the crossover with fcc structures being at $N \sim 500$.

The comparison of these theoretical predictions with the experiments is complicated by the fact that Au clusters are very often passivated during or after the formation process (Whetten *et al.*, 1996; Schaaff and Whetten, 2000), and it is difficult to determine to what extent the action of the passivating agents can modify the structures (Alvarez *et al.*, 1997). With this in mind, we try, however, to determine how the calculated crossover sizes compare with the experimental results. To this purpose, we must single out those experiments in which the observed clusters were able to reach their equilibrium structure. This was very likely the case in the work of Patil *et al.* (1993), who produced free Au clusters in inert-gas aggregation sources. The clusters were subsequently slowly heated up above their melting temperature and then slowly cooled down (for about one second). Finally, the clusters were deposited and observed. These clusters were identified as being fcc, even at the smallest sizes ($N \simeq 400$), in good agreement with the crossover sizes calculated by Baletto, Ferrando, *et al.* (2002; see Table I and Fig. 14). On the other hand, there have been several observations of large icosahedral structures,[9] at $N \gg 400$. For example, Ascencio *et al.* (1998, 2000) have observed by high-resolution electron microscopy a variety of structures (decahedron, truncated octahedron, icosahedron, and amorphous) for pas-

---

[7] See Grönbeck and Andreoni (2000), Häkkinen and Landman (2000), Bonacić-Koutecký *et al.* (2002), Gilb *et al.* (2002), Häkkinen *et al.* (2002), Wang *et al.* (2002), Zhao *et al.* (2003).

[8] See, for example, Doye and Wales (1998b), Li, Cao, and Jiang, (2000), Darby *et al.* (2002), Garzón *et al.* (2002).

[9] See Buffat *et al.* (1991), Marks (1994), Martin (1996), Ascencio *et al.* (1998), Ascencio *et al.* (2000), Koga and Sugawara (2003).

TABLE I. Potential parameters and cluster crossover sizes for several metals. Parameters p,q of the Rosato *et al.* (1989) potential; parameters $\sigma_1=pq/2$, σ_2, σ_3, and σ_A [see Eqs. (16) and (17)]; sizes where Δ is minimum (N_Δ^{Ih} for icosahedra and N_Δ^{Dh} for decahedra), and crossover sizes ($N_{Ih\to Dh}$, $N_{Dh\to fcc}$, and $N_{Ih\to fcc}$). in the case of the different noble and quasi-noble metals. The parameters of the potentials are taken from Baletto, Ferrando, *et al.* (2002) except for those of Ni, which are found in Meunier (2001) and Baletto, Mottet, and Ferrando (2003). The results on the crossover sizes are taken from Baletto, Ferrando, *et al.* (2002), except those for Ni which are published here for the first time. The results for σ_A are taken from Soler *et al.* (2000).

Metal	p	q	σ_1	σ_2	σ_3	σ_A	N_Δ^{Ih}	N_Δ^{Dh}	$N_{Ih\to Dh}$	$N_{Dh\to fcc}$	$N_{Ih\to fcc}$
Cu	10.55	2.43	13.1	0.062	0.35	0.24	309	20000	1000	53000	1500
Ag	10.85	3.18	17.2	0.065	0.29	0.54	147	14000	<300	20000	400
Au	10.53	4.30	22.6	0.082	0.16	1.86	147	1300	<100	500	<100
Ni	11.34	2.27	12.9	0.055	0.37	0.05	561	17000	1200	60000	2000
Pd	11.00	3.79	20.9	0.062	0.21	0.78	147	5300	<100	6500	<100
Pt	10.71	3.85	20.6	0.073	0.22	1.40	147	5300	<100	6500	<100

sivated particles of a few nanometer's diameter, with a prevalence, however, of (possibly defected) Marks and Ino decahedra. Defected clusters 2–4 nm in diameter have been detected by x-ray diffraction (Zanchet *et al.*, 2000). Moreover, in a recent experiment, Koga and Sugawara (2003) have analyzed a large sample of free Au clusters obtained in an inert-gas aggregation source, with diameters of 3–18 nm and found that icosahedra were the most frequent and decahedra second-most frequent, fcc clusters being absent. These results are again an indication in favor of kinetic effects and are discussed in Sec. V.B.3.

b. Silver clusters

As in the case of Au, the energetics of Ag clusters have been the subject of intensive study in all size ranges. For $N\leqslant 9$, Bonacić-Koutecký, Cespiva, *et al.* (1993, 1994) searched for the lowest-energy clusters by a self-consistent Hartree-Fock procedure which was able to produce structures in good agreement with the experiments (Ganteför *et al.*, 1990; Ho *et al.*, 1990; Alameddin *et al.*, 1992; Jackschath *et al.*, 1992). They found that the best isomers are planar up to the pentamer, as confirmed by Matulis *et al.* (2003) by density-functional calculations. Santamaria *et al.* (1994) found a planar structure also at $N=6$. Recent density-functional studies have considered $N\leqslant 12$ (Fournier, 2001), and $N=13$ (Oviedo and Palmer, 2002). The latter study suggested that the best isomer of 13 atoms is of low symmetry, and that even the cuboctahedron is more favorable than the icosahedron. By contrast, previous density-functional studies on larger Ag clusters (Jennison *et al.*, 1997) found that at $N=55$ the icosahedron is lower in energy than the cuboctahedron.

Larger clusters have been studied mainly by semi-empirical interatomic potentials. This approach has allowed global-minimum searches for N up to 100 atoms (Doye and Wales, 1998b; Erkoç and Yilmaz, 1999) and the comparison of selected magic structures belonging to the icosahedral, decahedral, and truncated octahedral motifs for N up to 40 000 atoms (Baletto, Ferrando, *et al.*, 2002). Doye and Wales (1998b) modeled Ag by the Sutton and Chen (1990) potential and optimized Ag clusters at $N\leqslant 80$, finding the same lowest-energy structures as Bonacić-Koutecký, Cespiva, *et al.* (1993) at $N=7,8,9$, and icosahedral global minima at $N=13$ and 55. Thirty of the global minima were icosahedral in character, but several decahedron and fcc clusters were found, the most stable being at $N=38$ (truncated octahedron)

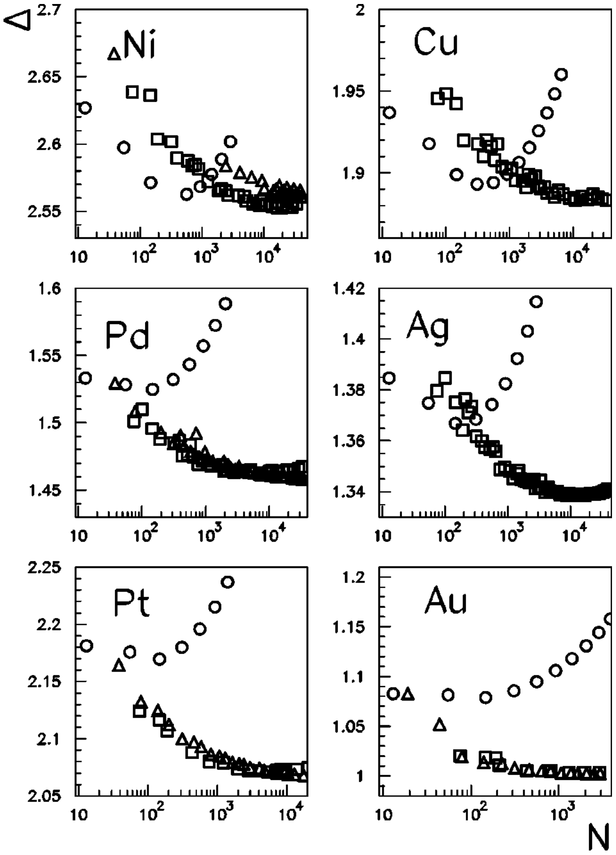

FIG. 14. Δ as a function of N for different cluster motifs in Ni, Cu, Pd, Ag, Pt, and Au: ○, iscosahedra; □, decahedra; △, trunacted octahedra. Data are taken from Baletto, Ferrando, *et al.* (2002), except for the data concerning Ni, which are original. For decahedra and truncated octahedra only the most favorable clusters are shown in the different size ranges.

and $N=71,75$ (decahedron). Mottet *et al.* (1997) modeled Ag by the Rosato *et al.* (1989) semiempirical potential, reproducing essentially the same behavior as the Sutton and Chen (1990) potential at small sizes. They showed that clusters of high stability can be obtained by removing the central atom in perfect icosahedra. In fact, a central vacancy allows neighboring atoms to better relax, expanding their intrashell distance. The same effect was also found in Cu and Au clusters. We note that, at variance with Au, there is no indication in Ag in favor of disordered structures at geometric magic numbers (38, 55, 75). Finally Baletto, Ferrando, *et al.* (2002) and Mottet *et al.* (2004) looked at the crossover sizes (see Table I) by an extensive comparison of clusters of the different motifs.

All the previous theoretical results agree in predicting that Ag follows the general trend outlined in Sec. III.A, with small icosahedra, intermediate-size decahedra, and large truncated octahedra clusters. This is in clear contrast with the inert-gas aggregation experiments by Reinhard, Hull, Ugarte, and Monot (1997), in which small clusters (~2 nm of diameter) were mainly decahedral (or fcc) while large clusters (above 5 nm) were mostly icosahedral. This discrepancy can only be explained by taking into account kinetic trapping effects leading to the growth of metastable structures, as discussed in Sec. V.B.3.

c. Copper clusters

The energetics of small Cu clusters has been extensively treated in a recent review by Alonso (2000); here we give a brief summary of the results for small sizes and then focus on larger clusters.

Several *ab initio* calculations[10] have been performed for $N\leqslant 10$, again comparing a set of reasonably good structures. There is evidence of planar structures up to $N=5$ or $N=6$ maximum, as suggested by recent density-functional calculations (Jug, Zimmerman, Calaminici, *et al.*, 2002). For $N=13$, density-functional calculations (Fujima and Yamaguchi, 1989) indicate that the icosahedron is favored over the cuboctahedron.

For larger size, up to $N\sim 100$, global optimization studies by semiempirical potentials have been performed. Doye and Wales (1989b) used the Sutton and Chen (1990) potential, while Darby *et al.* (2002) used the Gupta (1981) potential. In both cases, the best structure at $N=13$ is the icosahedron, in agreement with density-functional calculations, and there is no indication in favor of disordered structures at geometric magic numbers. Cu thus behaves like Ag, and very differently from Au. Baletto, Ferrando, *et al.* (2002) compared the energies of icosahedron, decahedron, and truncated octahedron clusters at larger sizes, finding that the crossover from icosahedral to decahedral structures is around 1000 atoms and that decahedron and truncated octahedron structures are in close competition up to 30 000 atoms at least (see Table I). Contrary to the Ag case, this behavior is in agreement with the inert-gas aggregation experiments of Reinhard, Hall, Berthoud, *et al.* (1997, 1998), who were able to identify a prevalence of small icosahedra, intermediate-size decahedra, and large fcc clusters, with a wide size interval in which decahedra and fcc clusters coexisted. The crossover size between icosahedron and decahedron structures is in agreement with the calculations.

d. Platinum clusters

The energetic stability of small Pt clusters has been addressed by fewer studies than the other metals treated here. Grönbeck and Andreoni (2000) performed a density-functional study in the size range $2\leqslant N\leqslant 5$, finding that the lowest-lying isomers are planar for both the tetramer and the pentamer. The preference for planar structures is in agreement with previous density-functional calculations by Yang *et al.* (1997), who also found planar structures for $N=6$ by a dynamical quenching procedure. In contrast, other *ab initio* calculations (Dai and Balasubramanian, 1995) on the tetramer gave preference to the tetrahedal structure, as in the density-functional results of Fortunelli (1999), who found that the lowest-lying isomer is indeed the tetrahedron, with a planar rhombic structure that was slightly higher in energy.

Sachdev *et al.* (1992) modeled Pt at larger sizes, by an embedded atom potential and made simulated annealing calculations, finding that both at 13 and at 55 atoms low-symmetry isomers are the lowest in energy. On the other hand, further global optimization results based on semiempirical modeling (Doye and Wales, 1998b; Baletto, Ferrando, *et al.*, 2002; Massen *et al.*, 2002; Sebetci and Güvenc, 2003) gave preference to the icosahedral structure at $N=13$. Doye and Wales (1998b) and Massen *et al.* (2002) found a low-symmetry structure at $N=55$, while Baletto, Ferrando, *et al.* (2002) found the icosahedral structure also at this size, though with small crossover sizes among icosahedral, decahedral, and truncated octahedral structural motifs (see Table I). *Ab initio* results are even fewer. Yang *et al.* (1997) found that at $N=13$ several low-symmetry structures are lower in energy than the icosahedron and the cuboctahedron. Watari and Ohnishi (1998) found that the cuboctahedron is more stable than the icosahedron at $N=13$ by density-functional calculations. Recently, Fortunelli and Aprà (2003) extended their calculations to $N=13$, 38, and 55. At $N=13$, they found that the Ino decahedron is lower in energy than the icosahedron and the cuboctahedron, but a structure of D_{4h} symmetry group originating from the symmetry breaking of the cuboctahedron is even lower. At $N=55$ the order of the structures is inverted, and the icosahedron becomes lower than the Ino decahedron and the cuboctahedron. Fortunelli and Aprà (2003) attributed the results at $N=13$ to the small size of the molecule, while the behavior at $N=55$ is intermedi-

---

[10] See Bauschlicher (1989), Bauschlicher *et al.* (1988, 1989, 1990), Fujima and Yamaguchi (1989), Massobrio *et al.* (1995), Jug, Zimmerman, Calaminici, *et al.* (2002), Jug, Zimmerman, and Köster (2002b).

ate between finite molecules and fully metallic systems. Very recent density-functional calculations by Aprà *et al.* (2004) show that rosette structures, originating from the disordering of one or two vertices in icosahedra of 55 atoms, are considerably lower in energy than the icosahedron itself. This result would support the preference of Pt for low-symmetry structures at icosahedral magic numbers.

e. Palladium clusters

The energetics of small Pd clusters have been investigated by several groups employing different methods.[11] Besides their catalytic properties, these clusters are very interesting because their lowest-lying isomers could have nonzero spin (Reddy *et al.*, 1993; Watari and Ohnishi, 1998), being thus magnetic. Zhang *et al.* (2003) have recently performed an extensive study of the stability of Pd clusters within the density-functional approach at $N \leqslant 13$. In this size range they compared several 1D, 2D, and 3D isomers; moreover, they considered a few selected structures at $N=19$ and 55. Their results indicate that the lowest-lying isomers are 3D starting with the tetramer (Zacarias *et al.*, 1999; Moseler *et al.*, 2001), and that icosahedral structures are favored over both decahedral and cuboctahedral structures for $N=13$ and 55. These results are in good agreement with previous calculations by Kumar and Kawazoe (2002). On the other hand, Watari and Ohnishi (1998) found that the cuboctahedron is more stable than the icosahedron at $N=13$ according to density-functional calculations. Moseler *et al.* (2001) were able to compare their results on vertical electron detachment energies for anionic clusters with the experimental data (Ervin *et al.*, 1988; Ho *et al.*, 1991; Ganteför and Eberhardt, 1996), obtaining a good agreement.

At larger sizes, *ab initio* results are few, being restricted to the comparison of a small set of selected structures at some special sizes. Kumar and Kawazoe (2002) have compared icosahedron with cuboctahedron and Ino decahedron clusters at $N=55$ and 147, finding that slightly distorted icosahedral structures are the lowest in energy in both cases. Nava *et al.* (2003) also found that a Jahn-Teller distorted icosahedron is lower in energy than a perfect icosahedron at $N=55$. Moreover, Nava *et al.* (2003) found that icosahedra and cuboctahedra are very close in energy at both $N=147$ and $N=309$, with the icosahedra prevailing at 147 and cuboctahedra at 309. By tight-binding calculations, Barreteau *et al.* (Barreteau, Desjonquères, and Spanjaard, 2000; Barrateau, Guirado-Lopez, *et al.*, 2000) found that the icosahedron is still lower in energy than the cuboctahedron at $N=309$, but not at $N=561$. However, it must be kept in mind that the cuboctahedron and the Ino decahedron are not usually favorable fcc and decahedron clusters. This observation is in agreement with previous density-functional calculations by Jennison *et al.* (1997), who showed that for $N=140$, the truncated octahedron is favored over the icosahedron structure obtained by removing seven vertex atom from the Ih_{147}, while in Ag the opposite happens.

Global optimization studies up to $N \simeq 100$ by the Sutton and Chen (1990) potential give for Pd the same results as for Ag, with icosahedron structure at $N=55$, as confirmed also in the optimization of the Gupta (1981) potential by Massen *et al.* (2002). At larger sizes, a comparison of the different structural motifs shows that Pd behaves in a similar way to Pt [with rather small crossover sizes (see Table I), and fcc clusters already in close competition with the other motifs at $N \sim 100$] when modeled by the Rosato *et al.* (1989) potential, while it behaves very similarly to Ag when treated by means of embedded atom potentials (Baletto, Ferrando, *et al.*, 2002). Calculations by Jennison *et al.* (1997) better support the results from the Rosato *et al.* (1989) potential, finding that fcc structures are more favored in Pd than in Ag. However, this point would need further investigation, and it is not resolved by the analysis of the available experimental data. José-Yacamán, Marín-Almazo, and Ascencio (2001) observed by transmission electron microscopy the thiol-passivated Pd nanoparticles in the range of 1–5 nm diameter, seeing a variety of structures, ranging from fcc (simple and twinned), to icosahedral, to decahedral, to amorphous structures. They were able to observe rather large icosahedral clusters, explaining their presence as being probably due to kinetic trapping effects.

f. Nickel clusters

As in the case of Cu, small Ni clusters have been recently reviewed by Alonso (2000). Reuse and Khanna (1995) and Reuse *et al.* (1995) performed several density-functional studies of small Ni clusters, concluding that the lowest-lying isomers are nonplanar for $N \geqslant 4$. At $N=7$, two isomers, the pentagonal bipyramid and the capped octahedron, are in close competition (Nayak *et al.*, 1996). The former is favored by density-functional (Nygren *et al.*, 1992) and embedded-atom (Boyakata *et al.*, 2001) calculations, while the latter is most likely to be observed in the experiments (Parks *et al.*, 1994), although the experimental data do not completely rule out the pentagonal bipyramid (Nayak *et al.*, 1996). Nayak *et al.* (1996) performed *ab initio* calculations, finding that these structures are almost degenerate in energy; then they performed molecular-dynamics simulations by the Finnis and Sinclair (1984) semiempirical potential, finding that the capped octahedron has a wider catchment basin, becoming thus much more favorable at high temperatures. This is clear evidence of an entropic effect (see Sec. IV.A). At $N=13$, Parks *et al.* (1994) experimentally identified the icosahedron as the most stable struc-

---

[11] See Valerio and Toulhoat (1996, 1997), Jennison *et al.* (1997), Zacarias *et al.* (1999), Barreteau, Desjonquères, and Spanjaard (2000), Barreteau, Guirado-López, *et al.* (2000), Efremenko and Sheintuck (2000), Guirado-López *et al.* (2000), Efremenko (2001), Krüger *et al.* (2001), Moseler *et al.* (2001), Roques *et al.* (2001), Kumar and Kawazoe (2002), Nava *et al.* (2003), Zhang *et al.* (2003).

ture. *Ab initio* calculations at the same size (Reuse and Khanna, 1995; Reuse *et al.*, 1995) have shown that the icosahedron is favored over the cuboctahedron, but the most stable isomer is obtained by distorting the icosahedron slightly to obtain a cluster with D_{3d} symmetry group. The experimental observations (Parks *et al.*, 1995, 1997, 1998) indicate a truncated octahedron structure at $N=38$, a capped decahedron structure at $N=39$, and (possibly defected) icosahedral structures at $N=55$. Theoretical results are in reasonable agreement with these experimental findings. Different global optimization results within semiempirical schemes (Doye and Wales, 1998b; Grygorian and Springborg, 2003) and tight-binding calculations (Lathiotakis *et al.*, 1996) predict fcc and icosahedral structures at $N=38$ and 55, respectively. Moreover, capped decahedral structures just above size 38 are found (Wetzel and DePristo, 1996; Andriotis and Menon, 2004). At larger sizes, the comparison of the different structural motifs by different semiempirical approaches (Cleveland and Landman, 1991; Mottet *et al.*, 2004) shows that the crossovers icosahedral→decahedral and decahedral→fcc take place at large sizes as in the case of Cu (see Table I).

4. General structural properties of noble-metal and quasi-noble-metal clusters

Here we sketch general trends among the six metals of the previous section with respect to three features: formation of planar clusters, magnitude of crossover sizes among the motifs, and preference for low-symmetry global minima at geometric magic sizes.

Concerning the preference for formation of planar structures, there is a clear indication of an increasing tendency going down from the 3*d* to the 5*d* series and from left to right in the Periodic Table. Thus Au has the strongest tendency, followed by Ag, Pd, and Pt, all three being at the same level (however, there is still some debate about planar Pt clusters); Cu and Ni have no preference at all for planar structures. Several groups have investigated the origin of this trend. Bravo-Pérez *et al.* (1999b) correlated the preference for planar structures in Au to the fact that nonadditive many-body interactions are stronger than additive two-body ones in this element. Bonacić-Koutecký *et al.* (2002) noticed that in planar Au clusters, *d* electrons contribute more to the bonding than in 3D structures; this would also qualitatively explain the weaker tendency to planar clusters for Ag, because in Ag the bonding is more of *s* type. Finally, Häkkinen *et al.* (2002) investigated Au_7^-, Ag_7^-, and Cu_7^- by density-functional calculations and demonstrated that the propensity of Au clusters to favor planar structures is correlated with the strong hybridization of the atomic 5*d* and 6*s* orbitals due to relativistic effects.

The tendency to form strained structures like icosahedra and decahedra, leading to large crossover sizes, and the tendency to present low-symmetry structures at geometric magic numbers have been discussed, in the framework of the same well-defined and quite reliable energetic model, by Baletto, Ferrando, *et al.* (2002) and Soler *et al.* (2000). What follows is a summary of these works. The energetic model is the Gupta (1981) or Rosato *et al.* (1989) potential, which predicts the correct surface reconstructions (Guillopé and Legrand, 1989) and reproduces quite accurately the diffusion barriers (Montalenti and Ferrando, 1999a, 1999b; Ala-Nissila *et al.*, 2002) for these metals. In this framework, the potential energy E of a cluster of N atoms is $E=\Sigma_{i=1}^{N}E_i$, where the energy of atom i is given by

$$E_i = A\sum_{j=1}^{n_v} e^{-p(r_{ij}/r_0-1)} - \xi\sqrt{\sum_{j=1}^{n_v} e^{-2q(r_{ij}/r_0-1)}}, \tag{11}$$

where n_v is the number of atoms within an appropriate cutoff distance (in the following we include only the first neighbors), and A,ξ,p,q are parameters fitted to the bulk properties of the element. The first term in Eq. (11) is a repulsive Born-Mayer energy, while the second is the attractive band energy. Following Tománek *et al.* (1985), one can eliminate the parameters A and ξ, in order to have a function of (p,q) and of the cohesive energy per atom E_{coh}. This is achieved by requiring that in the bulk crystal at equilibrium $E_i=E_{coh}$ and $\partial E_i/\partial r=0$ for $r=r_0$. The result is

$$E_i = \frac{|E_{coh}|}{12(p-q)}\left[q\sum_{j=1}^{n_v} e^{-p(r_{ij}/r_0-1)} - \sqrt{12}p\sqrt{\sum_{j=1}^{n_v} e^{-2q(r_{ij}/r_0-1)}}\right]. \tag{12}$$

This explicitly shows that the properties of the potential depend only on the parameters (p,q), E_{coh} and r_0 playing the role of scale factors on energy and distance. Since atomic distances r_{ij} in noncrystalline structures are not optimal, one can expect a metal that strongly increases its energy for a change in r_{ij} (i.e., that has a sticky interatomic potential) to have small crossover sizes (Doye *et al.*, 1995). In a solid at equilibrium, all 12 first neighbors are at $r_{ij}=r_0$. When one changes all r_{ij} by a common factor $r_{ij}\to(1+\varepsilon)r_{ij}$, developing the crystal energy per atom $E_i(\varepsilon)$ in Eq. (12) (with $n_v=12$) to the second order and dividing it by the equilibrium value $|E_{coh}|$, one obtains (Baletto, Ferrando, *et al.*, 2002)

$$\rho(\varepsilon) = \frac{E_i(\varepsilon)-E_i(0)}{|E_i(0)|} = \frac{1}{2}\varepsilon^2 pq. \tag{13}$$

Here $\sigma_1=\rho(\varepsilon)/\varepsilon^2=pq/2$ is essentially the product of the bulk modulus and the atomic volume divided by the cohesive energy per atom of the bulk crystal. Thus the larger the pq, the smaller the crossover sizes from icosahedra to decahedra $N_{Ih\to Dh}$ and from decahedra to fcc crystallites $N_{Dh\to fcc}$, as can be seen in Table I.

Let us now discuss the tendency to form low-symmetry structures at geometric magic sizes (referred to as the tendency to amorphization in the following). This tendency is due to a specific feature of the metallic bonding, which derives from its many-body character and relates the optimal distance of the bonding to the coordination of the atom (bond-order/bond-length correlation). This can be easily seen by taking a number of neighbors $1 \leqslant n_v \leqslant 12$ in Eq. (12), all at the same distance r. Minimization with respect to r leads to the optimum distance $r^*(n_v)$,

$$\frac{r^*(n_v)}{r_0} = 1 + \frac{1}{2(p-q)} \ln\left(\frac{n_v}{12}\right), \tag{14}$$

which is more and more contracted for decreasing n_v. It also leads to the energy

$$E^*(n_v) = -|E_{coh}|\left(\frac{n_v}{12}\right)^{(p-2q)/2(p-q)}. \tag{15}$$

The atoms on the surface of the cluster try to contract in order to minimize their elastic energy (Soler *et al.*, 2001). In the case of highly coordinated structures like the icosahedra (which have intrashell expanded distances), the optimization of the bond lengths is made at the expense of the number of bonds. Therefore one expects amorphization to be easy in the elements with high elastic energy (i.e., large pq) and strong contraction of the bonds with decreasing coordination, the latter leading to a weak dependence of E^* on n_v. The contraction of the bonds and the dependence of E^* on the coordination can be quantified by the following dimensionless parameters:

$$\sigma_2 = \frac{n_v}{r_0}\frac{dr^*}{dn_v} = \frac{1}{2(p-q)},$$

$$\sigma_3 = \frac{n_v}{E^*}\frac{dE^*}{dn_v} = \frac{p-2q}{2(p-q)}. \tag{16}$$

As is evident from Table I, all parameters agree in indicating that Au has by far the strongest tendency to amorphization, having the largest σ_1 and σ_2 and the smallest σ_3, followed by Pt and Pd; Ag and especially Cu and Ni have the weakest tendency.

On the same line of reasoning, Soler *et al.* (2000) defined a parameter based solely on experimental quantities to extend the estimate of the tendency to amorphization to other systems. This parameter is σ_A and is defined as the elastic energy δE_{el} that is needed to form an ordered surface with contracted atomic distances, divided by the amorphization energy δE_{am} which is required to form a scattered distribution of bond lengths. δE_{el} is expressed by means of the (Voigt-averaged) bulk and shear moduli B and G. ΔE_{am} is approximated by the enthalpy of melting ΔH_{melt}, which is an estimate of the energetic cost to form amorphous structures resembling those found in liquids. This leads to

$$\sigma_A = \frac{\delta E_{el}}{\Delta E_{am}} \simeq \frac{v(3B-5G)^2}{320 B \Delta H_{melt}}, \tag{17}$$

where v is the atomic volume. Equation (17) is valid for small clusters having almost all atoms on their surface. Elements with large σ_A are expected to have a stronger tendency to amorphization. As can be seen in Table I, the inspection of σ_A confirms the above trends, the only difference being the indication that Pt should have a stronger amorphization tendency than Pd, due essentially to the comparatively weaker enthalpy of melting of Pt (the ratio $\Delta H_{melt}/|E_{coh}|$ is much smaller in Pt than in Pd).

Finally, let us compare metals with Lennard-Jones clusters, in order to sketch a qualitative picture of the effects of many-body forces. If one applies the criterion of Eq. (13) to Lennard-Jones clusters, one finds a value of σ_1, which is even larger than those for Au, Pt, and Pd. This would suggest that Lennard-Jones systems have a weaker tendency to form icosahedral clusters than these metals, but this is not the case, since crossover sizes icosahedron → decahedron and icosahedron → fcc are much larger for Lennard-Jones clusters than for Au, Pt, or Pd. This happens because the bond-order/bond-length correlation of metallic elements tends to destabilize icosahedral structures. In fact, metals would prefer contracted interatomic distances for the low-coordination surface atoms, and bulk distances for the highly coordinated inner atoms. This is exactly the opposite of what happens in perfect icosahedral structures, which have contracted internal distances and expanded surface distances. Moreover, in some metals such as Pt, bond directionality effects (which are not included in the potentials considered in Table I) can be important (Fortunelli and Velasco, 2004) and favor the appearance of (111)-like hexagonal facets on the cluster surface (Aprà *et al.*, 2004), with a further destabilizing effect on icosahedral clusters.

5. Silicon clusters

Silicon nanoclusters are of great practical interest because of their intense photoluminescence at room temperature and the presence of quantum size effects. There is an ongoing debate about the size at which the most favorable clusters adopt the bulklike diamond structure. Bachels and Schäfer (2000) produced neutral Si clusters in a laser vaporization source and measured their binding energy in samples having average sizes $\bar{N}$ from 65 up to 890 atoms. They showed that the binding energy per atom E_b in this size range scales as $N^{1/3}$, this being characteristic of approximately spherical clusters (Kaxiras and Jackson, 1993a). At smaller sizes, different regimes in the behavior of E_b with N were found, as can be seen from Fig. 15. There, Bachels and Schäfer (2000) plotted, besides their results at large sizes, E_b for smaller clusters ($N \leqslant 7$) obtained from the results of other groups (Jarrold and Honea, 1991; Schmude *et al.*, 1993, 1995; Fuke *et al.*, 1994). Three regimes are clearly shown. For $N < 10$ the binding energy increases rapidly with the cluster sizes, and compact elementary units are built up. For $10 < N < 25$, E_b is practically independent of N, as would happen for prolate structures (Kaxiras and Jackson, 1993a). This agrees with the previous observation of small prolate Si clusters by Jarrold and Constant (1991). Finally, for larger clusters the $N^{1/3}$ behavior is recovered. Bachels and Schäfer (2000) were also able to produce metastable prolate structures at sizes up to

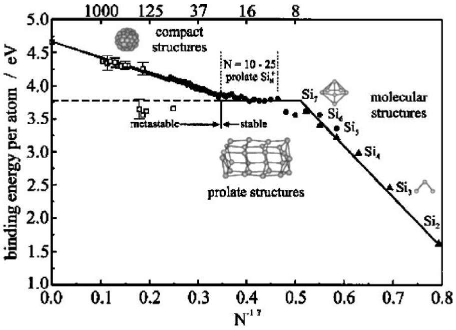

FIG. 15. Size dependence of the binding energies of neutral silicon clusters: □, binding energies of the two groups of cluster isomers found by calorimetric measurements; ●, data for neutral silicon clusters obtained from the collision-induced dissociation experiments of Jarrold and Honea (1991) on the corresponding silicon cluster cations, taking the experimentally determined photoionization potentials into account as from Fuke *et al.* (1994); ▲, the Knudsen mass spectrometric measurements of Schmude *et al.* (1993, 1995). The crossover from elongated to the spherical neutral silicon structures can be estimated from the binding energies to be located around $N=25$. The structure for an elongated Si_{26} cluster is taken from Grossman and Mitás (1995b). Adapted from Bachels and Schäfer, 2000.

about 170 atoms. These structures were mostly present in the part of the molecular beam with short dwell times.

How do these results compare to calculations? And is the transition size to quasispherical structures the same as the transition size to bulklike diamond structures? In the following we address these questions.

Theoretical results on the energetics of small silicon clusters have been obtained by quantum Monte Carlo, density-functional, and tight-binding calculations. The latter also permitted the application of global optimization methods such as simulated annealing (Yu *et al.*, 2002) and genetic algorithms (Ho *et al.*, 1998; Rata *et al.*, 2000; Wang, Wang, *et al.*, 2001).

For very small clusters, Raghavachari and Logovinsky (1985) found that the best clusters are planar only up to $N=4$; several calculations (Fournier *et al.*, 1992; Li *et al.*, 1999; Zickfeld, *et al.*, 1999; Yu *et al.*, 2002) found a generally good agreement with the above results. An important result at small sizes is that Si_{10} is a very stable cluster (Raghavachari and McMichael-Rohlfing, 1988; Grossman and Mitás, 1995a; Ramakrishna and Bahel, 1996; Li, Yin, *et al.*, 2000) so that it can act as a subunit of larger ones (see Fig. 16). For example, quantum Monte Carlo, density-functional (Mitás *et al.*, 2000), and tight-binding calculations (Yu *et al.*, 2002) find that the best structures at $N=20$ are simply formed by linking two Si_{10} subunits. Indeed, the most reliable explanation for the observation of prolate clusters is that they are built up by stacked subunits, whose structure is still under debate. Kaxiras and Jackson (1993a, 1993b) proposed that the subunits are sixfold rings; Raghavachari and McMichael-Rohlfing (1988), Jarrold and Bower (1992), and Ho *et al.* (1998) were in favor of tricapped trigonal prisms of nine atoms; Rata *et al.* (2000) found that Si_{20} is made of six- and eight-atom subunits. They also found that the dissociation energies and inverse mobilities calculated from their global minima were in excellent agreement with the experiments (Jarrold and Honea, 1991; Hudgins *et al.*, 1999) up to $N=18$, concluding that cluster formation is dominated by the energetics up to these sizes.

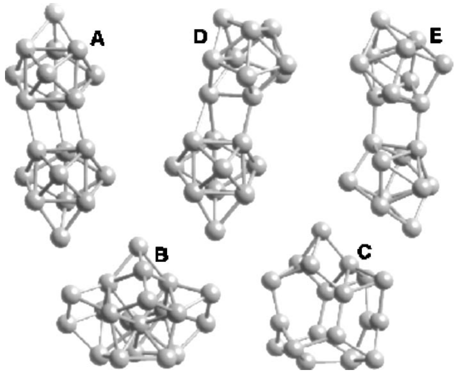

FIG. 16. The best isomers of Si_{20} according to Mitás *et al.* (2000). Structure E is the lowest in energy according to quantum Monte Carlo calculations. From Mitás *et al.*, 2000.

In summary, experiments and calculations agree in finding prolate structures of a few tens of atoms which are built up by small subunits in the range 6–10 atoms. This is also consistent with fragmentation experiments of clusters of about 150 atoms by Ehbrecht and Huisken (1999), yielding Si_6^+–Si_{11}^+ products.

Clusters are quasispherical for about $N>25$ (Hudgins *et al.*, 1999), even if they do not form crystalline structures at these sizes. Indeed, the experiments of Ehbrecht and Huisken (1999) could be interpreted as assuming that compact shapes at $N\sim150$ are built up by small subunits [the prolate metastable structures observed by Bachels and Schäfer (2000) being possibly unfolded versions of these clusters], and this agrees with the simulated annealing calculations by Yu *et al.* (2002). But this is not the only possibility, since Kaxiras and Jackson (1993a), Ho *et al.* (1998), and Mitás *et al.* (2000) have shown that quasispherical noncrystalline structures, which are not built up by stacking smaller subunits, become favorable at $N\geqslant20$. These sizes are large enough to allow the formation of cages containing at least one Si atom inside (Mitás *et al.*, 2000). These results compare rather well with the experiments of Bachels and Schäfer (2000). However, the theoretical determination of the most stable structures in medium-size Si clusters is a very complex task: see, for example, the debate about the structure of Si_{36} in Sun *et al.* (2003) and Bazterra *et al.* (2004).

Mélinon *et al.* (1997, 1998) demonstrated that the models based on quantum confinement in crystalline silicon clusters fail for films containing grains of less than 2 nm diameter (say $N\simeq200$). They were not able to observe any crystallization by transmission electron microscopy. On the other hand, if the grains are of 3 nm diameter, there is evidence of crystalline ordering (Ehbrecht *et al.*, 1997; Ehbrecht and Huisken, 1999; Ledoux *et al.*, 2000). This would indicate that the transition to crystalline structures is around $N=400$ atoms, as Yu *et al.* (2002) found by simulated annealing tight-binding calculations.

6. Clusters of fullerene molecules

The condensed-phase properties of C_{60} molecules have been the subject of considerable interest because of the unusual character of molecular interactions. In fact, above room temperature, C_{60} molecules can be considered as large spherical pseudoatoms which are free to rotate; the effective interaction between these pseudoatoms is extremely short-ranged relative to the large equilibrium pair separation. This is at the origin of peculiar properties. In fact, such sticky interactions (see Fig. 7) disfavor all strained configurations, like those occurring in icosahedra or in the liquid phase. Indeed, the existence of a liquid phase for bulk C_{60} (Hagen *et al.*, 1993; Caccamo *et al.*, 1997; Ferreira *et al.*, 2000) is still debated. Therefore clusters of C_{60} molecules are on the opposite side with respect to clusters of alkali metals, and we expect noncrystalline structures to be the global minima only for aggregates of a small number N of molecules.

This qualitative prediction has been confirmed by all existing calculations. We can divide these studies into two classes. The first uses an all-atom potential, with each carbon atom interacting with atoms of other molecules by a Lennard-Jones potential. This approach includes deviations from spherical symmetry, but at present allows global optimization only for small N. The second class uses spherically averaged potentials, such as the Girifalco (1992) potential, in which Lennard-Jones centers are continuously and uniformly distributed on the surface of a sphere, or the potential developed by Pacheco and Prates-Ramalho (1997), which is derived by fitting density-functional calculations. The Girifalco (1992) potential is purely two-body, whereas the Pacheco and Prates-Ramalho (1997) potential includes two-body and three-body terms (the latter, however, being of rather small importance).

All these approaches agree in predicting that icosahedral structures are favored only at very small N. All-atom potentials favor icosahedral structures up to $N=16$ (Doye *et al.*, 1997; Garcia-Rodeja *et al.*, 1997; Rey *et al.*, 1997), while calculations with the Girifalco (1992) potential, which is the stickiest, indicate that icosahedra are the lowest in energy only up to $N=13$ (Rey *et al.*, 1994; Wales, 1994a; Doye and Wales, 1996b). Finally, the Pacheco and Prates-Ramalho (1997) potential favors icosahedral structures up to $N=15$. Larger clusters are either based on decahedra or on close-packed structures, as shown by Doye *et al.* (2001), who performed an exhaustive basin-hopping global optimization study up to $N=105$ on the basis of both Pacheco and Prates-Ramalho (1997) and Girifalco (1992) potentials. Close-packed structures become more frequent as the size increases. Both potentials indicate that the most stable isomers are found at $N=38$ (truncated octahedron), $N=75$ [(2,2,2) Marks decahedron] and 101 [(2,3,2) Marks decahedron], and that $N=55$ is not a magic number. At that size, the icosahedron is higher in energy than the best decahedron structure by 0.3 and 2 eV according to the Pacheco and Prates-Ramalho (1997) and Girifalco (1992) potentials, respectively.

These results completely disagree with the experimentally observed structures. In fact, Martin *et al.* (1993) and Branz *et al.* (2000, 2002) found that clusters grown at low T and annealed at ~ 500 K (to allow the less bound surface molecules to evaporate) present a mass spectrum with a clear sequence of icosahedral magic numbers up to very large sizes, well above $N=100$ (see Fig. 17). The peak at $N=55$ is very evident, and no peaks are found at $N=38$ and 75. The mass spectra are qualitatively similar for neutral, positively and negatively charged clusters (Branz *et al.*, 2002). Recently, Rey *et al.* (2004) compared the neutral and singly-ionized cluster structures in a model including the Girifalco (1992) potential plus a point polarizable dipole electrostatic model. They found that the structures of ionized clusters are very similar to those of neutral clusters, thus confirming the observations. Branz *et al.* (2002) found decahedra and close-packed structures only after further annealing at higher T. This result indicates the possible existence of kinetic trapping effects in the formation of the clusters of C_{60} molecules (Baletto, Doye, and Ferrando, 2002), as we discuss in Sec. V.B.5. Trapping effects are overcome only after a strong annealing.

The resulting high-T experimental structures, however, still do not coincide with those predicted by the Girifalco (1992) and Pacheco and Prates-Ramalho (1997) potentials. In fact, there is a sequence of experimental magic numbers that can be attributed to the Leary tetrahedron at $N=98$ and to its fragments down to $N=48$, while the calculations do not attribute special stability to these structures. This discrepancy is probably due to the fact that even the Pacheco and Prates-Ramalho (1997) potential is too sticky; a slightly less sticky Morse potential gives the Leary tetrahedron as a magic structure (Doye *et al.*, 2001).

IV. THERMODYNAMICS OF FREE NANOCLUSTERS

In this section, we analyze the effects of raising the temperature on cluster structures. These effects may include solid-solid structural transitions and the melting of the cluster if the temperature is raised enough. Both solid-solid transitions and melting are cases that show the peculiar thermodynamic behavior of small finite systems such as clusters. Indeed, the thermodynamics of finite systems is a fascinating and complex field, involving many subtleties. Here we have no intention of being exhaustive and refer readers who need more complete treatments to existing monographs, from the classical book of Hill (1964) to the excellent book by Wales (2003). In the following we treat only those issues that

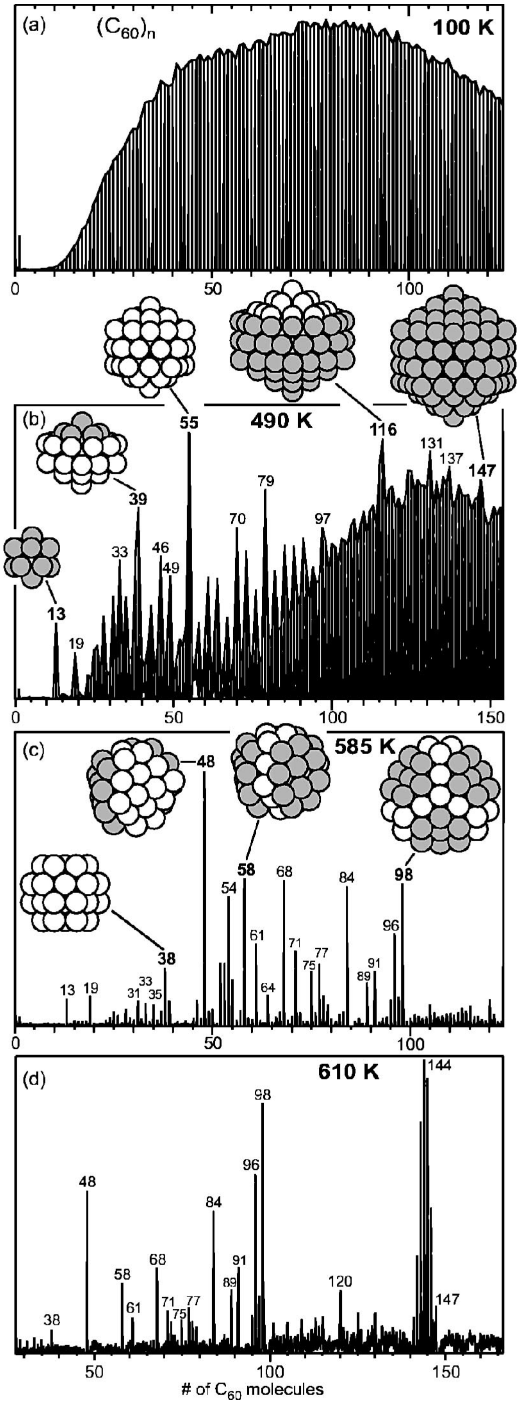

FIG. 17. Mass spectra of C_{60} clusters: panel (a), clusters produced at low T do not reveal any magic number; panel (b), after mild annealing to evaporate the less bound molecules, a clear series of icosahedral magic numbers emerges; panels (c) and (d), decahedra and close-packed magic numbers appear only after a high-T annealing. Adapted from Branz *et al.*, 2002.

have a direct bearing on temperature-dependent changes in the cluster structures.

Generally speaking, two points must be kept in mind about cluster thermodynamics. First, phase transitions in small systems are gradual, not sharp (Hill, 1964). A consequence of this fact is that there are bands of temperature and pressure within which two or more cluster structures may coexist. This coexistence is dynamic, like that of coexisting chemical isomers.[12] Second, thermodynamic properties (like the melting point) can be strongly size dependent, in analogy to what happens to the global-minimum structures. General trends for thermodynamic properties may be deduced on the basis of the following expression for the Gibbs free energy G (Hill, 1964). In a bulk system, $G=Ng(p,T)$ where $g(p,T)$ is the specific Gibbs potential. For a small system, we have also to consider contributions coming from surfaces, edges, etc. Thus we write G as

$$G = Ng(p,T) + b(p,T)N^{2/3} + c(p,T)N^{1/3} + d(p,T), \tag{18}$$

where the term in $N^{2/3}$ is a surface free energy, the term in $N^{1/3}$ is due to edge contributions, and the last term might be due, among other things, to the rotation of the cluster. In the limit $N \to \infty$, one has $G \to Ng$, the macroscopic relationship. But when the system is small all terms are important. The finite size of the clusters also implies that treatments in different thermodynamic ensembles (microcanonical and canonical) may give different behaviors for thermodynamic quantities such as the heat capacity (Bixon and Jortner, 1989; Jortner, 1992).

The thermodynamics of clusters have been studied by a variety of theoretical and simulation tools. These include Monte Carlo and molecular-dynamics simulations and analytical methods.[13]

In Sec. IV.A we focus on the role of entropic contributions to the free energy at increasing temperature, which may cause solid-solid structural transitions when the structure corresponding to the global energy minimum ceases to be the most likely at high T, so that other structures prevail. In Sec. IV.B we deal with the melting transition. There, we first discuss what is meant by melting (and premelting) in clusters, briefly reviewing experimental and simulation methods. Then we focus on the size dependence of the melting point, which may be very complex, as in the case shown in Fig. 18. We treat phenomenological theories for the (average) monotonic dependence of the melting point on size, and discuss the origin of its nonmonotonic variations. Finally, in Sec. IV.C we focus on some systems of particular interest.

A. Entropic effects and solid-solid transitions

Structural transitions can take place upon increasing the temperature for a given size because of entropic ef-

---

[12] See, for example, Honeycutt and Andersen (1987), Berry *et al.* (1988), Labastie and Whetten (1990), Bartell (1992), Matsuoka *et al.* (1992), Cleveland and Landman (1994), Schmidt *et al.* (1998), Jellinek (1999).

[13] Early studies are those of Lee *et al.* (1973), Briant and Burton (1975), Imry (1980), Nautchil and Petsin (1980), Natanson *et al.* (1983), Berry *et al.* (1984), Quirke and Sheng (1984), Amar and Berry (1986), Davis *et al.* (1987), Luo *et al.* (1987), Beck and Berry (1988), Reiss *et al.* (1988), Bixon and Jortner (1989).

fects. When the minimum-free-energy structure is different from the minimum-energy structure, we can define a temperature T_{ss} at which a solid-solid transformation occurs. In other words, for $T > T_{ss}$ the minimum-energy structure (which is always the most likely for $T \rightarrow 0$) ceases to be the most probable to the advantage of some other structure, which prevails because of entropic effects. Structural changes from fcc to decahedral and icosahedral structures as T increases have been predicted theoretically and seen in simulations of several systems [small Lennard-Jones (Doye and Calvo, 2001), Au (Cleveland *et al.*, 1998, 1999) and Cu clusters (Baletto *et al.*, 2004)]. Moreover, solid-solid entropy-driven structural transformations in Lennard-Jones clusters of about 200 atoms and with different structures have been observed in Monte Carlo simulations by Polak and Patrykiejew (2003). Recent experiments by Koga *et al.* (2004) support the existence of entropy-driven solid-solid transitions. Here we follow the theoretical treatment of Doye and Calvo (2001, 2002), dealing first with the classical harmonic approximation, and then introducing anharmonic and quantum corrections.

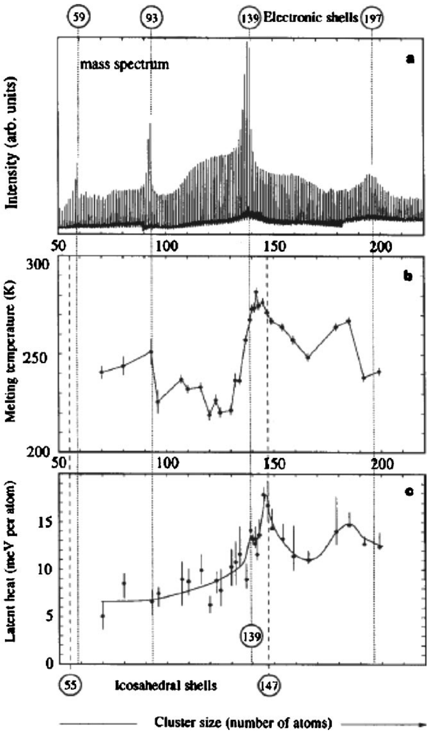

FIG. 18. Size-dependence of the measured melting temperatures and latent heat of melting for sodium clusters. These quantities are compared to the mass spectrum of the top panel, which shows electronic magic numbers. The correlations between the electronic magic sizes and the peaks in the melting temperature are rather weak, indicating that the melting behavior of small sodium clusters cannot be explained by simple models. Adapted from Schmidt *et al.*, 1998. Reprinted with permission from Nature http://www.nature.com/

1. Structural transitions in the harmonic approximation

Let $\mathcal{H}$ be the Hamiltonian of a cluster of size N:

$$\mathcal{H} = T(\{\mathbf{p}\}) + U(\{\mathbf{r}\}), \tag{19}$$

where $T(\{\mathbf{p}\}) = \Sigma_{i=1}^{N} p_i^2/2m$ is the kinetic energy and $U(\{\mathbf{r}\}) = U(\mathbf{r}_1, \ldots, \mathbf{r}_\mathbf{N})$ is the potential energy. Assume now that the cluster has a (nonlinear) structure, corresponding to a given minimum s of energy E_s^0. If the coupling of rotational and vibrational motions can be neglected, Z_s can be factored as

$$Z_s = Z_s^{tr} Z_s^{rot} Z_s^{vib}, \tag{20}$$

where Z_s^{tr} and Z_s^{rot} are related to the center-of-mass translation and to rigid rotational motions, respectively, while Z_s^{vib} is related to the vibrational motion around s. Z_s^{vib} depends on the internal coordinates $\xi_{s,i}$ where i ranges from 1 to $\kappa = 3N - 6$. For small oscillations, the vibrational motion can be treated within the harmonic approximation. In this case, it is convenient to choose the $\xi_{s,i}$ as the normal-mode coordinates, in order to write U as

$$U = E_s^0 + \frac{1}{2} \sum_{i=1}^{\kappa} \omega_{s,i}^2 \xi_{s,i}^2, \tag{21}$$

where the $\omega_{s,i}$ are the normal-mode frequencies. The transformation to normal modes allows an easy evaluation of Z_s^{vib}, which, in the classical case, is given by

$$\begin{aligned} Z_s^{vib} &\simeq \frac{e^{-\beta E_s^0}}{(2\pi\hbar)^\kappa} \prod_{i=i}^{\kappa} \int_{-\infty}^{\infty} d\xi_{s,i} d\dot{\xi}_{s,i} e^{-(\beta/2)(\omega_{s,i}^2 \xi_{s,i}^2 + \dot{\xi}_{s,i}^2)} \\ &= e^{-\beta E_s^0} \prod_{i=i}^{\kappa} \left(\frac{k_B T}{\hbar \omega_{s,i}} \right). \end{aligned} \tag{22}$$

The classical expressions for Z_s^{tr} and Z_s^{rot} are

$$Z_s^{tr} = \mathcal{V} \left(\frac{M k_B T}{2\pi\hbar^2} \right)^{3/2}, \quad Z_s^{rot} = \left(\frac{2\pi k_B T \bar{I}_s}{\hbar^2} \right)^{3/2}, \tag{23}$$

where $\mathcal{V}$ is the volume of the box in which the cluster is contained, M is the cluster mass, and $\bar{I}_s$ is the average inertial moment in s $[\bar{I}_s = (I_s^{xx} I_s^{yy} I_s^{zz})^{1/3}$, with I_s^{xx}, I_s^{yy}, and I_s^{xx} the principal moments of inertia].

To estimate the temperature dependence of the probability of finding the cluster in s, we have to compute the total partition function Z. Before doing so, we note that each minimum s has a number n_s of equivalent permutational isomers, of equivalent minima which are obtained by exchanging the coordinates of atoms of the same species. For homogeneous clusters, $n_s = 2N!/h_s$, where h_s is the order of the symmetry group of minimum s (Wales, 2003). If, at a given T, there are M_{min} minima with a non-negligible probability of being occupied, the probability p_s that the cluster is in the ensemble of the permutational isomers of minimum s can be evaluated by the superposition approximation (Doye and Wales, 1995). Within this approximation, Z is obtained by summing up the contributions from all significant minima. This gives

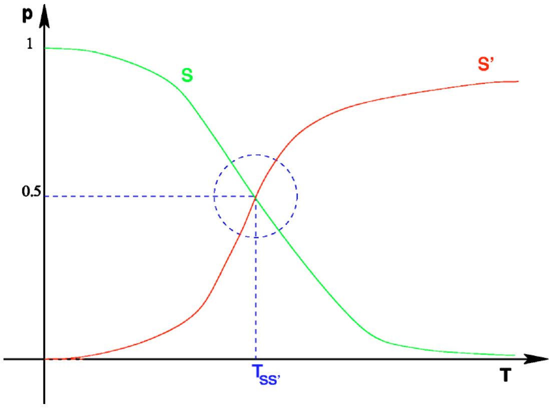

FIG. 19. (Color in online edition) Schematic representation of the probabilities p_S and $p_{S'}$ of the local energy minima S and S', with S' having higher energy than S vs temperature. In the temperature range close to the transition temperature $T_{SS'}$ the two structures coexist, being almost equally likely.

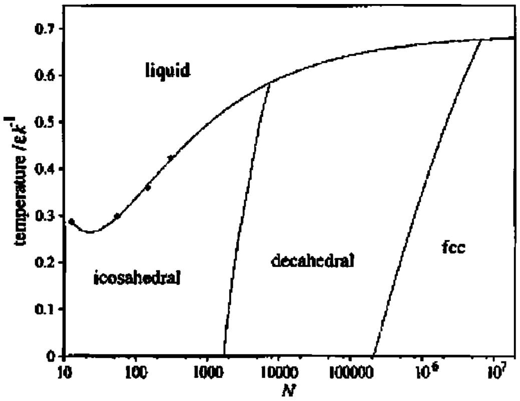

FIG. 20. Structural phase diagram in the N,T plane for Lennard-Jones clusters in the harmonic superposition approximation. From Doye and Calvo, 2002.

$$p_s = \frac{n_s Z_s}{Z} \simeq \frac{n_s Z_s}{\sum\limits_{\sigma=1}^{M_{min}} n_\sigma Z_\sigma} \simeq \frac{n_s \bar{I}_s^{3/2} e^{-\beta E_s^0} \Omega_s^{-\kappa}}{\sum\limits_{\sigma=1}^{M_{min}} n_\sigma \bar{I}_\sigma^{3/2} e^{-\beta E_\sigma^0} \Omega_\sigma^{-\kappa}}, \tag{24}$$

where $\Omega_s = (\Pi_i^\kappa \omega_{i,s})^{1/\kappa}$ is the geometric average of the vibrational frequencies of s.

Let us now consider the simplest case of a potential-energy surface having two minima, s and s' (with $E_s^0 < E_{s'}^0$), and calculate the ratio $p_s/p_{s'}$ between their occupation probabilities as a function of T. Assuming that $\bar{I}_s \simeq \bar{I}_{s'}$, one obtains

$$\frac{p_s}{p_{s'}} = \frac{Z_s n_s}{Z_{s'} n_{s'}} = e^{-\beta \Delta E^0} \left[\frac{n_s}{n_{s'}} \left(\frac{\Omega_{s'}}{\Omega_s} \right)^{\kappa} \right], \tag{25}$$

where $\Delta E^0 = E_s^0 - E_{s'}^0$. Since $\Delta E^0 > 0$ we have two cases:

(i) if $n_s/\Omega_s^\kappa > n_{s'}/\Omega_{s'}^\kappa$, s is favored over s' for all temperatures;

(ii) if $n_s/\Omega_s^\kappa < n_{s'}/\Omega_{s'}^\kappa$, for $T > T_{ss}$, s' becomes more favored than s and thus a solid-solid transition is possible; see Fig. 19.

From the above equations, we estimate T_{ss} as

$$T_{ss} = \frac{\Delta E^0}{k_B[\ln(n_{s'}/n_s) + \kappa \ln(\Omega_s/\Omega_{s'})]}. \tag{26}$$

To find a solid-solid transition, not only must case (ii) hold, but T_{ss} must be below the melting range of the cluster.

How do entropic contributions behave in typical cases? Doye and Calvo (2002) throughly analyzed Lennard-Jones clusters within the harmonic superposition approximation. They grouped together the minima pertaining to each motif (icosahedron, decahedron, and fcc), thus being able to estimate transition temperatures between structural motifs and not simply between pairs of minima. They found that the entropic contributions shift upwards through icosahedral→decahedral and decahedral→fcc crossover sizes with increasing temperature, as can be seen in the (coarse-grained) structural phase diagram of Fig. 20. This happens because icosahedral structures have on average smaller vibrational frequencies than decahedral ones, the latter having softer vibrations than fcc clusters (Doye and Calvo, 2002). Metals modeled by Sutton and Chen (1990) potentials behave in a qualitatively similar way (Doye and Calvo, 2001). A discussion of the observation of solid-solid transitions in experiments and simulations on specific systems is given in Sec. IV.C. Here we only remark that solid-solid transitions may be extremely slow in typical situations, so that observing them may require a substantial overheating of the initial structure (Koga *et al.*, 2004), to surmount the energy barriers leading to escape from the initial basin.

2. Anharmonic and quantum corrections

The harmonic superposition approximation is often accurate for cluster thermodynamics up to temperatures close to the melting range, as shown for Ag_{38} and Cu_{38} by Baletto *et al.* (2004). However, there are cases in which this approximation is not sufficient, and anharmonic effects must be included (Doye and Wales, 1995). Solid-solid transitions can be close to the melting temperature, in which case anharmonic effects are not negligible. Moreover, the harmonic approximation may strongly overestimate the probability of minima that have low-barrier escape paths. An example of failure of the harmonic approximation is found by Wang, Blastein-Barojas, *et al.* (2001) and Doye and Calvo (2003).

One can introduce anharmonic effects via T-dependent frequencies, i.e., $\tilde{\Omega}_s(T) = \Omega_s(1 - \beta_s^0/\beta)$, where β^0 is a measure of the anharmonicity. This then gives for the transition temperature, neglecting the permutational contribution,

$$\beta_{ss}^{anHA} = \frac{\kappa}{\Delta E^0} \left[\ln(\Omega_s/\Omega_{s'}) + \ln\left(\frac{\beta - \beta_s^0}{\beta - \beta_{s'}^0} \right) \right], \tag{27}$$

where the second term represents the first order approximation to the anharmonic correction to β_{ss}^{anHA}

$=1/k_B T_{ss}^{anHA}$. To apply the previous equation it is necessary to estimate β_0 but the available methods do not allow one to treat large sizes.

Quantum corrections can be inserted both in Z_s^{rot} and Z_s^{vib}. Since quantum corrections to Z_s^{rot} should become important only at very low temperatures, we now consider only the corrections to Z_s^{vib}. These corrections are very easily introduced within the harmonic approximation. The quantum partition function of a set of oscillators is given by

$$Z_s^{vib} = e^{-\beta E_s^0} \prod_{i=1}^{\kappa} [2\sinh(\beta\hbar\omega_{i,s}/2)]^{-1}. \tag{28}$$

The classical limit is valid when it is possible to approximate the $\sinh(\beta\hbar\omega_{i,s}/2)$ with its argument; thus it is valid for high temperatures. The introduction of quantum oscillators modifies the expression of the ratio between the occupation probabilities of two minima s and s' in the following way:

$$\frac{p_s}{p_{s'}} = e^{-\beta\Delta E^0} \left[\frac{n_s}{n_{s'}} \frac{\prod_i^{\kappa} \sinh(\beta\hbar\omega_{i,s'}/2)}{\prod_i^{\kappa} \sinh(\beta\hbar\omega_{i,s}/2)} \right]. \tag{29}$$

In particular, we note that here the temperature dependence is also in the vibrational contribution and not only in the Boltzmann factor. To understand when quantum corrections are needed we may refer to the Debye temperature Θ_D. If the temperature of the system is above $0.70\Theta_D$ the system can be treated as classical to a good approximation, while at lower temperature we also need to take quantum effects into account (Ashcroft and Mermin, 1976). Calvo *et al.* (2003) satisfactorily explained the finite-temperature spectroscopic properties of $\mathrm{CaAr_N}$ clusters including quantum and anharmonic corrections in their calculations.

B. Melting of nanoclusters

The concepts of solid and liquid states, which are commonly employed when discussing extended systems, can be applied to clusters. In fact, at low temperature, the particles of a cluster spend most of the time making small-amplitude vibrations around the global minimum, in analogy to what happens in bulk solids. If the temperature is increased, other minima begin to be populated, and this is associated with the onset of some diffusive motion. Finally, if the temperature becomes high enough, the cluster explores the basins of a huge number of minima, with fast rearrangements, thus behaving like a liquid droplet. Within this description, cluster melting is seen as an isomerization transition, with the number of probable isomers increasing drastically after some threshold temperature. A nice example of this behavior for $\mathrm{Ag_6}$ clusters is given by Garzón, Kaplan, *et al.* (1998). However, there are several differences between the solid-liquid transition of clusters and that of its bulk counterpart:

(i) The melting point is reduced (with a few known exceptions) with a complex dependence on size.

(ii) The latent heat is smaller; this can be understood, for example, by noting that disordering the surface costs less than disordering inner atoms.

(iii) The transition does not take place sharply at one definite temperature, but smoothly over a finite temperature range. There, solid and liquid phases may coexist dynamically in time (Berry *et al.*, 1988; Lynden-Bell and Wales, 1994). When one observes the cluster over a long time interval, there will be subintervals in which the cluster appears to be solid and others in which the cluster is fully liquid.

(iv) The heat capacity can become negative in microcanonical environments (Schmidt *et al.*, 2001). This means that the microcanonical average kinetic energy may be a nonmonotonically increasing function of the total energy in the range of the transition (Bixon and Jortner, 1989).

(v) The melting transition depends on cluster structure and chemical ordering (this being, indeed, a nonequilibrium effect).

Often the melting transition is preceded by *premelting phenomena*. To quote Calvo and Spiegelman (2000), "premelting phenomena are characteristic of isomerizations taking place in a limited part of the configuration space," for example, isomerizations involving surface atoms only (in this case the term *surface melting* is used). Premelting phenomena are often singled out by additional peaks in the specific heat vs temperature.

1. Experimental methods

Following Haberland (2002), experiments studying cluster melting can be divided into two classes:

(i) study of the change of some physical property across the melting point (for example, changes in photon or x-ray diffraction patterns)

(ii) measurement of the caloric curve $E=E(T)$, that is, the cluster's internal energy E as a function of T.

Takagi (1954) made the first observation of the melting point depression by transmission electron microscopy. This is a standard technique for studying the size-dependent melting point of small particles by monitoring the changes in the diffraction pattern associated with the disordering of the structure. Electron and x-ray diffraction and nanocalorimetry techniques have been used to study melting in deposited clusters (Lai *et al.*, 1996; Peters *et al.*, 1998; Efremov *et al.*, 2000). At present these methods are, however, not applicable to free, mass-selected clusters in vacuum for two reasons: first, no method of temperature measurement is known in this case, and the density of mass-selected clusters is so small that it is extremely difficult to collect a diffraction signal. In any case, as the size decreases, the diffraction techniques become increasingly inaccurate due to line broadening. Several experiments have tried to measure the melting behavior of free cluster, mainly by methods belonging to class (i). Even *et al.* (1989) and Buck and Ettischer (1994) looked for some spectroscopic evidence. Electron diffraction from a (not mass-selected) supersonic expansion gives Debye-Scherrer like diffraction rings, whose intensity is a measure of cluster temperature. This method was pioneered by Farges *et al.* (1981) and later intensively studied by Hovick and Bartell (1997). Martin *et al.* (1994) were the first to publish a size dependence of the melting temperature of free clusters. They showed that the structure on mass spectra of large sodium clusters can depend sensitively on the temperature. The disappearance of structure was interpreted as being due to melting. Another method has been proposed by Shvartsburg and Jarrold (2000) to measure the melting temperature T_m for small tin clusters, with the surprising result that they melt higher than bulk tin. Here, cluster ions are injected into a helium-gas atmosphere, and are pulled by an electric field through the gas. The collisions with the gas produce an effective friction force. Clusters having a small collision cross section experience a smaller friction force and arrive first. A new approach to the study of the melting processes in gallium nanoparticles embedded in a matrix has been recently developed by Parravicini *et al.* (2003a, 2003b). This method is based on capacitance measurements through the derivative of the dielectric constant with respect to T.

Calorimetry experiments have been performed on deposited clusters (for example, Lai *et al.*, 1996, considered tin clusters on a SiN substrate) and free clusters. Free-cluster calorimetry has been applied by Haberland's group (Schmidt *et al.*, 1997, 1998, 2001; Kusche *et al.*, 1999) to Na clusters and by Bachels *et al.* (2000) to Sn clusters. Haberland's method consists of two steps, the preparation of size-selected clusters of known temperature and the determination of their energy. A beam of cluster ions is produced and thermalized in a heat bath at temperature T_1; a mass spectrometer is used to select a single cluster size. Then the clusters are irradiated by a laser beam and absorb several photons. The basic idea of the experiment is that absorbtion of photons of energy $\delta U = h\nu$ will raise the temperature beyond T_1. The photon energy quickly relaxes into vibrations and heats the cluster to a temperature T_2 at which the clusters do not emit atoms on the time scale of the experiment (several microseconds). Only the adsorption of more photons from the laser pulse raises the temperature above T_{evap}, the temperature needed for evaporation of atoms from the cluster. The size distribution of the remaining cluster ions is measured, and this is a very sensitive measure of the cluster internal energy. The increased temperature of the cluster, T_2, is then identified by increasing the cluster source temperature until the thermally heated clusters show the same photofragmentation behavior as the laser-heated ones. A second mass spectrometer measures the distribution of the fragment ions produced. Different numbers of absorbed photons lead to clearly separated groups of fragments in the mass spectrum, with the distance between two groups corresponding to exactly the energy of one photon. This allows one to calibrate the mass scale in terms of energy. If the temperature of the heat bath is varied, the internal energy of the selected clusters changes and thus also the number of evaporated atoms (see Fig. 21).

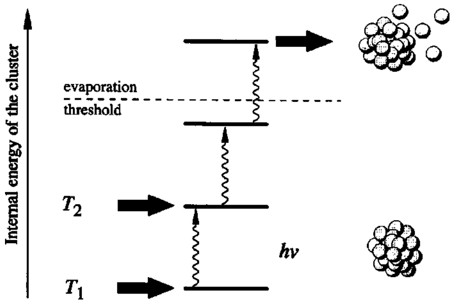

FIG. 21. Schematic representation of the experimental method for measuring $E(T)$ for free clusters. Adapted from Schmidt *et al.*, 1998. Reprinted with permission from Nature http://www.nature.com/

In the method of Bachels *et al.* (2000) Sn clusters are produced by a laser ablation source using a pulsed nozzle whose temperature is variable. Cluster temperatures should deviate from nozzle temperatures only by 10–20 K. Neutral clusters are studied, so that there is no mass selection; the width of the distribution of the cluster sizes can be of the order of 60% of the average size. Energy is measured by a sensitive pyroelectric foil in which the clusters impinge, causing a temperature increase which leads to a measurable voltage jump.

2. Computational methods

Here we first discuss the quantities that may be used to single out the melting transition, and then we briefly review the most common computational methods.

The most common method for studying the melting transition is the calculation of the caloric curve, that is, the total cluster energy E as a function of T, in a simulation where the cluster is heated up from a low-T solid configuration. $E(T)$ may show a smooth jump in the melting region (see Fig. 22), corresponding to a peak in the heat capacity $c(T) = \partial E / \partial T$, as in Fig. 23. However, the caloric curve is not always an efficient indicator, because the jump may be small and difficult to find, or even absent. When properly calculated, peaks in the heat capacity can indicate the melting temperature T_m. However, when multiple peaks are present, the assignment of the melting point may become difficult. One may identify T_m with the temperature of the highest peak, but sometimes this criterion fails (see the discussion in Frantz, 2001).

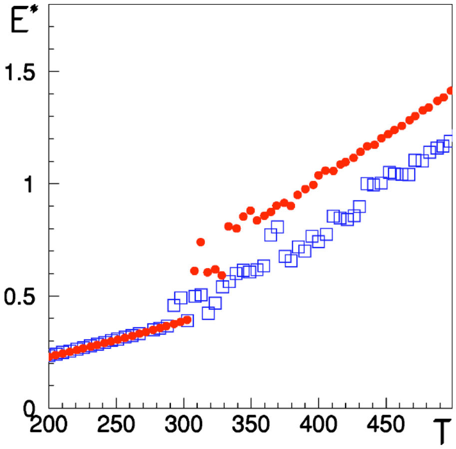

FIG. 22. (Color in online edition) Caloric curves from a molecular-dynamics melting simulation: ●, Ag_{38}; ■, Cu_{38}. The heating rate is of 0.1 K/ns. The clusters are modeled by the Rosato *et al.* (1989) potential. E^* is the average total energy E of the cluster after the subtraction of the global-minimum energy and of the kinetic and harmonic contributions: $E^* = E - E_{GM} - 3(N-1)k_B T$. The jump in the caloric curve is clear for Ag_{38}, and less evident for Cu_{38}. Figure courtesy of Christine Mottet.

In general, criteria for distinguishing solidlike and liquidlike phases and sensitive indicators of the melting transition are needed.

Solidlike and liquidlike phases can be distinguished if an order parameter Q can be found such that the Landau free energy $F_l(Q)$ is bistable for a range of temperatures. Then two distinct phases can be identified and can be said to coexist (Wales, 2003, and references therein). The Landau free energy is defined as $F_l(Q) = k_B T \ln P(Q) + \text{const}$, where $P(Q)$ is the probability of observing a value Q of the order parameter for the transition in the simulation run. Thus, in an equivalent way, one can find that the probability distribution of the order parameter has two minima in the canonical ensemble. As $N \to \infty$, the free-energy barrier between these minima is expected to increase and the phase transition tends to the first-order bulk phase transition.

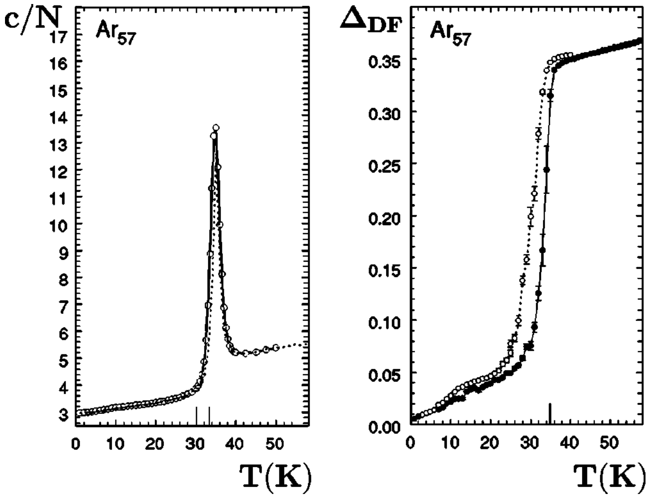

FIG. 23. Heat capacity and bond-length fluctuations in the 57-atom Lennard-Jones cluster. Left panel, heat capacity curves. Open circles and solid line represent the results of parallel tempering simulations, while the dotted line and the thin solid line are the results of Metropolis Monte Carlo runs of different length. Right panel, Δ_{DF} calculated in two Monte Carlo simulations of different length (the longer one corresponds to the open circles). The temperature at which Δ_{DF} starts its strong increase corresponds well to the temperature of the heat capacity peak. The heat-capacity c and Δ_{DF} are given in reduced units (see Frantz, 2001). Adapted from Frantz, 2001.

The practical problem is now to find an adequate set of order parameters. A possible order parameter is the total potential energy E_p or just the difference between the configurational energy and the global-minimum energy (Lynden-Bell and Wales, 1994; Shah *et al.*, 2003). Other parameters are related to the local ordering, such as the orientational bond order parameters Q_L (Steinhardt *et al.*, 1983), or the signatures[14] of the common-neighbor analysis (Faken and Jónsson, 1994). The radial distribution function is also routinely monitored. This is useful also to single out surface disordering phenomena (Qi *et al.*, 2001; Huang and Balbuena, 2002).

Solidlike and liquidlike phases may also be distinguished by their different mobility. In bulk systems, the Lindemann criterion is commonly used. The atomic vibrational amplitude $\langle \Delta r^2 \rangle^{1/2}$ is defined as a disorder parameter Δ_L; experiments and simulations show that its critical value is around 0.10–0.15 in units of the atomic spacing (Bilgram, 1987; Lowen, 1994). For irregular finite systems, however, the pure Lindemann criterion is not appropriate; a better idea is to introduce the distance-fluctuation measure Δ_{DF}, as proposed by Etters and Kaelberer (1977) and Berry *et al.* (1988):

---

[14] In the common-neighbor analysis a signature is assigned to each pair of neighbors. This signature is a triplet of integers (r,s,t), where r is the number of common nearest neighbors of two atoms of the pair, s is the number of nearest-neighbor bonds among the r common neighbors, and t is the length of the longest chain that can be formed with the s bonds. We have found that the monitoring of the signatures $(r,s,t) = (5,5,5)$, (4,2,1), (4,2,2) is sufficient to distinguish icosohedral, decahedral, and fcc structures over a wide range of sizes (Baletto, Mottet, and Ferrando, 2001a; Baletto, 2003) during growth simulations. The (5,5,5) signature indicates pairs located along a (locally) fivefold symmetry axis. The (4,2,1) signature is associated with pairs with fcc neighborhood. The (4,2,2) signature is associated with pairs comprising an atom of a (locally) fivefold axis and an atom outside the axis. In perfect fcc clusters one expects to find a large percentage of (4,2,1) signatures and no (5,5,5) and (4,2,2) signatures. Comparing icosahedral and decahedral clusters in the same size range, one finds that the percentage of (5,5,5) signatures is much larger in icosahedra, while the percentage of (4,2,1) signatures is larger in decahedra. Tables with the values of the percentages for these signatures are found in the dissertation of Baletto (2003; see also Baletto, Mottet, and Ferrando, 2001a).

$$\Delta_{DF} = \frac{2}{N(N-1)} \sum_{i<j} \frac{\sqrt{\langle \Delta r_{ij}^2 \rangle}}{\langle r_{ij} \rangle}, \tag{30}$$

where r_{ij} is the distance between atoms i and j, $\langle \Delta r_{ij}^2 \rangle = \langle (r_{ij} - \langle r_{ij} \rangle)^2 \rangle$. The key difference between the Lindemann and distance-fluctuation criteria is that the latter is based on the fluctuation of the distance between pairs of atoms while the former is based on the fluctuation of individual atoms relative to their average position. The critical value of Δ_{DF} for a solid-liquid transition has been suggested to be around 0.03–0.05 (Zhou *et al.*, 2002). Some caveats are necessary when using Δ_{DF}. As pointed out by Frantz (1995, 2001), Δ_{DF} depends on the length of the simulation run. For very long simulations, a value $\Delta_{DF} \sim 0.1$ can be obtained even at low temperatures, at which the cluster is simply making isomerizations among permutational isomers in its solid form. However, computing Δ_{DF} can be a very sensitive method for monitoring qualitatively the melting transition from below (Frantz, 2001).

In order to have quantitative information on the mobility of the cluster particles, while avoiding the shortcomings of Δ_{DF}, one can consider quantities that do not depend on the simulation length. Rytkönen, Valkealahti, and Manninen (1998) monitored the average rate of change in the nearest neighbors of the cluster atoms. Another possibility is to compute the number of distinct basins visited per unit time.

The melting of nanoclusters has largely been studied by standard simulation methods such as molecular dynamics and Monte Carlo (see, for example, Frenkel and Smit, 1996). Unlike the Monte Carlo method, which is based on a fictitious dynamics, molecular dynamics closely mimics the true dynamics of the system. This allows the calculation of equilibrium time-dependent correlation functions, like those related to the diffusion of the cluster particles. Molecular dynamics also permits the realistic simulation of melting and freezing processes, which take place on finite time scales and thus may include kinetic effects. On the other hand, Monte Carlo can be faster in sampling the configuration space, being thus more appropriate if one is interested in static quantities only.

In fact, a major problem when calculating thermodynamic properties by simulation is quasiergodicity, that is, the incomplete sampling of the configurational space that may occur in the phase-change region. Quasiergodicity can lead to overestimated transition temperatures in molecular-dynamics caloric curves (Calvo and Guet, 2000) if the heating rate is too fast.

Various methods have been employed to reduce the systematic errors resulting from quasiergodicity, including the histogram, jump-walking, smart-walking, and parallel tempering methods.[15] Many of these methods are based on the coupling of configurations obtained from ergodic higher-T simulations to the quasiergodic lower-T simulations. Monte Carlo J-walking methods, for example, couple the usual small-scale Metropolis moves made by a lower-T random walker with occasional large-scale jumps that move the random walker out of confined regions of configurational space. These large-scale jumps are to configurations that are obtained in higher-T simulations. Calvo *et al.* (2000) and Neirotti *et al.* (2000) showed that parallel tempering is remarkably successful in overcoming quasiergodicity and in calculating accurate heat-capacity curves. In parallel tempering, several simulations are run in parallel at different temperatures. Periodically, exchange moves are attempted between configurations at nearby temperatures, and accepted or rejected according to the Metropolis rule.

3. Size dependence of the melting point

The size dependence of the cluster melting point for a given material usually shows a monotonic decrease with decreasing size, and has irregular variations on a fine scale. Here we first deal with the justification for the monotonic trend and then treat the fine-scale nonmonotonic variations.

The average dependence of a melting point with size N has been derived by means of a few phenomenological models. The classical calculation by Pawlow (1909) has been further extended and modified by several groups. A recent account of some of these developments is given by Chushak and Bartell (2001b). Here we derive Pawlow's formula following the approach of Buffat and Borel (1976). We consider a cluster of size N and of spherical shape. At a given pressure p, its melting temperature is $T_m(N)$, which has to be compared with the bulk melting temperature $T_m(\infty)$. In analogy with bulk melting, one identifies the solid-liquid transition by equating the chemical potentials μ_s and μ_l of the solid and of the liquid, so that $T_m(N)$ at a given pressure p follows from the solution of this equation:

$$\mu_s(p,T) = \mu_l(p,T). \tag{31}$$

This equation means that the chemical potential of a fully liquid and of a fully solid cluster are equal at melting. The chemical potential can be expanded around its value at the triple point; we retain first-order terms only:

$$\mu(p,T) = \mu(p_0,T_0) + \frac{\partial \mu}{\partial T}(T - T_0) + \frac{\partial \mu}{\partial p}(p - p_0). \tag{32}$$

From the Gibbs-Duhem equation $(-Vdp + SdT + Nd\mu = 0)$ it follows that

$$\frac{\partial \mu}{\partial T} = -s, \quad \frac{\partial \mu}{\partial p} = \frac{1}{\rho}, \tag{33}$$

where $s = S/N$ is the entropy per particle and $\rho = V/N$ is the number density. From Eqs. (31)–(33), and taking into account that $\mu_s(p_0,T_0) = \mu_l(p_0,T_0)$, one obtains

---

[15] See, for example, Frantz *et al.* (1990), Labastie and Whetten (1990), Calvo *et al.* (2000), Ghayal and Curotto (2000), Neirotti *et al.* (2000), Frantz (2001), Fthenakis *et al.* (2003).

$$-s_l(T-T_0)+\frac{1}{\rho_l}(p_l-p_0)=-s_s(T-T_0)+\frac{1}{\rho_s}(p_s-p_0). \tag{34}$$

Here, one must distinguish between the pressure p_s of a solid cluster and the pressure p_l of a liquid cluster. In fact, the pressure inside a small object of radius r is larger than the external pressure because of the Laplace contribution $p_{Lap}=2\gamma/r$ to the pressure, where γ is the interface tension of the cluster and r is its radius. Since a liquid and a solid cluster of N atoms can differ both in interface tension (γ_{lv} for the liquid-vapor interface, γ_{sv} for the solid-vapor interface) and in radius, they can have different Laplace pressure terms,

$$p_l=p_{ext}+\frac{2\gamma_{lv}}{r_l}, \quad p_s=p_{ext}+\frac{2\gamma_{sv}}{r_s}. \tag{35}$$

For a cluster of $r\sim 10$ nm, typical interface tensions are of the order of 10^3 erg/cm^2, so that the Laplace pressure is much larger than p_{ext} under the usual conditions. Thus p_{ext} can be neglected in Eq. (35). Moreover, for spherical clusters,

$$\frac{r_s}{r_l}=\left(\frac{\rho_l}{\rho_s}\right)^{1/3}. \tag{36}$$

Substituting Eqs. (35) and (36) into Eq. (34), neglecting p_{ext}, and taking into account that $L=T_0(s_l-s_s)$ is the latent heat of melting per particle, one obtains

$$1-\frac{T_m(N)}{T_m(\infty)}=\frac{2}{\rho_s r_s L}\left[\gamma_{sv}-\gamma_{lv}\left(\frac{\rho_s}{\rho_l}\right)^{2/3}\right]. \tag{37}$$

Since $r_l\propto N^{1/3}$, one finds that Eq. (37) can be rearranged to the form (Reiss *et al.*, 1988)

$$T_m(N)=T_m(\infty)\left[1-\frac{\mathcal{C}}{N^{1/3}}\right], \tag{38}$$

where $\mathcal{C}$ is a constant. This formula gives a very simple dependence for $T_m(N)$ which can thus be considerably lower than $T_m(\infty)$ (Buffat and Borel, 1976; Lewis *et al.*, 1997; Rytkönen, Valkealahti, and Manninen, 1998). An expression for $\mathcal{C}$ easily follows from Eq. (37), but the quantities involved in that expression may not be easy to evaluate. Moreover, several rather crude approximations are involved in Eq. (37), so that usually $\mathcal{C}$ is considered as a fitting parameter.

Several attempts have been made to improve Pawlow's theory. Buffat and Borel (1976) included higher-order terms in Eq. (32), and solved numerically the resulting equation. Including higher-order terms is in principle more accurate, but these terms increase the number of unknown parameters to be evaluated. Reiss and Wilson (1948), Hanszen (1960), and finally Sambles (1971) refined Pawlow's model by including the possibility of surface melting, that is, of having clusters (of total radius r) made of an inner core of radius $r-\delta$ and an external liquid shell of thickness δ. The melting temperature is found by imposing the equilibrium condition on this solid-core/liquid-shell particle. A derivation for the case of metallic particles was given by Kofman *et al.* (1994) and Vanfleet and Mochel (1995); here we briefly sketch their approach. The extension of this approach to molecular clusters (by including van der Waals forces) can be found in Levi and Mazzarello (2001).

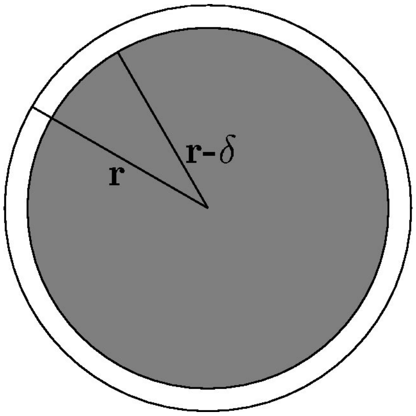

FIG. 24. A particle with a solid core of radius $r-\delta$ and a liquid shell of thickness δ.

Let us consider a particle like that in Fig. 24, containing N_l particles in the liquid shell. Its free energy G is given by

$$G=(N-N_l)\mu_s+N_l\mu_l+4\pi r^2\left[\gamma_{sl}\left(\frac{r-\delta}{r}\right)^2+\gamma_{lv}+S'e^{-\delta/\zeta}\right], \tag{39}$$

where

$$S'=\gamma_{sv}-\left[\gamma_{lv}+\gamma_{sl}\left(\frac{r-\delta}{r}\right)^2\right]. \tag{40}$$

Here ζ is the characteristic length of the interaction among atoms in liquid metals, and the term $S'e^{\delta/\zeta}$ takes into account the effective interaction between the solid-liquid and liquid-vapor interfaces. This effective interaction is repulsive and favors the formation of a liquid shell between the solid core and the vapor. For T not too far from $T_m(\infty)$ one may approximate $N_l(\mu_l-\mu_s)\simeq V_l\rho L[T_m(\infty)-T]/T_m(\infty)$, where $V_l=4\pi[r^3-(r-\delta)^3]/3$ is the volume of the liquid layer, and the density difference between liquid and solid is neglected ($\rho_l=\rho_s=\rho$). Minimizing G with respect to δ, one finds the following solution for $T_m(N)$:

$$1-\frac{T_m(N)}{T_m(\infty)}=\frac{2\gamma_{sl}}{\rho L(r-\delta)}(1-e^{-\delta/\zeta})+\frac{S'r^2}{\rho L\zeta(r-\delta)^2}e^{-\delta/\zeta}. \tag{41}$$

Pawlow's result of Eq. (37) is recovered in the limit $\zeta\to 0$, which means a sharp interface, or equivalently, no effective repulsive interaction between the solid-liquid and the liquid-vapor interfaces. For molecular clusters, this effective interaction is proportional to $1/\delta^2$ instead of $e^{-\delta/\zeta}$ (Levi and Mazzarello, 2001).

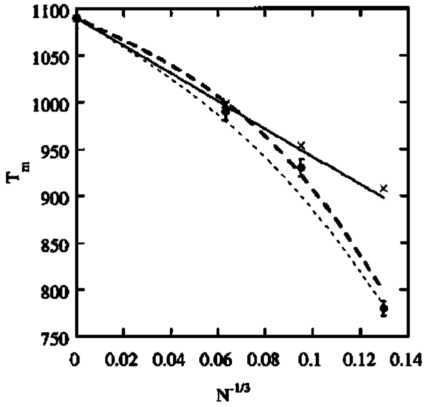

FIG. 25. Melting point of gold clusters from molecular-dynamics simulations (black dots), and comparison with different theoretical results: solid line, Pawlow's theory; ×, second-order corrections from Buffat and Borel (1976); heavy dashed curves, the liquid-shell model by Sambles (1971), Eq. (42); thin dashed curves, second-order corrections to Sambles's formula. Reprinted with permission from Chushak and Bartell (2001b). Copyright 2001 American Chemical Society.

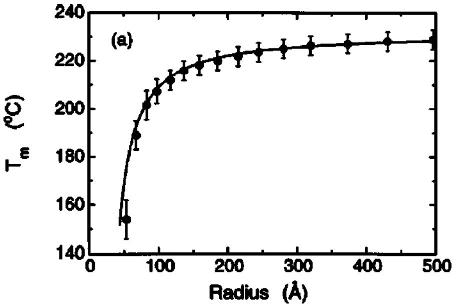

FIG. 26. Comparison of theoretical and experimental melting points of supported tin clusters: ●, experiment; solid line, the fitting by means of Eq. (42). From Lai *et al.*, 1996.

Following a somewhat different line of reasoning, Chushak and Bartell (2001b) derived a similar expression, which is close to those found by Hanszen (1960) and Sambles (1971):

$$1-\frac{T_m(N)}{T_m(\infty)}=\frac{2}{\rho_l L}\left\{\frac{\gamma_{sl}}{r-\delta}+\frac{\gamma_{lv}}{r}\left[1-\left(\frac{\rho_s}{\rho_l}\right)^{2/3}\right]\right\}. \qquad (42)$$

If γ_{sl} is evaluated as $\gamma_{sv}-\gamma_{lv}$ (that is, if the liquid shell perfectly wets the solid core), and $\delta=0$, Eq. (42) reduces to Eq. (37).

Both Eqs. (41) and (42) are more accurate than Pawlow's result down to small sizes (see Fig. 25). Peters *et al.* (1998) found that the solid-core/liquid-shell model gives a better fit of the experimental melting temperatures of supported lead clusters. Chushak and Bartell (2001b) and Wang, Zhang, *et al.* (2003) melted a series of selected fcc clusters of gold and copper, respectively, by molecular-dynamics simulations within an embedded-atom energetic model. They found that Eq. (38) is accurate down to $N\sim10^3$ and 5×10^2 for Au and Cu, respectively. At smaller sizes, Eq. (42) is in better agreement with the simulation data in the case of Au. Other simulation results are given by Ercolessi *et al.* (1991), Lewis *et al.* (1997), and Qi *et al.* (2001). Lai *et al.* (1996) obtained an excellent fit to their experimental data on the melting of tin clusters (see Fig. 26) by the formula of Hanszen (1960); the same data were successfully refitted by means of Eq. (41) (Bachels *et al.*, 2000).

When the size dependence of the melting point is examined on a fine scale, irregular variations are found, especially at small sizes, where the addition or the removal of a single atom can have dramatic effects. There is a good agreement among several simulation results in predicting that clusters of special stability, such as icosahedral clusters at magic sizes (55, 147, etc.), melt at higher temperatures than predicted by Eq. (38) [see, for example, the cases of Lennard-Jones, Na, and noble-metal clusters (Rytkönen, Valkealahti, and Manninen, 1988; Valkealahti and Manninen, 1993; Frantz, 2001)]. However, the situation can be more complicated.

Schmidt *et al.* (1998) measured the melting point of Na clusters up to 200 atoms. They found an irregular behavior of T_m, with few well-defined peaks, as shown in Fig. 18, and L showed the same kind of behavior. The peaks in $T_m(N)$ and L were not well correlated with those in the mass spectrum, corresponding to the closing of electronic shells. These results showed that the most abundant clusters and the highest-melting-point clusters do not always coincide. In a recent experiment, Schmidt *et al.* (2003) were able to measure the energy and the entropy change in the melting of Na clusters. They found that the peaks in $T_m(N)$ are driven by the energy difference between the liquid and the solid phases. The entropy difference is closely correlated to the energy difference and simply causes a damping of the energetic effects. This would show that the main indicator for a high T_m is the energetic separation of the global minimum from higher isomers. However, it is not yet clear whether entropic differences are always correlated to energetic differences, or whether this is a trait of Na clusters.

The irregular variations of the melting point in Lennard-Jones clusters were studied by Frantz (2001), who thoroughly analyzed the range $26\leqslant N\leqslant 60$ by the parallel tempering technique. Frantz (2001) found that the peaks in $T_m(N)$ were generally well correlated with those of other stability indicators, such as the energetic separation of the second isomer from the global minimum $E_{SM}(N)-E_{GM}(N)$, $\Delta_1(N)$, and $\Delta_2(N)$ [see Eq. (6)]. An exception was $N=58$, a magic size for the stability indicators, but not corresponding to a peak of $T_m(N)$.

Finally, even though the melting point in nanoclusters is usually depressed, some evidence of exceptions to this rule is beginning to accumulate. The first experimental evidence of an exception is due to Shvartsburg and Jarrold (2000), who studied the melting of Sn clusters. Small Sn clusters have a rather elongated structure, which should change to nearly spherical upon melting. No signature of this change was observed by Shvartsburg and Jarrold (2000), so they concluded that Sn cluster ions containing 10–30 atoms have a melting point at least 50 K above the bulk one. This behavior has been confirmed by Joshi *et al.* (2002), who performed *ab initio* molecular-dynamics simulations of the melting of Sn_{10}. They found that binding in such a small cluster is indeed covalent, and that the specific heat of Sn_{10} shows a shoulder around 500 K due to a permutational rearrangement of atoms that preserves the trigonal prism core of the ground state. Only at much higher temperatures, $T \simeq 1500$ K, does this core distort and break up, yielding a peak in the specific heat around 2300 K. Joshi *et al.* (2003) also simulated the melting of Sn_{20}, finding that it has a lower melting point than Sn_{10}, but one that is still much higher than that of bulk Sn. Chuang *et al.* (2004) have found by *ab initio* Langevin molecular dynamics that Sn_6, Sn_7, and Sn_{13} also melt at a higher T than bulk Sn.

Small Sn clusters seem not to be the only ones to melt at higher temperature than the bulk crystal. There is recent experimental and theoretical evidence for gallium clusters (Breaux *et al.*, 2003; Chacko *et al.*, 2004), whose high melting point is attributed to the fact that, in contrast to bulk Ga, binding in small clusters is fully covalent. Finally, in their simulations, Akola and Manninen (2001) observed a bulklike behavior of Al_{13}^{-} above the Al bulk melting temperature.

As a final remark, we note that thermodynamic effects on structural stability and the melting of nanoclusters suggest a more general definition of the stability, including temperature effects (Baletto, Rapallo, *et al.*, 2004).

C. Studies of selected systems

1. Lennard-Jones clusters

There are several computational studies of melting in Lennard-Jones clusters, especially at magic icosahedral sizes. Early molecular-dynamics studies on the melting of Ar clusters by Briant and Burton (1975) indicated a relatively sharp first-order-like transition at T below the bulk melting temperature. This result was later confirmed. At $N=55$ and $N=147$ all simulations indicate relatively sharp jumps in the caloric curves at $T \simeq 35$ K and $T \simeq 42$ K, and the radial distributions confirm that whole clusters melted during the transitions (Etters and Kaelberer, 1975; Honeycutt and Andersen, 1987; Matsuoka *et al.*, 1992). At $N=13$ the cluster fluctuates back and forth between the two phases and a consistent determination of T_m is very difficult. The breadth of the solid-liquid transition is also revealed for Ar_{13} adsorbed on a surface (Blaisten-Barojas *et al.*, 1987), where the cluster changes from an icosahedral, solidlike structure at low T to a set of liquidlike structures at high T. Clusters containing 309 or more atoms are observed to desorb atoms at temperatures where the core is still solid (Rytkönen *et al.*, 1997). Thus it is very complicated to define their melting point, if the heating rate is slow. Fast heating rates can, however, cause the superheating of the cluster. Rytkönen, Valkealahti, and Manninen (1998) found a rather good agreement with Eq. (38), except that T_m at small sizes and for icosahedral structures is higher than predicted analytically. To investigate how the melting takes place, Rytkönen *et al.* calculated the radial distribution function, finding that, at nonmagic icosahedral sizes, there is a clear tendency to surface melting while the cores preserve an icosahedral morphology.

Frantz (1995, 2001) made a detailed systematic study of small Lennard-Jones clusters by Monte Carlo simulations. He found that the smallest clusters presented an irregular dependence of their thermodynamic properties on size. For $N > 25$ some trends were pronounced. Icosahedral packing was dominant (with the exception of the truncated octahedron at $N=38$) and the heat capacity peak parameters formed two overlapping sequences as a function of N, depending on whether the overlayer had Mackay or anti-Mackay stacking. In clusters with an anti-Mackay overlayer, the heat-capacity peak shifted towards higher T and became smaller at increasing N, while clusters with Mackay rearrangements had small, low-T peaks that generally shifted to higher T and grew in size as N increased. There was a sequence of magic numbers, $N=36,39,43,46,49,55$, at which the heat-capacity peak was stronger. As already discussed in Sec. IV.B.3, this sequence correlates well with that extracted from the binding energy differences.

2. Sodium clusters

Experiments by Martin *et al.* (1994) and Schmidt *et al.* (1998) have revealed a complex dependence of $T_m(N)$ for Na clusters. Its irregular small-size behavior has already been discussed in Secs. IV.B.3. Liu *et al.* (2002) performed a systematic simulation study of the melting of different morphologies over a wide size range. They found that the melting points for all sizes and structural types were in a narrow T range (200–300 K) and all clusters presented a liquid-gas transition around 1000 K.

Another interesting point about the melting of Na clusters, which is of great general interest, is the presence of premelting effects. A detailed study of this topic at $8 \leqslant N \leqslant 147$ atoms has been performed by Calvo and Spiegelman (2000) by a Monte Carlo thermodynamical analysis close to the solid-liquid transition, within a semiempirical modeling by Gupta (1981) potentials. Up to 147 atoms, the thermodynamics appears to be directly related to the lowest-energy structures, and melting by steps is favored by the presence of surface defects. For $N < 75$ the T_m presents a strong nonmonotonic behavior with N, which is typical of geometric size effects. For larger sizes the transition becomes more and more similar to the bulk case. Calvo and Spiegelman (2000) find evidence of premelting phenomena at small sizes, with the caloric curves presenting multimodal behavior with increasing T. Simple isomerization between a few structures, surface melting, or competition between several funnels on the energy landscape may be the causes of this premelting. Premelting seems to be the rule for small Na clusters, the only exceptions being the very stable magic icosahedral structures. The secondary peaks in the heat capacity become less pronounced at $N > 100$, indicating that premelting becomes less important. Calculations by Gupta potentials and *ab initio* schemes (Rytkönen, Häkkinen, and Manninen 1998, 1999; Reyes-Nava *et al.*, 2002) agree reasonably well with the experiments, but several aspects of the melting behavior of Na clusters are still to be understood. Calvo and Spiegelman (2004) have recently reexamined the melting behavior of Gupta Na clusters in the size range around 130 atoms, finding that the potential is somewhat inadequate because it predicts strong premelting effects that are not observed in the experiments. These premelting effects are related to the surface melting of the outer icosahedral shell.

3. Noble-metal and transition-metal clusters

In the case of metallic clusters, the literature is extensive, especially for Au clusters.[16] To begin, we remark that, although the melting point is depressed, its reduction is smaller than that of Lennard-Jones clusters, and it is strongly material dependent (Jellinek *et al.*, 1986; Garzón and Jellinek, 1991; Jellinek and Garzón, 1991). Usually melting is accompanied by a peak in the specific heat, and by a substantial rearrangement of the cluster. But there are exceptions. For example, the simulations by Westergren *et al.* (2003) revealed that Pd_{34} melts without an accompanying peak in the heat capacity, and the atoms become mobile without any significant change in geometric structure. García-Rodeja *et al.* (1994) and Lee *et al.* (2001) studied several transition and noble metals, at very small sizes, around 13 atoms, modeled by Gupta potentials. Their simulation results were in agreement with those obtained by Güvenc and Jellinek (1992). The salient result is that the behavior of Ni, Cu, Pd, Ag, and Pt is similar, the main difference being that Pd_{13} presents a more complex anharmonic behavior than Ag (Westergren and Nordholm, 2003). The 13-atom clusters undergo a structural transition from a rigid, solidlike icosahedral structure to a nonrigid, liquidlike one via an intermediate temperature range in which both forms coexist. The caloric curves do not present any sharp transition, and T_m is found by monitoring Δ_{DF} [Eq. (30)] and looking for a maximum in the specific heat. The instability of some specific atom can play a key role in melting, as in the case of the capped atoms at $N=14$. The atom added to the 13-atom icosahedron can diffuse rapidly at T below the melting region, and this causes a small peak in the specific heat (García-Rodeja *et al.*, 1994; Lee *et al.*, 2001) so that T_m is smaller than for the 13-atom cluster. Similar behavior is found at $N=20$ for the capped double icosahedron. In contrast, when the double icosahedron is not the global minimum, the heat capacity has an unexpected behavior. For example, Pd_{19} shows a distinct abrupt change at $T \sim 400$ K and a rounded-off broad peak at higher T (Lee *et al.*, 2001).

Li, Ji, *et al.* (2000) made a thorough analysis at $N=55$ for Au, Ag, and Cu by means of molecular-dynamics simulations. Ag_{55} and Cu_{55} showed abrupt changes during the meltinglike transitions, while the transition of Au_{55} seemed to proceed for a relatively broader interval, with Δ_{DF} increasing gently from 300 up to 600 K and with a small, ladderlike energy jump in the caloric curve. The degrees of reduction for T_m were different among the three metals. Compared to Ag and Cu, Au exhibited the largest size-induced drop of T_m. This confirms the trends of Table I, since Cu also gives the most stable icosahedron cluster from the thermodynamic point of view.

At $N=38$ a complex melting behavior for Cu was found by Baletto *et al.* (2004), using molecular-dynamics simulations. A solid-solid transition took place from the truncated octahedron at the global minimum. Then the cluster rearranged itself into defected decahedron structures before melting, in analogy with the behavior of the Lennard-Jones cluster of the same size (Doye *et al.*, 1998). On the other hand, Ag_{38}, which has the same global-minimum structure as Cu_{38}, does not exhibit any solid-solid transition to defected decahedral structures. At this size Au presents a coexistence phase region among different isomers already at $T \sim 250$ K (Garzón *et al.*, 1999).

Molecular-dynamics simulations of the melting transitions for crystalline nickel clusters above $N \sim 750$ show that $T_m(N)$ closely follows Eq. (38) (Qi *et al.*, 2001), while, for $N < 500$, icosahedral structures present higher T_m and large latent heat. Similar results are found also for Cu (Wang, Zhang, *et al.*, 2003). For smaller N, the icosahedral packing is more stable and presents higher melting points than those derived from Eq. (38) (Valkealahti and Manninen, 1993).

Gold clusters have been studied intensively in recent years (see Cleveland *et al.*, 1998, 1999; Lee *et al.*, 2001; Li *et al.*, 2002). All these studies agree that a solid-solid structural transformation from the low-T optimal structures to icosahedral structures takes place below the melting temperature. Detailed analysis of the atomic trajectories and of the structural evolution indicates that this solid-to-solid transition is essentially without diffusive motion, occurring quickly and involving many (small) cooperative displacements of the atoms. The structural transformation is driven by the vibrational and configurational entropy at elevated T (Luo *et al.*, 1987; Ajayan and Marks, 1988). A thorough molecular-dynamics simulation study was made by Liu *et al.* (2001). Different morphologies were compared up to $N \sim 25\,000$. At intermediate sizes, for all type of morphologies, Liu *et al.* (2001) found that the melting process occurs in three stages: a relatively long time of surface disordering and reordering, a relatively short time of surface melting, and finally a rapid overall melting. Concerning the differences among the structural motifs, starlike decahedra are the hardest to melt, while icosahedron clusters are the easiest, with regular decahedra being in between. Small cuboctahedra, up to $N=309$ at

---

[16] See Buffat and Borel (1976), Garzón and Jellinek (1993), Cleveland *et al.* (1997, 1998, 1999), Li, Ji, *et al.* (2000; Li, Lee, *et al.*, 2002), Lee *et al.* (2001), and Koga *et al.* (2004).

least, transform into icosahedra before melting, while large ones do not. Contrary to the other motifs, T_m of icosahedra saturates at $N > 12\,000$. Liu *et al.* (2001) also compared different structures at identical sizes, finding that transition temperatures could differ by as much as 75 K. This nonequilibrium effect indicates the differences in kinetic stability of the different structures against heating.

Very recently Koga *et al.* (2004) were able to heat up metastable gold icosahedra produced in an inert-gas aggregation source (see Sec. V.B.3). Upon heating to $T = 1273$ K, which is only 64 K below the bulk melting temperature of Au, they were able to produce a clearly dominant fraction of decahedron structures in the range 6–12 nm diameter. A considerable fraction of fcc clusters was obtained only heating above the bulk melting temperature, and only for diameters above 10 nm. Since all calculated crossover sizes decahedron→fcc at 0 K are much smaller (Cleveland *et al.*, 1997; Baletto, Ferrando, *et al.*, 2002), these experimental results give support to the hypothesis of an upward displacement of the crossover size with increasing temperature, in agreement with the predictions of the harmonic theory (Doye and Calvo, 2001), as can be seen in Fig. 20.

4. Silicon clusters

Wang, Wang, *et al.* (2001) performed a systematic simulation study of structural transitions and thermodynamic properties of small Si clusters within a tight-binding molecular-dynamics scheme. They confirmed previous results on the thermodynamics of very small clusters found by means of empirical many-body potentials (Stillinger and Weber, 1985; Blaisten-Barojas and Levesque, 1986; Tchofo-Dinda *et al.*, 1995), and also considered larger sizes. Their canonical Monte Carlo simulations revealed that the melting point of Si clusters changes dramatically when the global-minimum structures change from prolate and cagelike (for $N = 17$ in this study) to an atom-centered and nearly spherical morphology. The nearly spherical clusters present a much broadened melting region, extending from 750 to 1300 K. This is because, in nearly-spherical structures, the cluster core is more tightly bonded than the surface atoms, and a much higher temperature is needed to disorder it. In the range $650 < T < 1050$ K, the nearly spherical clusters keep their structure, although there is a noticeable surface diffusion. After that, melting can take place via two pathways. The first possibility is that, as T increases, the clusters develop to the prolate morphology up to 1200 K, then break into subunits, which finally become less and less stable until the clusters disorder completely. The other possibility is that the clusters develop from quasispherical to prolate to molten oblate structures. Atoms in prolate cagelike structures are more stable than the surface atoms of the nearly spherical structures. The melting of cagelike structures often accompanies the overall deformation and fragmentation of the cage framework. Thus a much higher temperature is needed to break the cage, but the whole cluster melts at temperatures comparable with other nearly spherical structures.

V. KINETIC EFFECTS IN THE FORMATION OF NANOCLUSTERS

From the results reported in the previous sections, one can see that there are discrepancies between the results of energetic and/or thermodynamic calculations and the real outcomes of the experiments, viz., the structures that are actually observed in the production of free solid clusters. In some cases, the disagreement is of such a qualitative nature that it is unlikely to be due to the failure of the energetic or of the thermodynamic modeling. To cite just the most striking cases, we mention the observation of small decahedra and large icosahedra in the inert-gas aggregation experiments on the production of Ag clusters (Reinhard, Hall, Ugarte, and Monot, 1997), the production of large icosahedral clusters of C_{60} molecules (Martin *et al.*, 1993; Branz *et al.*, 2000, 2002), and the detection of octahedral Al clusters presenting only (111) facets (Martin *et al.*, 1992). Moreover, there is still quantitative disagreement between the theoretical estimates (based on the total energy optimization) and the experimental data about the crossover sizes for Ar clusters (Ikeshoji *et al.*, 2001). These results indicate that kinetic effects must be taken into account to explain the actual free-cluster formation in the experiments. As discussed in Sec. II, the time scale of nanocluster formation in typical sources ranges from a fraction of a millisecond to a few milliseconds. On this time scale, clusters may not be able to reach the minimum free-energy structure, thus remaining trapped in some metastable configuration that can have a very long lifetime, especially when the clusters are further cooled down after their solidification.

In studying the formation process of solid clusters in contact with a thermal bath, such as the inert-gas atmosphere in inert-gas aggregation sources, we can think of two alternative models. In both models, clusters grow mainly by the addition of single atoms (de Heer, 1993).

In the first model (Sec. V.A), which is suited for high growth temperatures, the cluster solidifies after its growth is completed, that is, at a further cooling stage taking place outside the growth chamber. In this case, the final cluster structure does not depend on the kinetics of the growth process, because the cluster remains a liquid droplet while growing, but rather depends on the kinetics of the cooling after growth, which may take place on time scales like those discussed in Sec. V.A, namely, in the range of $1 - 10^{-2}$ K/ns. This model will be referred to as the *liquid-state growth model*. It is simulated by freezing a liquid droplet until it solidifies, usually at constant N and decreasing T. In fact, there are systems (such as the noble gases) in which evaporation of atoms is non-negligible at temperatures close to the melting point, because melting and boiling temperatures are close to each other. Evaporating atoms can thus play an important role even in the cooling of solid clusters. In contrast, metals present huge differences between melting and boiling points, so that evaporative cooling is negligible for solid metallic clusters.

In the second model (Sec. V.B), which is suited for relatively low growth temperatures, clusters solidify while they are still growing.[17] This model will be referred to as the *solid-state growth model*. In this model, the final outcome is determined by the kinetics of the growth process itself. Solid-state growth is simulated by adding single atoms to a small initial seed at constant temperature (Baletto, Mottet, and Ferrando, 2000a, 2000b).

Finally (see Sec. V.C), there are cases in which growth proceeds not only by the addition of single atoms, but also by the collision and coalescence of already formed clusters.

A. Freezing of liquid nanodroplets

When simulating cluster freezing, the relevant parameter is the rate r_c at which the temperature T is rescaled, in order to mimic a thermal contact with a cold atmosphere. For example, the cluster can be cooled down by small steps δT at each time interval δt so that $r_c = \delta T/\delta t$. In an inert-gas atmosphere, one can estimate that a cluster of radius R and area $A_{eff}=4\pi R^2$ will collide with gas atoms with a frequency ϕ^G_{exp} given by

$$\phi^G_{exp} \sim \frac{P_G A_{eff}}{\sqrt{2\pi m_G k_B T_G}}, \tag{43}$$

where P_G and T_G are the pressure and the temperature, respectively, of the inert gas of mass m_G. In the harmonic approximation, the energy loss is given by

$$\frac{\delta T}{\delta t} \sim \phi^G_{exp} \frac{\delta E}{3Nk_B}, \tag{44}$$

where δE is the energy transfer at each collision, and since $A_{eff} \propto N^2$ and $N \propto R^3$ we obtain $\delta T/\delta t \propto 1/R$. Following Westergren *et al.* (1998), we can estimate that the loss for each collision (for example with a helium atom) δE is 1–10 meV. Using typical parameters for the gas, $P_G \sim 1-100$ mbar, $T_G \sim 300$ K (Reinhard, Hall, Ugarte, and Monot, 1997; Koga and Sugawara, 2003) and considering $R \sim 1$ nm, we have $\delta T/\delta t$ in the range 0.01–1 K/ns.

1. Lennard-Jones clusters

Ikeshoji *et al.* (2001) studied the freezing of Lennard-Jones clusters by molecular-dynamics simulations. Contrary to what happens for metals, the melting and boiling points of these clusters are rather close in temperature, so that the evaporation of atoms during the solidification process is non-negligible. Because of that, Ikeshoji *et al.* (2001) considered two ways of cooling clusters down. The thermostat method decreased temperature in a canonical simulation, while the evaporation method let the cluster evaporate atoms in a simulation at constant energy. They considered 380 clusters in the range $160 < N < 2200$, finding that there was a transition at increasing size from icosahedra to a mixture of structures (decahedron, fcc, hcp, and icosahedron). The transition did not depend on the cooling method, and took place for $N \simeq 450$. This is lower than the transition size (750 atoms) observed in experiments on argon clusters (Farges *et al.*, 1986), but it is closer than any other estimate based on total energy optimization, thus indicating the possible presence of kinetic trapping effects. Moreover, calculated and experimental diffraction patterns were in good agreement. Besides pure clusters, Ikeshoji *et al.* (2001) considered binary Lennard-Jones systems, finding that the formation of large icosahedra was favored by the size mismatch. This finding may furnish a qualitative explanation of the experimental observation of large icosahedron clusters in binary (metallic) systems (Saha *et al.*, 1997, 1999).

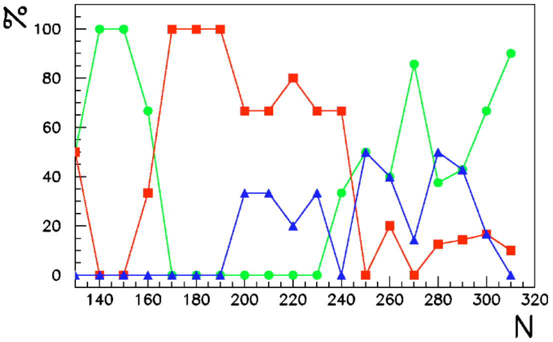

FIG. 27. (Color in online edition) Percentages of the different structures obtained in molecular-dynamics simulations of Ag cluster freezing at $r_c=1$ K/ns for $130<N<310$: ●, icosahedral structures; ■, decahedra; ▲, fcc clusters. Adapted from Baletto, Mottet, and Ferrando, 2002.

2. Silver clusters

Baletto, Mottet, and Ferrando (2002) studied the freezing of Ag liquid nanodroplets by molecular-dynamics simulations with realistic cooling rates r_c in the range 0.1–5 K/ns. They made a systematic study of Ag freezing at $130 \leqslant N \leqslant 310$, and in addition considered the freezing at the icosahedral magic numbers 147, 309, 561, and 923. The latter simulations were made to investigate the possibility of obtaining large metastable Ag icosahedra by freezing liquid droplets, in order to ascertain whether the liquid-state growth model could explain the experimental observation of metastable icosahedra by Reinhard, Hall, Ugarte, and Monot (1997).

The results for $130 \leqslant N \leqslant 310$ are summarized in Fig. 27. On a coarse-grained description, the energetic calculations by Baletto, Ferrando, *et al.* (2002) showed that icosahedral clusters are the best up to $N \simeq 170$; then the best structures are decahedral, except for the icosahedral magic number $N=309$, while fcc clusters become competitive with the decahedra for $N > 600$. The freezing simulations of Baletto, Mottet, and Ferrando (2002)

---

[17] Clusters may solidify during growth at constant temperature after reaching a critical size.

TABLE II. Numbers of icosahedron (Ih), decahedron (Dh), and fcc structures at magic icosahedral sizes. The results are obtained from five molecular-dynamics simulations for each cooling rate r_c and for each size. Adapted from Baletto, Mottet, and Ferrando, 2002.

r_c (K/ns)	N	N_{Ih}	N_{Dh}	N_{fcc}
1	147	5		
	309	4	1	
	561	2	2	1
	923	1		4
5	147	5		
	309	3		2
	561	2		3
	923		1	4
20	147	5		
	309	2	1	2
	561	1	3	1
	923	1	3	1

gave the following results. At r_c=1 K/ns, particles solidified as icosahedra in the range 135<N<165. Around N=165 there was a transition to decahedron clusters, which were the most frequent for 170<N<245. About 20% of the runs gave fcc structures in this range, and a few icosahedron clusters were formed. For 245<N<310, the dominant structures at the end of the freezing were icosahedra, but fcc clusters were also common, especially in the range N∼250–260 and N∼280–300, in which they made up more than 50%. At slower cooling rates, r_c=0.12 K/ns, the percentage of fcc and icosahedron particles in the range 170<N<245 dropped practically to zero, indicating that decahedron clusters are likely to be the most favored from the thermodynamic point of view in this size range. On the other hand, at faster cooling rates, r_c=5 K/ns, the percentage of fcc clusters in the range 245<N<310 decreased in favor of decahedron clusters, while the dominant proportion of icosahedra remained practically constant.

From the freezing results at the icosahedral magic numbers 147, 309, 561, and 923, it was possible to extract the following tendency (see Table II and Fig. 28). The percentage of icosahedral structures at the end of the freezing process decreased with cluster size for all cooling rates, passing from 100% at N=147 to less than 20% at N=923. There was no evidence of changes in the results when r_c ranged within 1–20 K/ns, probably indicating that these rates are sufficient to mimic a freezing process taking place close to equilibrium.

In summary, the simulations showed that it is not possible to avoid the formation of a large percentage of small icosahedra (2–3 nm diameter) if freezing takes place after the growth is completed. Moreover, the probability of forming large icosahedra by freezing liquid Ag droplets with realistic cooling rates is small. Both findings are in contrast with the experimental results of Reinhard, Hall, Ugarte, and Monot (1997), who did not find strong evidence of small icosahedra, while they observed a dominant percentage of icosahedra at large sizes. Therefore, one can rule out the liquid-state growth model as an explanation for the outcome of this experiment.

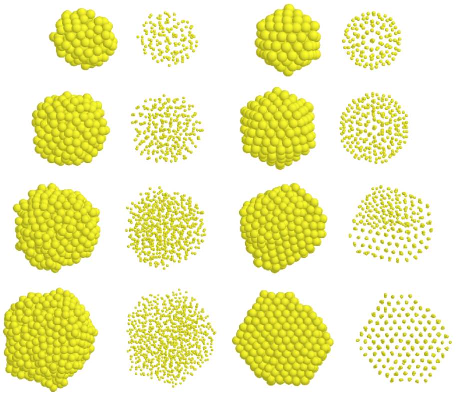

FIG. 28. (Color in online edition) Molecular-dynamics simulation of silver cluster freezing. On the left, we show the initial configurations of Ag liquid nanodroplets at magic icosahedral numbers (147, 309, 561, and 923), while on the right, there are typical final structures obtained by cooling at 1 K/ns: from top to bottom, 147-atom icosahedron; 309-atom icosahedron; a decahedron at 561 [strongly asymmetric and with an island on hcp stacking above (Baletto and Ferrando, 2001)]; a fcc polyhedron at 923.

3. Gold clusters

Chushak and Bartell (2001a, 2001b) studied the solidification of Au nanoclusters by molecular-dynamics simulations. However, their method is rather different from that applied to Ag clusters by Baletto, Mottet, and Ferrando (2002). Chushak and Bartell (2001a, 2001b) started from high-T liquid clusters of rather large sizes (459, 1157, and 3943 atoms). These clusters were then cooled down very quickly, at a rate r_c=5×10^4 K/ns, to a temperature of about 700 K, at which their most stable form is solid. At this temperature, production runs of 1 ns were performed. After that, clusters were further quenched down to 300 K, again with a fast rate (300 K/ns). As a result of this cooling procedure Chushak and Bartell found that icosahedron clusters were preferentially produced, even though they should not be the lowest-energy structures at these sizes (see Baletto, Ferrando, *et al.*, 2002). In this case, icosahedron clusters were produced with high probability during freezing because of the width of the icosahedron funnel (Doye, 2004) with respect to the funnels leading to either close-packed or decahedral structures. This is a kinetic trapping effect, which is stronger at rapid cooling rates, and agrees with the results on Ag freezing by Baletto, Mottet, and Ferrando (2002).

Nam *et al.* (2002) have studied the mechanism by which metastable gold icosahedron clusters are frozen out of nanodroplets using molecular-dynamics simulations within the embedded-atom model. Their simula-

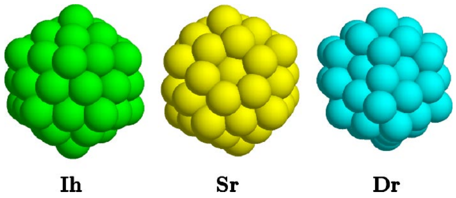

FIG. 29. (Color in online edition) Platinum cluster structures at $N=55$. From left to right icosahedron (Ih), single rosette (Sr), and double rosette (Dr). The Ih is the lowest in energy, the Sr and the Dr are, respectively, 0.48 and 0.42 eV higher in energy.

tions started from a liquid droplet at 1500 K, which was cooled down at a rapid rate of 100 K/ns. Again, the majority of clusters solidified in the icosahedral symmetry, with the solidification starting at the cluster surface, in such a way that a well-ordered, close-packed surface with fivefold symmetry points was formed while the cluster was still amorphous inside. The formation of such a surface triggered the solidification process towards the formation of icosahedra: Nam *et al.* (2002) noticed that when ordering began at the surface, the final result was an icosahedron cluster. Conversely, if the surface did not order first, the final cluster was either decahedral or fcc.

4. Entropic effects and kinetic trapping in Pt_{55}

As a paradigm showing the peculiar interplay between entropic and kinetic trapping effects, we report on a molecular-dynamics study of the melting of Pt_{55} (Baletto, 2003), modeled by the Rosato *et al.* (1989) potential. Within this model, Pt_{55} presents the competing structures of Fig. 29: the icosahedron, the single rosette (Sr), and the double rosette (Dr), which are, respectively, the minimum-energy structure, the high-T minimum-free-energy structure, and a structure frequently found in growth simulations (Baletto, 2003). The single and double rosettes are obtained by modifying the external shell of the Ih_{55}. In the single rosette, a single vertex atom is displaced to form a hexagonal ring (the *rosette*) together with its nearest-neighbor atoms on the surface. The two rosettes of the double rosette are at nearby vertices, giving a close resemblance to the global minimum of Au_{55} found by Garzón, Michaelian, *et al.* (1998) and shown in Fig. 13. In the melting simulations (see Fig. 30), the single rosette becomes the most favored structure for $600<T<700$ K. In this range, the cluster still oscillates among icosahedral, single-rosette, and double-rosette structures. Finally, it melts above 750 K. This is due to entropic effects. In fact, calculations within the harmonic approximation (see Sec. IV.A.1) show that the probability of finding the single rosette becomes considerable above 600 K, while the probability of the double rosette always remains much smaller. Constant-T simulations on long time scales (several μs) of the evolution of Pt_{55} above 600 K confirm this scenario, showing also that the harmonic approximation is qualitatively right in predicting that the single rosette is more probable than the double, but it is quantitatively poor because it underestimates the probability of both with respect to the probability of the icosahedron (see Fig. 31). Another entropy-driven effect concerns decahedral structures. Even though some decahedral structures are lower in energy than the single and double rosette, we find that the entropic contribution favors single rosettes and

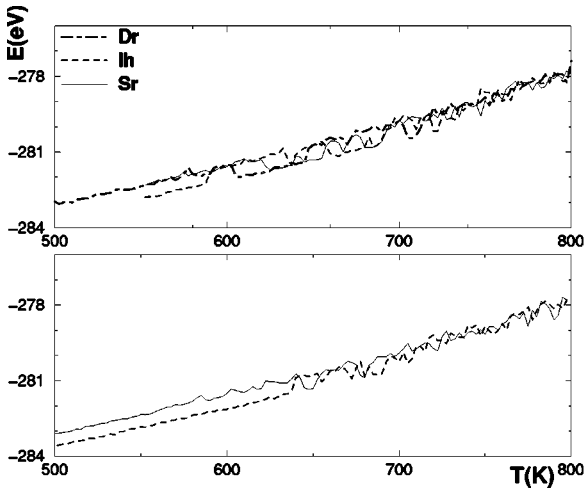

FIG. 30. Melting and freezing molecular-dynamics simulations of Pt_{55} clusters. In the upper panel we show the melting caloric curves for for three structures: dashed line, icosahedral (Ih); solid line, single rosette (Sr); dash-dotted line, double rosette (Dr). For $600<T<700$ K, all melting curves exhibit several oscillations among the three structures. The lower panel shows two freezing curves. The dashed line ends with an icosahedral structure, while the solid line ends with a single-rosette structure. This is an example of the interplay of entropic and kinetic effects. Due to entropic effects, the Sr structure is the most likely in the temperature range in which the cluster begins to solidify. This structure may then be preserved down to low temperatures by a trapping effect.

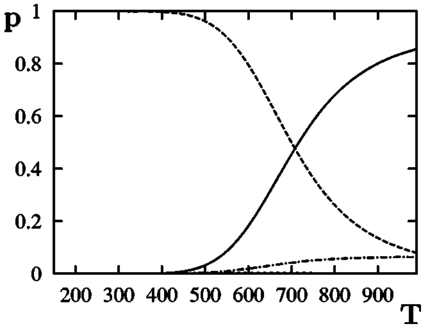

FIG. 31. Probabilities of the different structures of Pt_{55} vs T in the harmonic superposition approximation: solid line, the probability of the single rosette; dashed line, probability of the icosahedron; dash-dotted line, probability of the double rosette; dotted line (which coincides with the T axis on this scale), probability of the decahedron. The last always have a very small probability, even if they are energetically favored with respect to the single rosette, which is the best structure from the entropic point of view and becomes the most likely at high T.

double rosettes over decahedral structures even at low temperatures.

The freezing simulations in Fig. 30 show an interplay of kinetic and entropic effects. The cluster starts to solidify at $T \simeq 700$ K, a temperature range in which the single rosette is the most probable structure. Then the cluster is likely to remain kinetically trapped in this structure down to low temperatures.

5. Copper, nickel, and lead clusters

Valkealahti and Manninen (1997) performed a systematic molecular-dynamics study of the freezing of Cu nanodroplets within the effective-medium model. They varied r_c in the range 1000–10 K/ns, thus also considering rates that are rather close to the experimental ones, and analyzed a wide range of sizes up to about 4000 atoms. In their simulations, the clusters solidified as icosahedra at small icosahedral magic numbers (up to $N=147$); small clusters with other sizes and large clusters could solidify as twinned fcc structures. No evidence of unfaulted truncated octahedron or decahedron clusters was found. The fact that icosahedron clusters are dominant at small sizes but not at larger ones is in agreement with the experimental findings of Reinhard, Hall, Berthoud, *et al.* (1997), who found, however, some evidence in favor of intermediate-size decahedron clusters.

Qi *et al.* (2001) have studied the freezing of several Ni clusters at sizes from 336 to 8007 atoms by molecular-dynamics simulations within the embedded-atom potential. In their simulations, they performed heating and cooling cycles at very fast rates (4000 K/ns): starting from a solid cluster they increased T to melt the structure, and then cooled it down again. As a result, they found icosahedron clusters after freezing for $N<500$, and fcc clusters for larger sizes. All these studies confirm the tendency to form icosahedral clusters only after freezing small liquid droplets, in agreement with the previous cases, whereas at larger sizes other structures are dominant.

The first study of the solidification of Pb clusters was made by Lim *et al.* (1994); they considered a single cluster of about 8000 atoms, obtaining an icosahedron after fast quenching, in disagreement with their own energetic calculations (Lim *et al.*, 1992), which predicted that the cuboctahedron would be lower in energy than the icosahedron. This topic has been recently analyzed in a more systematic way by Hendy and Hall (2002), who quenched a large variety of liquid Pb droplets in the size range between 600 and 6000 atoms. In their simulations, the liquid droplet was quenched suddenly below the cluster melting point, and then equilibrated for 10 ns. Up to 4000 atoms, they found mostly icosahedra with a reconstructed surface, showing that they are lower in energy than any other known structure in the same size range. The freezing of clusters of about 6000 atoms produced faulted fcc structures. The production of icosahedron clusters agrees with the experimental observation of icosahedron particles of 3–6 nm diameter by Hyslop *et al.* (2001) in inert-gas aggregation experiments.

B. Solid-state growth

Even though the liquid-state growth model can explain some kinetic effects in the growth of nanoclusters (see, for instance, the cases of lead and argon clusters treated in Sec. V.A), there are still several experimental results that cannot be explained by it: the growth of large icosahedra in clusters of Ag and of C_{60} molecules, and the growth of octahedra in Al clusters. For these systems, it turns out that the solid-state growth model is much more appropriate.

In the following, we deal first with a very general mechanism for the solid-state growth of metastable icosahedra (Sec. V.B.1); then we treat (Sec. V.B.2) the molecular-dynamics simulation results for noble-metal and quasi-noble-metal clusters at small sizes (Baletto, Mottet, and Ferrando, 2001b). These simulations were run with very slow fluxes, in order to test the solid-state growth model against the energetics and thermodynamics results. In Sec. V.B.3, results on the growth of Ag and Au clusters of intermediate and large size are reported. Finally Secs. V.B.4 and V.B.5 are devoted to the growth of aluminum and C_{60} clusters, respectively.

1. Universal mechanism of the solid-state growth of large icosahedra

Before focusing on specific systems, we treat a very general mechanism which we believe to be responsible for the observation of large metastable icosahedra in several systems (see Ag, Au, and C_{60} below). This mechanism consists of two steps. The first is the solid-solid transformation of a decahedron into an icosahedron, the second the shell-by-shell growth of the icosahedron to reach large sizes. This is a very peculiar example of structural transformation, because it has a clear kinetic origin, occurs only through solid states, and does not depend on the interparticle potential, but is essentially due to geometric reasons. First of all, we note that this transformation is possible because a decahedron is a fragment of a larger icosahedron, so that by proper addition of atoms, a decahedron can grow towards an icosahedron. However, this is only a possibility, and a further ingredient is necessary to render this transformation kinetically favored. This key ingredient is the fact that on the (111)-like facets of a decahedron are found a larger number of stable adsorption sites of hcp stacking than of fcc stacking (Baletto and Ferrando, 2001).

Islands of fcc stacking preserve the decahedral rearrangement in columns, around the fivefold symmetry axis, while hcp islands break the decahedral symmetry (see Fig. 32) and can lead to the transformation towards a larger icosahedron. A decahedron plus a hcp island is a part of a larger icosahedron. The displacement of a hcp island to the fcc stacking costs a considerable amount of energy, which increases with the stickiness of the potential. While the growth of islands of fcc stacking leads simply to a larger decahedron [this is the *umbrella growth model* (Martin *et al.*, 1991b)], the nucleation of hcp islands can be the starting point for transforming a

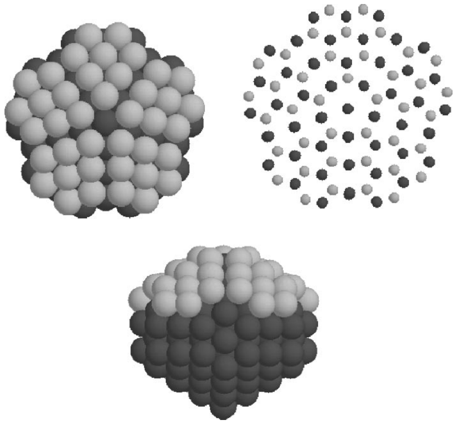

FIG. 32. A 146-atom decahedron plus an hcp island above a cap. The black dots indicate fcc adsorption sites, the gray dots the hcp sites. The fcc sites on the edges between facets are not stable for single adatoms. Compared to adsorption on icosahedral clusters, the fcc and hcp sites correspond to Mackay and anti-Mackay sites, respectively.

decahedron into a larger icosahedron. The island can be either one or two layers thick, leading to transformations to icosahedra of different sizes, through different rearrangement pathways (Baletto, Mottet, and Ferrando, 2001a). The size at which a solid-state decahedron→icosahedron transformation can take place depends strongly on temperature. A larger starting decahedron requires a higher temperature.

While a growing decahedron can transform into an icosahedron, there is no natural growth sequence from icosahedron to decahedron structures, because an icosahedron is not a fragment of a larger decahedron. To transform a growing icosahedron into a decahedron, a complete rearrangement of the cluster is necessary. This rearrangement becomes likely only at high temperatures, close to the melting point, as proved by the experiments of Koga *et al.* (2004). Therefore we can well understand that it is rather common to find wide temperature ranges in which kinetic trapping into icosahedral structures dominates the growth sequence. The solid-state decahedron→icosahedron transformation thus allows us to explain several experimental results: from small decahedra, larger icosahedra are grown, which can then grow further in a shell-by-shell mode preserving their symmetry.

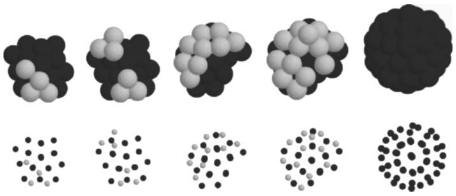

FIG. 33. The solid-state decahedron→icosahedron transformation obtained in growth simulation of clusters of C_{60} molecules. The same kind of transformation is also found in simulations of Ag cluster growth. Ag and C_{60} present completely different interactions, soft and sticky, respectively. Adapted from Baletto, 2003.

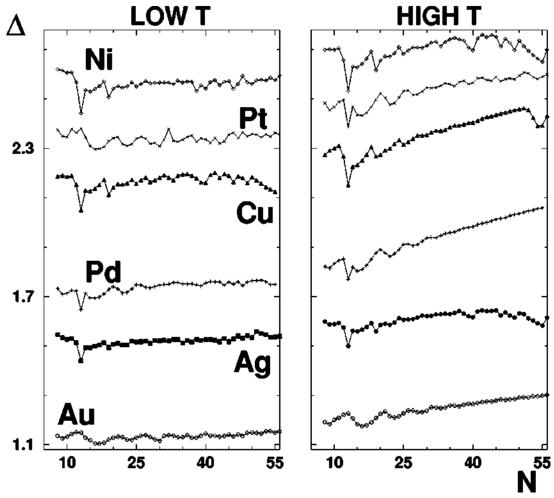

FIG. 34. Growth simulations of small metallic clusters. Δ as a function of cluster size at different temperatures: low temperatures (200 K for Au and Ag, 300 K for Ni and Pt, 400 K for Cu and Pd) on the left and high temperatures (400 K for Au and Ag, 600 K for Ni, 700 K for Pd, Pt, and Cu). Minima in Δ single out the most stable structures.

The above considerations lead to a general observation about the possibility of building up noncrystalline (especially icosahedral) structures in nanoclusters. In fact, even though a sticky potential disfavors these structures, at the same time it enhances kinetic trapping effects, because diffusion barriers are high and rearrangements involving many particles become very difficult (Wales, 1994b; Baletto, Doye, *et al.*, 2003). These kinetic effects very likely lead to the growth of icosahedra (see Fig. 33).

2. Growth of small noble-metal and transition-metal clusters

Here we analyze simulations of the growth of small Cu, Ag, Au, Ni, Pd, and Pt clusters modeled by the Rosato *et al.* (1989) potential, in order to single out qualitative differences in the behavior of these elements. To this purpose, we show in Fig. 34 the quantity Δ [Eq. (5)] as a function of the cluster size for growth simulations at different temperatures, depending on the metals, with fixed $\tau_{dep}=98$ ns. In this case, Δ is defined by putting into Eq. (5) the temperature-dependent total energy E of the cluster, averaged at each size over several snapshots, instead of the zero-temperature binding energy E_b. Stable structures are singled out by minima in Δ. Finally we focus on the growth of Ag and Cu clusters at $N=38$, to show that in this case kinetic trapping effects are overwhelming. In fact, the global-minimum structure, which is a truncated octahedron according to this energetic model, is grown with a non-negligible probability only in a narrow temperature range for a given flux.

Growth sequences for Cu and Ni clusters are clearly dominated by icosahedral or polyicosahedral structures,

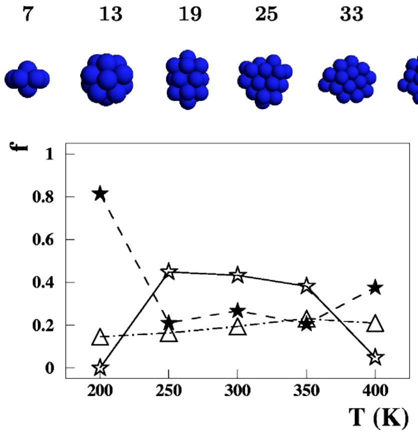

FIG. 35. (Color in online edition) Ag_{38} growth simulation results. In the top row, snapshots from a simulation at $T=200$ K are shown at different sizes. The structures of the snapshots pertain to the global minima up to $N=33$; then growth is kinetically trapped into defected decahedron structures, which are neither energetically nor entropically favored. The graph shows the structural frequencies f_{TO}, f_{Dh}, f_{LS} of different structures at $N=38$ and at different growth temperatures: open stars, truncated octahedra; solid stars, decahedra; triangles, low-symmetry structures. The lines are only guides to the eyes. At low temperatures, strong kinetic trapping into decahedral structures occurs. This is followed by an intermediate temperature regime where the three structural motifs are essentially equally likely. At high temperatures, entropic effects favor decahedral and low-sym-metry structures at the expense of the truncated octahedron. Adapted from Baletto *et al.*, 2004.

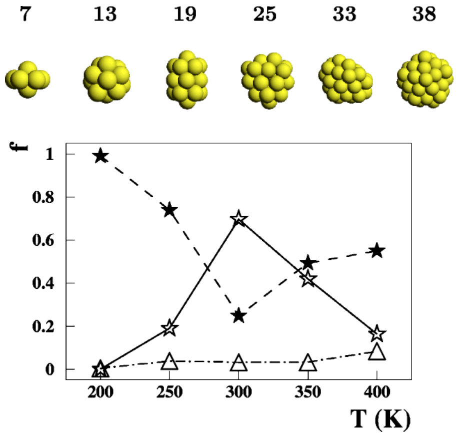

FIG. 36. (Color in online edition) Cu_{38} growth simulation results. Symbols as in Fig. 35. In the top row, snapshots from a Cu simulation at $T=400$ K are reported. Again, the snapshots reproduce the global minima up to $N=33$. On the contrary, the growth structure at $N=38$ is not the global minimum but a Dh, which is entropically favored at this temperature. Around 200 K, there is a strong kinetic trapping into Dh structures formed at smaller sizes. At intermediate temperatures the TO structure is preferentially grown; at high T, Dh structures again prevail due to entropic effects. Adapted from Baletto *et al.*, 2004

as can be seen in Fig. 34. The magic sizes are 13, 19, 25, 40, 43, 46, 49, and 55, with 13, 19, and 55 being of special stability. The sequences are well reproducible over a wide range of growth temperatures. The main difference between Ni and Cu is that in Ni it is easier to obtain truncated octahedra of 38 atoms, even at relatively low temperatures (400 K). In this case, growth continues with the cluster trapped in non icosahedral structures. Growth sequences for Ag show the same kind of structures, but they are reproducible over a narrower temperature range. In contrast, the growth sequences of Au reveal completely different magic sizes. Icosahedral structures are completely unfavored. The minima at $N=13$ and 19 are absent, replaced by peaks at $N=16$ and 22. At $N=30$ we find a decahedral minimum, which survives up to $T\sim300$ K. At higher temperatures the clusters oscillate among different structures over a time scale shorter than τ_{dep} so that they can be considered either melted or quasimelted. There is no evidence of entropic effects favoring the transition to icosahedral structures. Finally, Pt and Pd show an intermediate behavior between Cu, Ni, and Ag on the one side, and Au on the other. For Pd, there is a minimum at $N=13$, but there is no evidence of any other magic size up to the Ih_{55}, which is likely to be grown. In Pt, minima are found at $N=13$ (as in Cu) and 22 (as in Au). At high T, it is possible to grow truncated octahedra of 38 atoms. Very interesting behavior takes place around for Pt_{55}, as anticipated in Sec. V.A.4, with the probable growth of rosette structures, either because of kinetic trapping in incomplete icosahedral structures formed at lower sizes, or because of the onset of entropic effects at high temperatures.

A complex interplay of thermodynamic and kinetic effects takes place in the growth simulations of Ag_{38} and Cu_{38} (Baletto, Rapallo, *et al.*, 2004). At this size, the global minimum is a truncated octahedron, which is in competition with a series of defected decahedron structures (mostly based on decahedra of 23 atoms covered by islands), and in the case of Ag, with a low-symmetry structure that is neither a defected decahedron nor a close-packed cluster. In the case of copper, these decahedron structures become favored over the truncated octahedra at temperatures around 350 K, because of entropic effects. Moreover, for sizes just below $N=38$, the global minima are defected decahedra in both Ag and Cu. For these reasons, the truncated octahedron is not likely to be grown in the simulations. Performing several simulations at $T=200$, 250, 300, 350, and 400 K, and observing the structures grown at $N=38$, one obtains the results reported in Figs. 35 and 36. At 200–250 K, kinetic trapping into decahedron structures is the fate of essentially all simulations, so that the magic structure never coincides with the global minimum, which is also the free-energy minimum in this temperature range. This kinetic trapping is due to the fact that the global minima in the range 30–37 atoms are decahedral (with the single exception of Cu_{37}). In the interval 300–350 K, kinetic trapping becomes less effective, even if it is still somewhat present. In this range, the truncated structures are still quite likely at equilibrium, and they are indeed observed, together with decahedra and low-symmetry structures (the latter in Ag only). Above 350 K, again decahedral structures prevail in Cu_{38}, as at low temperature. However, this is not due to kinetic trapping, but to an entropic effect, because at these temperatures decahedral structures are the most likely at equilibrium.

3. Growth of intermediate- and large-size Ag and Au clusters

The experiments of production of Ag clusters in inert-gas aggregation sources (Reinhard, Hall, Ugarte, and Monot, 1997) show that the abundances of small clusters (2 nm diameter) are not dominated by icosahedral structures, while icosahedra are the most abundant structures for much larger sizes. Here we discuss how these results can be explained in the framework of a solid-state growth model (Baletto, Mottet, and Ferrando, 2000b, 2001a).

Let us consider first the sizes around 150 atoms, that is, diameters of about 2 nm. In this range, the molecular-dynamics growth simulations show that a *reentrant morphology transition* takes place. This means that, at a given deposition flux, there is an intermediate temperature window (400–500 K for fluxes of experimental interest) in which decahedral structures are preferentially grown, while at low and high temperatures icosahedra are obtained.

In fact, at intermediate temperatures, Ag clusters are able to optimize their shape up to $N \sim 100$ [the best structure is the (2,3,2) decahedron at 101 atoms] and then remain trapped in decahedral structures. This leads to the formation of a metastable decahedron cluster around $N=150$ [the (3,2,2) decahedron cluster at 146 atoms is the best in this range] instead of the lower-energy icosahedra related to the $N=147$ icosahedron. At higher temperatures ($T > 550$ K), the clusters are liquid up to $N \simeq 130$, and the final outcomes at $N \simeq 150$ are icosahedra. Finally, at low temperatures ($T < 450$ K), the cluster has sufficient kinetic energy to optimize its shape only up to 75 atoms. Then it remains trapped in this structure and evolves towards the (6,1,1) decahedron at $N=100$. When this decahedron is almost completed, the addition of further atoms causes the nucleation of hcp islands on the facets and starts the formation of larger icosahedra. This is an example of a solid-state decahedron →icosahedron transformation (Baletto and Ferrando, 2001). Typical simulation results are summarized by the snapshots shown in Fig. 37.

The metastable decahedra at $N \simeq 150$ can have very long lifetimes. Baletto, Mottet, and Ferrando (2000b) calculated the lifetime τ_{Dh} of the (3,2,2) decahedron in the range $550 \leqslant T \leqslant 650$ K, finding an activated behavior of the kind $\tau_{Dh} = \tau_{Dh}^0 \exp[\Delta E/(k_B T)]$. After estimating the prefactor τ_{Dh}^0 and the activation barrier ΔE, they were able to extrapolate a lifetime of several milliseconds at 450 K. This should indicate that this structures is likely to survive on the experimental time scale.

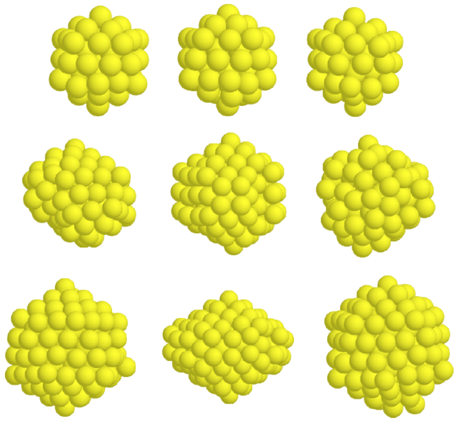

FIG. 37. (Color in online edition) Snapshots of silver cluster growth at $\tau_{dep}=7$ ns from three simulations at three different temperatures: left column, 400 K, middle column, 500 K, right column, 600 K. In each column, the snapshots are taken at sizes of 55, 105, and 147 atoms from top to bottom. At 75 decahedra are preferentially grown up to 500 K. Icosahedral structures of 147 atoms are obtained in the simulations at 400 and 600 K, and a decahedron at 500 K. At 55 atoms, we obtain an icosahedron at 400 and 500 K (the structure at 600 K is rapidly fluctuating).

The reentrant morphology transition is due to kinetic trapping and not to entropic effects. In fact, on the basis of the considerations reported in Sec. IV.A, from Eq. (25) it follows that, for $N=147$, p_{Dh}/p_{Ih} monotonically increases with T.

Let us now consider a growth sequence leading to the formation of small decahedra and of large metastable icosahedra, in agreement with the results of the experiments by Reinhard, Hall, Ugarte, and Monot (1997). This sequence is obtained for $400 < T < 500$ K and is essentially a solid-state decahedron→icosahedron transformation followed by a shell-by-shell trapping in icosahedral structures, as reported in Fig. 38. In fact, continuing the deposition on a metastable decahedron

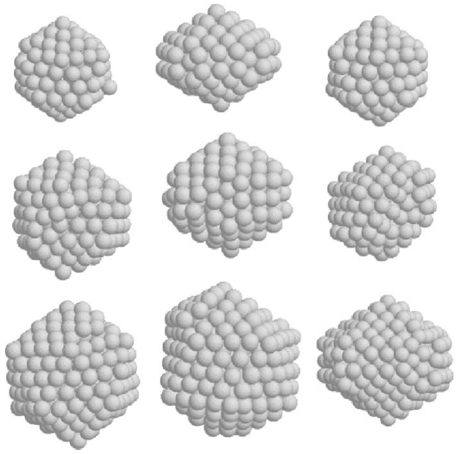

FIG. 38. Growth sequences of intermediate-size Ag clusters at different T: from left to right, 400, 450, and 600 K. In the top row, $N \simeq 150$, in the middle row $N \simeq 200$, and in the bottom row $N \simeq 300$.

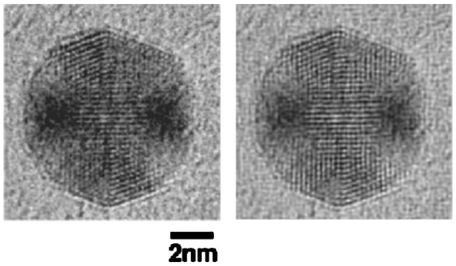

FIG. 39. High-resolution electron microscopy image of a large icosahedral Au cluster grown in an inert-gas aggregation source and then deposited on an inert substrate. Adapted from Koga and Sugawara, 2003.

of ~150 atoms, an island of hcp stacking is nucleated. This island can be either one or two layers thick, leading to the formation of icosahedra with $N=309$ or 561, respectively (Baletto, Mottet, and Ferrando 2001a). For $T>600$ K, icosahedral structures are never obtained for $N>180$. The deposition of a few tens of atoms above $N=147$ causes a sharp transition towards decahedra of 192 atoms. This grows passing through different decahedral structures, towards one with $N=318$ by the nucleation of islands of fcc stacking. For $T>650$ K, fcc structures are preferentially grown. This happens because around $N=201$ and $N=314$, decahedral and fcc clusters are in close competition from the energetic point of view. Because of that, when temperature is high enough and the energy differences become less important, the growing cluster can pass through different faulted fcc and asymmetric decahedral structures, growing finally as a fcc structure. At low temperatures, around 400 K, icosahedra are preferentially grown around $N=150$, and these icosahedra continue growing in a shell-by-shell mode.

The growth of Au clusters has also been investigated, and there is evidence for kinetic trapping effects of the same kind as those found in Ag. In a recent experiment, Koga and Sugawara (2003) generated and analyzed a huge population of Au clusters with diameters in the range 3–18 nm. The clusters were produced in an inert-gas aggregation source with carrier helium gas, then deposited on an amorphous carbon substrate and analyzed by high-resolution electron microscopy. Some of these clusters are shown in Figs. 2 and 39. Analysis of the cluster population revealed a striking feature: for all sizes, most of the clusters were icosahedral (see Fig. 40), with a proportion of about 90% at small sizes, slowly decreasing to 60–70 % at large sizes. The remaining clusters were mostly of decahedral symmetry, while a very few fcc clusters were observed. This result is in disagreement both with the energetic calculations (Cleveland *et al.*, 1997; Baletto, Ferrando, *et al.*, 2002) and with the experimental observation of Patil *et al.* (1993) indicating very low crossover sizes from the icosahedron to the other motifs. Patil *et al.* (1993) observed Au clusters after melting and very slow refreezing; they were thus very likely observing equilibrated clusters. Koga and Sugawara (2003) attributed the observation of large icosahedra to a kinetic trapping effect (Baletto, Mottet, and Ferrando, 2000a, 2001a), caused by the shell-by-shell growth of small icosahedral clusters. At the moment, simulations on Au cluster growth are not available to rule out the possibility of a liquid-state growth process, but the formation of such large icosahedra by the freezing of liquid droplets seems unlikely in the light of the results reported in Sec. V.A.2 and by Baletto, Mottet, and Ferrando (2002).

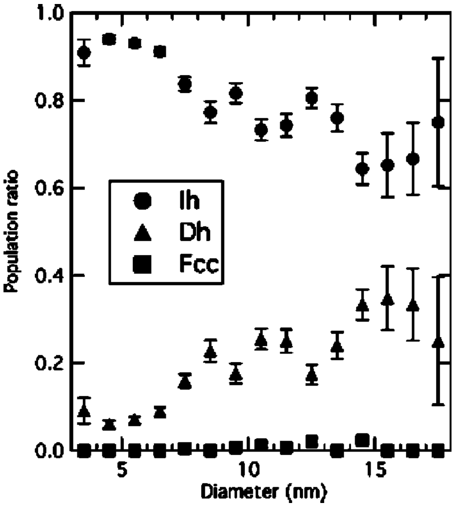

FIG. 40. Experimental population distributions of icosahedral, decahedral, and fcc Au clusters grown in an inert-gas aggregation experiment. Adapted from Koga and Sugawara, 2003.

4. Aluminum clusters

The formation of Al clusters was studied experimentally by different groups (Lermé *et al.*, 1992; Martin *et al.*, 1992). The mass spectra presented regular oscillations, whose maxima were equally spaced by a quantity $\delta N^{1/3}$ when the cluster abundance was plotted as a function of $N^{1/3}$ (see Fig. 41). The numerical value of the spacing turned out to be $\delta N^{1/3} \simeq 0.22$. Valkealahti *et al.* (1995) nicely explained these features as being of geometric origin within the octahedral growth model. In this model, each maximum corresponds to the addition of a single close-packed layer on one of the eight facets of the octahedron. Let us consider an octahedron with n_1 close-packed layers in the direction of one of its eight facets. This octahedron has $N_{oct}(n_1)$ atoms. When we

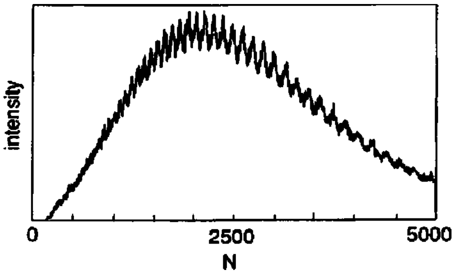

FIG. 41. Experimental mass spectrum of aluminum clusters. Adapted from Valkealahti *et al.*, 1995.

add a further layer above one facet, the number of atoms becomes $N_{oct}(n_1+1)$. Valkealahti *et al.* (1995) demonstrated that

$$\delta N^{1/3} = [N_{oct}(n_1+1) - N_{oct}(n_1)]^{1/3} = \frac{1}{6}\left(\frac{3}{2}\right)^{2/3} \qquad (45)$$

in very good agreement with the experiments.

In a subsequent molecular-dynamics study, Valkealahti and Manninen (1998) analyzed the possibility of growing octahedral clusters starting from truncated octahedra. As a first step towards understanding the growth mechanism, they calculated diffusion barriers for adatoms and dimers, finding very interesting mechanisms such as chain diffusion, which allows direct mass transport between two nonadjacent (111) facets through an intermediate (100) facet. Then, in their growth simulations, they took a truncated octahedron of 586 atoms as a starting seed, and deposited atoms one by one at constant temperature ($T=400$ K) with a rather fast deposition rate ($\tau_{dep}=0.5$ ns) up to a total of 201 deposited atoms. The results demonstrated the possibility of transforming a truncated octahedron into an octahedron by the following mechanism. When depositing on the truncated octahedron, atoms are very likely to fall on (111) facets, where they can diffuse fast. When an adatom reaches the border with a (100) facet, it can exchange easily with an edge atom, which is then trapped on the (100) facet. The reverse process [exchange from a (100) to a (111) facet] is very difficult because the adsorption energy is much more favorable on (100) than on (111) facets. The accumulation of atoms on (100) facets leads naturally to the formation of an octahedron exposing only (111) facets. This mechanism was confirmed later by molecular-dynamics growth simulations of Ag and Au clusters (Baletto, Mottet, and Ferrando, 2000a) that were performed starting from a truncated octahedron of $N=201$ but with a much slower deposition rate. The growth simulations of truncated octahedron clusters have revealed the formation of stacking faults (Valkealahti and Manninen, 1998; Baletto, Mottet, and Ferrando, 2000a). Manninen and Manninen (2002) and Manninen *et al.* (2003) showed that clusters with stacking faults are also obtained in global optimization on an fcc lattice with all possible (111) stacking faults allowed, in the case of different model potentials.

5. Clusters of C_{60} molecules

In the case of C_{60} clusters, growth takes place in the solid state. Baletto, Doye, and Ferrando (2002) simulated their growth with τ_{dep} between 100 and 200 ns and $T<600$ K, modeling the interactions by the Girifalco (1992) potential. Some results are shown in Fig. 42, where snapshots from typical growth simulations at different T and $\tau_{dep}=100$ ns are reported at some significant sizes. All the sequences $T<525$ K develop along the same line and lead to the formation of a well-ordered icosahedron of 55 atoms. At $N=13$ the structure is always icosahedral, in agreement with the global optimization results. Similarly, around $N=25$ the structure usually resembles the global minimum, although this is not necessarily the case in between these sizes. Only at very low T (<300 K) does the structure remain trapped in the icosahedral shape after 13 molecules. The 25-molecule structure is decahedral but with an island on the bottom (111) faces of the cluster. This structure plays a key role, because growth is dominated by kinetic trapping effects beyond this size, since a complete solid-state decahedron→icosahedron transformation takes place. Furthermore, the structure is a fragment of the icosahedron with $N=55$, and continued growth around the bottom apex of the decahedron provides a pathway to this structure, with its apex ending up at the center of the resulting icosahedron (Baletto *et al.*, 2001a).

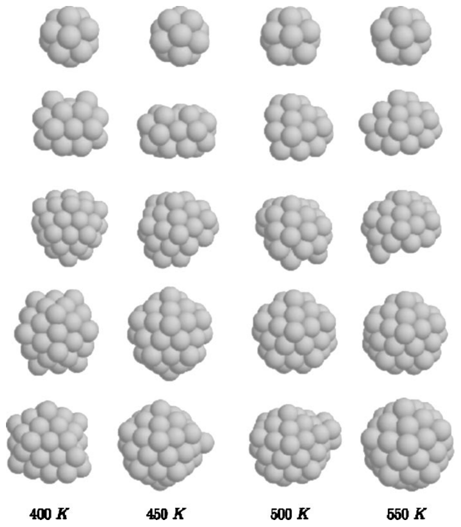

FIG. 42. Growth sequences of C_{60} clusters for $\tau_{dep}=100$ ns and different temperatures. From top to bottom snapshots at $N=13$, 25, 38, 45, and 55 particles are shown. Adapted from Baletto, Doye, and Ferrando, 2002.

This growth pattern bears no resemblance to the sequence of global minima, which develops through either close-packed or decahedral structures. In particular, the $(C_{60})_{38}$ global minimum is a truncated octahedron, while the growth simulations always give structures with fivefold symmetries. The same happens at $N=45$, and finally a Mackay icosahedron results at $N=55$. If the growth is continued for $N>55$, a well-ordered anti-Mackay overlayer (Martin, 1996) develops on the surface of the icosahedron, in agreement with the sequence of magic numbers observed experimentally for $55<N<100$ (Branz *et al.*, 2000, 2002). Decahedral and fcc structures are only obtained in a few cases at rather high growth temperatures (525–550 K), as found by Baletto, Doye, and Ferrando (2002). If one uses the Pacheco and Prates-Ramalho (1997) potential, the growth of nonicosahedral structures becomes more likely, but icosahedra are still obtained in most cases.

Let us discuss how these simulation results compare to the experiments by Branz *et al.* (2000, 2002) discussed in Sec. III.E.6. The experimental data concerning the formation of icosahedral clusters are easily explained by the outcome of the simulations by Baletto, Doye, and

Ferrando (2002): further annealing of the growth structures indicates that it is indeed quite easy to eliminate the less bound molecules from the surfaces of the clusters, thus leaving only icosahedral magic clusters.

On the other hand, the experimental results obtained after annealing at higher T (close to 600 K) are more difficult to explain: close-packed or decahedral clusters were mostly observed in the experiments (Branz *et al.*, 2000, 2002). In principle, these clusters could be formed in two ways:

(i) the high-T annealing allows some of the icosahedral clusters obtained at lower temperatures to rearrange in such a way that they are able to reach the structure with minimum free energy;

(ii) the high-T annealing causes the evaporation of almost all icosahedral clusters, and only the few (already existing) nonicosahedral clusters, which are more stable, survive and are observed.

Moelcular-dynamics simulations of the annealing of icosahedral clusters of different sizes at high temperatures (650–750 K) have never produced a rearrangement of the cluster to either decahedral or close-packed structures (Baletto, Doye, and Ferrando, 2002). Instead, dissolution by desorption of molecules (with some local rearrangement within the structure) occurs. These results are consistent with mechanism (ii) but we cannot draw a firm conclusion. Some structural transformations from icosahedral to decahedral structures have been observed in extremely long (0.1 ms) simulations by Branz (2001) and Branz *et al.* (2002) at $T \sim 700$ K, where, however, the number of atoms was forced to remain constant in a closed simulation box, and this forbade cluster dissolution, which is, at this temperature, dominant. Unfortunately, at the moment it is not possible to simulate dissolution at 600 K, because the time scales involved are too long.

C. Coalescence of nanoclusters

The coalescence of supported clusters is of great importance in the field of surface nanostructuring. This topic has been the subject of an excellent review paper by Jensen (1999). Here we intend to focus on the coalescence of free clusters, a mechanism that can be important for free-cluster formation, especially in the late stages of the growth process, when already formed clusters can collide and join together. Some experimental evidence in favor of this mechanism may be inferred from the results of Patil *et al.* (1993), who found the formation of polycrystalline Au clusters in an inert-gas aggregation source and attributed them to the encounter and coalescence of different smaller units. However, we remark that polycrystalline clusters may also result as the outcome of the freezing of single liquid droplets (Valkealahti and Manninen, 1997).

Lewis *et al.* (1997) studied the coalescence of free Au clusters by molecular-dynamics simulations. They coupled the clusters to a thermostat, to keep the temperature constant during the coalescence process, and therefore their results are probably better applied to supported clusters, which can exchange energy with the substrate at a rapid rate. They considered the coalescence between two solid clusters, a liquid and a solid cluster, and two liquid clusters. The coalescence of two liquid clusters takes place rapidly. A single spherical cluster is formed by the deformation of the two clusters in such a way as to optimize the contact surface, without interdiffusion. Later on, interdiffusion takes place, but the spherical shape is reached over much shorter time scales by a collective rearrangement phenomenon. The coalescence of a solid and a liquid cluster proceeds in two stages. At first the contact surface is maximized rapidly, on the same time scale as the coalescence of liquid clusters. At this stage the cluster is far from being spherical but has a faceted ovoidal shape. After that the spherical shape is reached by a slow process driven mainly by surface diffusion. The rapid changes seen at short times are due to elastic and plastic deformations. At long times the presence of facets slows down the diffusion (Baletto and Ferrando, 2001), so that coalescence times are much longer (Mazzone, 2000) than predicted by the macroscopic theory of sintering (Nichols

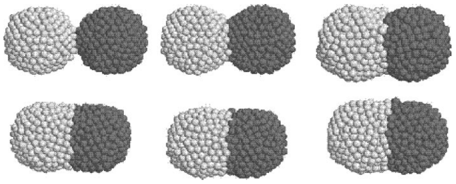

FIG. 43. Molecular-dynamics simulation of the coalescence of two 565-atom lead icosahedra initially at 300 K. The sequence of snapshots at 3.75-ps intervals shows the early growth of the neck after the initial contact. Adapted from Hendy *et al.*, 2003.

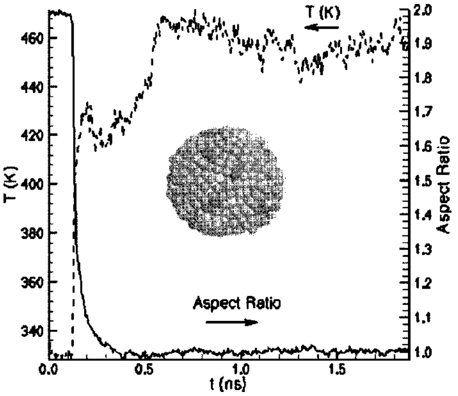

FIG. 44. Evolution of the temperature and of the aspect ratio during the molecular-dynamics simulation of the coalescence of two 565-atom lead icosahedra at the initial temperature of 300 K. At the point of first contact between clusters (approximately 30 ps after the beginning of the simulation) the temperature rises sharply due to the release of surface energy. The inset shows the final cluster structure, which is almost spherical. The spherical shape is quickly reached, since the aspect ratio is very close to one after 1 ns. Adapted from Hendy *et al.*, 2003.

and Mullins, 1965; Jensen, 1999) via surface diffusion. Finally, the coalescence of two solid clusters (simulated also by Zhu, 1996 for Cu clusters) is a complex phenomenon, which takes place on a slow time scale and may involve either the formation of a single domain cluster or of complicated structures presenting grains. This depends on size and structure of the initial clusters, at variance with the previous cases. Moreover, the nucleation of a critical island on the surface can govern the rearrangement kinetics (Combe *et al.*, 2000).

Recently Hendy *et al.* (2003) simulated the coalescence of free lead clusters in the microcanonical ensemble, without coupling the clusters to a thermostat. This seems to be the most appropriate method when dealing with free clusters produced in inert-gas aggregation sources. In fact, when two clusters come into contact, many new bonds form, causing a considerable release of surface energy. This can cause a noticeable temperature increase (more than 100 K for clusters of $N \simeq 500$). Since cooling rates are less than 1 K/ns [see Eq. (44)], and the initial stage of coalescence develops in a few ns (see Figs. 43 and 44), the inert gas is not likely to affect the process strongly by taking energy away. The temperature increase makes the coalescence process much faster, by enhancing surface diffusion. Hendy *et al.* (2003) considered the coalescence of two solid surface-reconstructed icosahedral clusters (Hendy and Hall, 2001) of 565 atoms. They found that, depending on the initial temperature and the sizes of the two clusters, the final aggregate could be either solid or liquid. When the final temperature T_f of the resulting cluster of 1130 atoms was below T_m of the Ih_{565}, the coalescence took place through solid states. On the other hand, when T_f was above T_m of the resulting cluster of 1130 atoms, the final cluster was liquid. Finally, when T_f was in between the two melting temperatures, the aggregate melted at first and solidified again at a later stage.

VI. CONCLUSIONS AND PERSPECTIVES

In this review we have tried to present an overview of the physical properties of nanoclusters, with the aim of showing the interplay of energetic, thermodynamic, and kinetic factors in building up the structures that are produced in the experiments or observed in the simulations. We hope that we have demonstrated that the physics of nanoclusters can be understood only by taking into account all three factors and relating them to the features of the interparticle potential. Among these features, the potential range is always a guideline for understanding the qualitative features of structural properties and transformations. For example, we have seen that soft interparticle interactions admit noncrystalline clusters as minimum-energy isomers. In contrast, for sticky interparticle potentials, crystalline structures are energetically favored, but at the same time kinetic trapping phenomena are enhanced. The latter often cause the growth of noncrystalline structures in the actual experiments. In metallic systems, the bond-order/bond-length correlation plays a crucial role in destabilizing some cluster structures, such as the icosahedra, and favoring the formation of low-symmetry structures. Finally, bond directionality is crucial in semiconductor clusters and in some metals, too.

Several examples have shown that the interplay of energetics, thermodynamics, and kinetics is crucial, and that a satisfactory explanation of the experimental outcomes is very often impossible on the basis of energetic considerations alone. This can have deep consequences for the very important issue of controlling the shapes of the produced nanoclusters, which is of great technological importance. Given that the interplay of the three factors is crucial, each one is extremely interesting by itself and poses stimulating theoretical challenges.

The development of reliable methods for modeling the energetics of nanoclusters is a rapidly developing field, both from the point of view of *ab initio* calculations, well suited for precise calculations on small systems, and from the point of view of semiempirical modeling, which is needed to treat larger systems and to simulate long time scales. In cluster science, these approaches are complementary and are both necessary. Since the best structure of a cluster of given size and composition is generally unknown, the semiempirical modeling, which has a much lower computational cost, is the starting point for selecting good candidates for subsequent *ab initio* local structural optimization. We have seen that there are already several examples in the literature showing that this approach is extremely fruitful, and now the challenge is to extend it to large sizes and complex systems (for example, nanoalloys). The search for good structural candidates is performed by global optimization methods. The literature on these methods and their applications to clusters has exploded in the last few years; several different procedures have been proposed, with important progress towards the understanding of the requirements for building up efficient global optimization algorithms. The main point here is that the most efficient algorithms work after transforming the original PES to a multidimensional staircase. In the field of global optimization, there is still the need to develop algorithms for complicated systems and large sizes. The latter task is, however, limited by the intrinsic NP-hard nature of the global optimization problem itself (see footnote 3 and Wille and Vennik, 1985). Thus there is no hope in optimizing very large clusters, although good putative global minima are found by the present algorithms by exploring only a very small fraction of the huge number of local minima. The reason why these algorithms work lies in the features of the PES, which may present funnels in which optimization is fast, and in the favorable transformation of the thermodynamics of the system when working on the staircase PES.

The thermodynamics of nanoclusters is a very active research field, with several problems under debate. For example, the relation between elementary interactions and the type of phase changes in clusters is still to be understood to a large extent for realistic model potentials. Moreover, the effect of chemical composition on melting and on structural transitions has been the subject of very few studies. Finally, the approach of the bulk limit is not yet well understood. Each of these problems poses complex theoretical and computational challenges.

The study of the growth kinetics of nanoclusters is a field that is just starting to develop. Here, a systematic study of small systems by the available methods is still to be performed. Moreover, new methods should be developed, first of all to extend the size of the simulated systems and the time scale of the simulations, and then to treat the formation of clusters in complex environments, such as formation in liquid solutions or on surfaces, interaction with passivating agents and adsorbed molecules, and so on.

In conclusion, we hope that our review article has given at least some idea of the present development of the fascinating and lively subject of cluster science.

ACKNOWLEDGMENTS

The authors are grateful to Jonathan Doye, Alessandro Fortunelli, Ignacio Garzón, Hellmut Haberland, Roy Johnston, Andrea Levi, Christine Mottet, Arnaldo Rapallo, and Giulia Rossi for their help and suggestions. The authors acknowledge financial support from the Italian MIUR under the project 2001021133. R.F. acknowledges financial support from CNR for the project SSA-TMN in the framework of ESF EUROCORES-SONS.

REFERENCES

Ahlrichs, R., and S. D. Elliott, 1999, Phys. Chem. Chem. Phys. **1**, 13.

Ajayan, P. M., and L. D. Marks, 1988, Phys. Rev. Lett. **60**, 585.

Akola, J., and M. Manninen, 2001, Phys. Rev. B **63**, 193410.

Ala-Nissila, T., R. Ferrando, and S. C. Ying, 2002, Adv. Phys. **51**, 949.

Alameddin, G., J. Hunter, D. Cameron, and M. M. Kappes, 1992, Chem. Phys. Lett. **192**, 122.

Alivisatos, A. P., 2001, Sci. Am. (Int. Ed.) **285**, 66.

Alivisatos, A. P., K. P. Johnsson, X. G. Peng, T. E. Wilson, C. J. Loweth, M. P. Bruchez, and P. G. Schultz, 1996, Nature (London) **382**, 609.

Alonso, J. A., 2000, Chem. Rev. (Washington, D.C.) **100**, 637.

Alvarez, M. M., J. T. Khoury, T. G. Schaaff, M. Shafigullin, I. Vezmar, and R. L. Whetten, 1997, Chem. Phys. Lett. **266**, 91.

Amar, F. G., and R. S. Berry, 1986, J. Chem. Phys. **85**, 5943.

Amara, P., D. Hsu, and J. E. Straub, 1993, J. Phys. Chem. **97**, 6715.

Anderson, J. B., and J. B. Fenn, 1985, Phys. Fluids **8**, 780.

Andriotis, A. N., and M. Menon, 2004, J. Chem. Phys. **120**, 230.

Aprà, E., F. Baletto, R. Ferrando, and A. Fortunelli, 2004, Phys. Rev. Lett. **93**, 065502.

Ascencio, J. A., C. Gutiérrez-Wing, M. E. Espinosa, M. Marín, S. Tehuacanero, C. Zorrilla, and M. José-Yacamán, 1998, Surf. Sci. **396**, 349.

Ascencio, J. A., M. Pérez, and M. José-Yacamán, 2000, Surf. Sci. **447**, 73.

Ashcroft, N. W., and N. D. Mermin, 1976, *Solid State Physics* (Saunders College, Orlando).

Aziz, R. A., F. R. W. McCourt, and C. C. K. Wong, 1987, Mol. Phys. **61**, 1487.

Bacelo, D. E., R. C. Binning, and Y. Ishikawa, 1999, J. Phys. Chem. A **103**, 4631.

Bachels, T., H. J. Güntherodt, and R. Schäfer, 2000, Phys. Rev. Lett. **85**, 1250.

Bachels, T., and R. Schäfer, 2000, Chem. Phys. Lett. **324**, 365.

Baguenard, B., M. Pellarin, J. Lermé, J. L. Vialle, and M. Broyer, 1994, J. Chem. Phys. **100**, 754.

Bailey, M. S., N. T. Wilson, C. Roberts, and R. L. Johnston, 2003, Eur. Phys. J. D **25**, 41.

Baletto, F., 2003, Ph.D. thesis (Universita di Genova).

Baletto, F., J. P. K. Doye, and R. Ferrando, 2002, Phys. Rev. Lett. **88**, 075503.

Baletto, F., J. P. K. Doye, C. Mottet, and R. Ferrando, 2003, Surf. Sci. **532**, 898.

Baletto, F., and R. Ferrando, 2001, Surf. Sci. **490**, 361.

Baletto, F., R. Ferrando, A. Fortunelli, F. Montalenti, and C. Mottet, 2002, J. Chem. Phys. **116**, 3856.

Baletto, F., C. Mottet, and R. Ferrando, 2000a, Surf. Sci. **446**, 31.

Baletto, F., C. Mottet, and R. Ferrando, 2000b, Phys. Rev. Lett. **84**, 5544.

Baletto, F., C. Mottet, and R. Ferrando, 2001a, Phys. Rev. B **63**, 155408.

Baletto, F., C. Mottet, and R. Ferrando, 2001b, Eur. Phys. J. D **16**, 25.

Baletto, F., C. Mottet, and R. Ferrando, 2002, Chem. Phys. Lett. **354**, 82.

Baletto, F., C. Mottet, and R. Ferrando, 2003, Phys. Rev. Lett. **90**, 135504.

Baletto, F., A. Rapallo, G. Rossi, and R. Ferrando, 2004, Phys. Rev. B **69**, 235421.

Barranco, M., J. Navarro, and A. Poves, 1997, Phys. Rev. Lett. **78**, 4729.

Barreteau, C., M. C. Desjonquères, and D. Spanjaard, 2000, Eur. Phys. J. D **11**, 395.

Barreteau, C., R. Guirado-López, D. Spanjaard, M. C. Desjonquères, and A. M. Oleś, 2000, Phys. Rev. B **61**, 7781.

Bartell, L. S., 1992, J. Phys. Chem. **96**, 108.

Bauschlicher, C. W., 1989, Chem. Phys. Lett. **156**, 91.

Bauschlicher, C. W., S. R. Langhoff, and H. Partridge, 1989, J. Chem. Phys. **91**, 2412.

Bauschlicher, C. W., S. R. Langhoff, and H. Partridge, 1990, J. Chem. Phys. **93**, 8133.

Bauschlicher, C. W., S. R. Langhoff, and P. R. Taylor, 1988, J. Chem. Phys. **88**, 1041.

Bazterra, V. E., O. Oña, M. C. Caputo, M. B. Ferraro, P. Fuentealba, and J. C. Facelli, 2004, Phys. Rev. A **69**, 053202.

Beck, T. L., and R. S. Berry, 1988, J. Chem. Phys. **88**, 3910.

Becke, A. D., 1988, Phys. Rev. A **38**, 3098.

Becke, A. D., 1996, J. Chem. Phys. **98**, 5648.

Becker, O. M., and M. Karplus, 1997, J. Chem. Phys. **106**, 1495.

Berry, R. S., T. L. Beck, H. L. Davis, and J. Jellinek, 1988, *Evolution of Size Effects in Chemical Dynamics* (Wiley, New York), p. 75.

Berry, R. S., J. Jellinek, and G. Natanson, 1984, Phys. Rev. A **30**, 919.

Bilgram, J. H., 1987, Phys. Rep. **153**, 1.

Binns, C., 2001, Surf. Sci. Rep. **44**, 1.

Biswas, R., and D. R. Hamann, 1986, Phys. Rev. B **34**, 895.

Bixon, M., and J. Jortner, 1989, J. Chem. Phys. **91**, 1631.

Bjørnholm, S., J. Borggreen, O. Echt, K. Hansen, J. Pedersen, and H. D. Rasmussen, 1990, Phys. Rev. Lett. **65**, 1627.

Bjørnholm, S., J. Borggreen, O. Echt, K. Hansen, J. Pedersen, and H. D. Rasmussen, 1991, Z. Phys. D: At., Mol. Clusters **19**, 47.

Blaisten-Barojas, E., I. L. Garzón, and M. Avalos-Borja, 1987, Phys. Rev. B **36**, 8447.

Blaisten-Barojas, E., and D. Levesque, 1986, Phys. Rev. B **34**, 3910.

Bobadova-Parvanova, P., K. A. Jackson, S. Srinivas, M. Horoi, C. Köhler, and G. Seifert, 2002, J. Chem. Phys. **116**, 3576.

Bonacić-Koutecký, V., J. Burda, R. Mitrić, M. Ge, G. Zampella, and P. Fantucci, 2002, J. Chem. Phys. **117**, 3120.

Bonacić-Koutecký, V., L. Cespiva, P. Fantucci, and J. Koutecký, 1993, J. Chem. Phys. **98**, 7981.

Bonacić-Koutecký, V., L. Cespiva, P. Fantucci, J. Pittner, and J. Koutecký, 1994, J. Chem. Phys. **100**, 490.

Bonacić-Koutecký, V., P. Fantucci, C. Fuchs, C. Gatti, J. Pittner, and S. Polezzo, 1993, Chem. Phys. Lett. **213**, 522.

Bonacić-Koutecký, V., P. Fantucci, and J. Koutecký, 1988, Phys. Rev. B **37**, 4369.

Bonacić-Koutecký, V., P. Fantucci, and J. Koutecký, 1991, Chem. Rev. (Washington, D.C.) **91**, 1035.

Borgia, I., B. Brunetti, I. Mariani, A. Sgamellotti, F. Cariati, P. Fermo, M. Mellini, C. Viti, and G. Padeletti, 2002, Appl. Surf. Sci. **185**, 206.

Boustani, I., W. Pewestorf, P. Fantucci, V. Bonacić-Koutecký, and J. Koutecký, 1987, Phys. Rev. B **35**, 9437.

Boyukata, M., Z. B. Güvenc, S. Ozcelik, P. Durmus, and J. Jellinek, 2001, Int. J. Quantum Chem. **84**, 208.

Brack, M., 1993, Rev. Mod. Phys. **65**, 677.

Branz, W., 2001, Ph.D. thesis (University of Stuttgart).

Branz, W., N. Malinowski, A. Enders, and T. P. Martin, 2002, Phys. Rev. B **66**, 094107.

Branz, W., N. Malinowski, H. Schaber, and T. P. Martin, 2000, Chem. Phys. Lett. **328**, 245.

Bravo-Pérez, G., I. L. Garzón, and O. Novaro, 1999a, J. Mol. Struct.: THEOCHEM **493**, 225.

Bravo-Pérez, G., I. L. Garzón, and O. Novaro, 1999b, Chem. Phys. Lett. **313**, 655.

Breaux, G. A., R. C. Benirschke, T. Sugai, B. S. Kinnear, and M. F. Jarrold, 2003, Phys. Rev. Lett. **91**, 215508.

Briant, C. L., and J. J. Burton, 1975, J. Chem. Phys. **63**, 2045.

Brühl, R., R. Guardiola, A. Kalinin, O. Kornilov, J. Navarro, T. Savas, and J. P. Toennies, 2004, Phys. Rev. Lett. **92**, 185301.

Buck, U., and I. Ettischer, 1994, J. Chem. Phys. **100**, 6974.

Buffat, P., and J.-P. Borel, 1976, Phys. Rev. A **13**, 2287.

Buffat, P.-A., M. Flueli, R. Spycher, P. Stadelmann, and J.-P. Borel, 1991, Faraday Discuss. **92**, 173.

Caccamo, C., D. Costa, and A. Fucile, 1997, J. Chem. Phys. **106**, 255.

Callegari, C., K. K. Lehmann, R. Schmied, and G. Scoles, 2001, J. Chem. Phys. **115**, 10 090.

Calvo, F., and C. Guet, 2000, J. Chem. Phys. **113**, 1315.

Calvo, F., J. P. Neirotti, D. L. Freeman, and J. D. Doll, 2000, J. Chem. Phys. **112**, 10 350.

Calvo, F., and F. Spiegelman, 2000, J. Chem. Phys. **112**, 2888.

Calvo, F., and F. Spiegelman, 2004, J. Chem. Phys. **120**, 9684.

Calvo, F., F. Spiegelman, and M.-C. Heitz, 2003, J. Chem. Phys. **118**, 8739.

Car, R., and M. Parrinello, 1985, Phys. Rev. Lett. **55**, 2471.

Castleman, A. W., and K. H. Bowen, 1996, J. Phys. Chem. **100**, 12 911.

Ceperley, D. M., 1994, Rev. Mod. Phys. **67**, 279.

Chacko, S., K. Joshi, D. G. Kanhere, and S. A. Blundell, 2004, Phys. Rev. Lett. **92**, 135 506.

Cheng, H.-P., R. N. Barnett, and U. Landman, 1993, Phys. Rev. B **48**, 1820.

Cheng, L., W. Cai, and X. Shao, 2004, Chem. Phys. Lett. **389**, 309.

Chin, S. A., and E. Krotscheck, 1992, Phys. Rev. B **45**, 852.

Chin, S. A., and E. Krotscheck, 1995, Phys. Rev. B **52**, 10 405.

Christensen, O. B., and M. L. Cohen, 1993, Phys. Rev. B **47**, 13 643.

Chuang, F.-C., C. Z. Wang, S. Ögüt, J. R. Chelikowsky, and K. M. Ho, 2004, Phys. Rev. B **69**, 165 408.

Chushak, Y., and L. S. Bartell, 2001a, Eur. Phys. J. D **16**, 43.

Chushak, Y. G., and L. S. Bartell, 2001b, J. Phys. Chem. B **105**, 11 605.

Clemenger, K., 1985, Phys. Rev. B **32**, 1359.

Cleveland, C. L., and U. Landman, 1991, J. Chem. Phys. **94**, 7376.

Cleveland, C. L., and U. Landman, 1994, J. Phys. Chem. **98**, 6272.

Cleveland, C. L., U. Landman, T. G. Schaaff, M. N. Shafigullin, P. W. Stephens, and R. L. Whetten, 1997, Phys. Rev. Lett. **79**, 1873.

Cleveland, C. L., W. D. Luedtke, and U. Landman, 1998, Phys. Rev. Lett. **81**, 2036.

Cleveland, C. L., W. D. Luedtke, and U. Landman, 1999, Phys. Rev. B **60**, 5065.

Coleman, T., and D. Shalloway, 1994, J. Global Optim. **4**, 171.

Combe, N., P. Jensen, and A. Pimpinelli, 2000, Phys. Rev. Lett. **85**, 110.

Cottancin, E., J. Lermé, M. Gaudry, M. Pellarin, J.-L. Vialle, M. Broyer, B. Prével, M. Treilleux, and P. Mélinon, 2000, Phys. Rev. B **62**, 5179.

Cox, H., R. L. Johnston, and J. N. Murrell, 1999, J. Solid State Chem. **145**, 517.

Dai, D., and K. Balasubramanian, 1995, J. Chem. Phys. **103**, 648.

Darby, S., T. V. Mortimer-Jones, R. L. Johnston, and C. Roberts, 2002, J. Chem. Phys. **116**, 1536.

Davis, H. L., J. Jellinek, and R. S. Berry, 1987, J. Chem. Phys. **86**, 6456.

Daw, M. S., and M. I. Baskes, 1984, Phys. Rev. B **29**, 6443.

Deaven, D. M., and K. M. Ho, 1995, Phys. Rev. Lett. **75**, 288.

Deaven, D. M., M. Tit, J. R. Morris, and K. M. Ho, 1996, Chem. Phys. Lett. **256**, 195.

de Heer, W. A., 1993, Rev. Mod. Phys. **65**, 611.

Desjonqueres, M. C., and D. Spanjaard, 1998, *Concepts in Surface Physics* (Springer, Berlin).

Dietz, T. G., M. A. Duncan, D. E. Powers, and R. E. Smalley, 1981, J. Chem. Phys. **74**, 6511.

Doye, J. P. K., 2003, J. Chem. Phys. **119**, 1136.

Doye, J. P. K., 2004, unpublished.

Doye, J. P. K., and F. Calvo, 2001, Phys. Rev. Lett. **86**, 3570.

Doye, J. P. K., and F. Calvo, 2002, J. Chem. Phys. **116**, 8307.

Doye, J. P. K., and F. Calvo, 2003, J. Chem. Phys. **119**, 12 680.

Doye, J. P. K., A. Dullweber, and D. J. Wales, 1997, Chem. Phys. Lett. **269**, 408.

Doye, J. P. K., and S. C. Hendy, 2003, Eur. Phys. J. D **22**, 99.

Doye, J. P. K., and D. J. Wales, 1995, J. Chem. Phys. **112**, 9659.

Doye, J. P. K., and D. J. Wales, 1996a, Science **271**, 484.

Doye, J. P. K., and D. J. Wales, 1996b, Chem. Phys. Lett. **262**, 167.

Doye, J. P. K., and D. J. Wales, 1998a, Phys. Rev. Lett. **80**, 1357.

Doye, J. P. K., and D. J. Wales, 1998b, New J. Chem. **22**, 733.

Doye, J. P. K., and D. J. Wales, 2001, Phys. Rev. Lett. **86**, 5719.

Doye, J. P. K., D. J. Wales, and R. S. Berry, 1995, J. Chem. Phys. **103**, 4234.

Doye, J. P. K., D. J. Wales, W. Branz, and F. Calvo, 2001, Phys. Rev. B **64**, 235409.

Doye, J. P. K., D. J. Wales, and M. A. Miller, 1998, J. Chem. Phys. **109**, 8143.

Efremenko, I., 2001, J. Mol. Catal. A: Chem. **173**, 19.

Efremenko, I., and M. Sheintuck, 2000, J. Mol. Catal. A: Chem. **160**, 445.

Efremov, M. Y., F. Schiettekatte, M. Zhang, E. A. Olson, A. T. Kwan, R. S. Berry, and L. H. Allen, 2000, Phys. Rev. Lett. **85**, 3560.

Ehbrecht, M., and F. Huisken, 1999, Phys. Rev. B **59**, 2975.

Ehbrecht, M., B. Kohn, F. Huisken, M. A. Laguna, and V. Paillard, 1997, Phys. Rev. B **56**, 6958.

Ercolessi, F., W. Andreoni, and E. Tosatti, 1991, Phys. Rev. Lett. **66**, 911.

Ercolessi, F., M. Parrinello, and E. Tosatti, 1988, Philos. Mag. A **58**, 213.

Erkoç, S., and T. Yilmaz, 1999, Physica E (Amsterdam) **5**, 1.

Ervin, K. M., J. Ho, and W. C. Lineberger, 1988, J. Chem. Phys. **89**, 4514.

Etters, R. D., and J. Kaelberer, 1975, Phys. Rev. A **11**, 1068.

Etters, R. D., and J. Kaelberer, 1977, J. Chem. Phys. **66**, 5112.

Even, U., N. Ben-Horin, and J. Jortner, 1989, Phys. Rev. Lett. **62**, 140.

Faken, D., and H. Jónsson, 1994, Comput. Mater. Sci. **2**, 279.

Farges, J., M.-F. de Feraudy, B. Raoult, and G. Torchet, 1981, Surf. Sci. **106**, 95.

Farges, J., M. F. de Feraudy, B. Raoult, and G. Torchet, 1983, J. Chem. Phys. **78**, 5067.

Farges, J., M. F. de Feraudy, B. Raoult, and G. Torchet, 1985, Surf. Sci. **156**, 370.

Farges, J., M. F. de Feraudy, B. Raoult, and G. Torchet, 1986, J. Chem. Phys. **84**, 3491.

Farges, J., M.-F. de Feraudy, B. Raoult, and G. Torchet, 1988, Adv. Chem. Phys. **70**, 45.

Ferreira, A. L. C., J. M. Pacheco, and J. P. Prates-Ramalho, 2000, J. Chem. Phys. **113**, 738.

Finnila, A. B., M. A. Gomez, C. Sebenik, C. Stenson, and J. D. Doll, 1994, Chem. Phys. Lett. **219**, 343.

Finnis, M. W., and J. E. Sinclair, 1984, Philos. Mag. A **50**, 45.

Fortunelli, A., 1999, J. Mol. Struct.: THEOCHEM **493**, 233.

Fortunelli, A., and E. Aprà, 2003, J. Phys. Chem. **107**, 2934.

Fortunelli, A., and A. M. Velasco, 2004, Int. J. Quantum Chem. **99**, 654.

Fournier, R., 2001, J. Chem. Phys. **115**, 2165.

Fournier, R., S. B. Sinnott, and A. E. DePristo, 1992, J. Chem. Phys. **97**, 4149.

Frantz, D. D., 1995, J. Chem. Phys. **102**, 3747.

Frantz, D. D., 2001, J. Chem. Phys. **115**, 6136.

Frantz, D. D., D. L. Freeman, and J. D. Doll, 1990, J. Chem. Phys. **93**, 2769.

Freeman, D. L., and J. D. Doll, 1985, J. Chem. Phys. **82**, 462.

Freeman, D. L., and J. D. Doll, 1996, Annu. Rev. Phys. Chem. **47**, 43.

Frenkel, D., and B. Smit, 1996, *Understanding Molecular Simulations* (Academic Press, San Diego).

Fthenakis, Z., A. N. Andriotis, and M. Menon, 2003, J. Chem. Phys. **119**, 10 911.

Fujima, N., and T. Yamaguchi, 1989, J. Phys. Soc. Jpn. **58**, 1334.

Fuke, K., K. Tsukamoto, F. Misaizu, and M. Sanekata, 1994, J. Chem. Phys. **99**, 7807.

Ganteför, G., and W. Eberhardt, 1996, Phys. Rev. Lett. **76**, 4975.

Ganteför, G., M. Gauss, K. H. Meiwes-Broer, and H. Lutz, 1990, J. Chem. Soc., Faraday Trans. **86**, 2483.

Garcia-Rodeja, J., C. Rey, and L. J. Gallego, 1997, Phys. Rev. B **56**, 6466.

Garcia-Rodeja, J., C. Rey, L. J. Gallego, and J. A. Alonso, 1994, Phys. Rev. B **49**, 8495.

Garzón, I. L., M. R. Beltrán, G. Gonzalez, I. Gutierrez-Gonzalez, K. Michaelian, J. A. Reyes-Nava, and J. I. Rodriguez-Hernandez, 2003, Eur. Phys. J. D **24**, 105.

Garzón, I. L., and J. Jellinek, 1991, Z. Phys. D: At., Mol. Clusters **20**, 235.

Garzón, I. L., and J. Jellinek, 1993, Z. Phys. D: At., Mol. Clusters **26**, 316.

Garzón, I. L., I. G. Kaplan, R. Santamaria, and O. Novaro, 1998, J. Chem. Phys. **109**, 2176.

Garzón, I. L., K. Michaelian, M. R. Beltrán, A. Posada-Amarillas, P. Ordejón, E. Artacho, D. Sánchez-Portal, and J. M. Soler, 1998, Phys. Rev. Lett. **81**, 1600.

Garzón, I. L., K. Michaelian, M. R. Beltrán, A. Posada-Amarillas, P. Ordejón, E. Artacho, D. Sánchez-Portal, and J. M. Soler, 1999, Eur. Phys. J. D **9**, 211.

Garzón, I. L., and A. Posada-Amarillas, 1996, Phys. Rev. B **54**, 11 796.

Garzón, I. L., J. A. Reyes-Nava, J. J. Rodriguez-Hernandez, I. Sigal, M. R. Beltrán, and K. Michaelian, 2002, Phys. Rev. B **66**, 073403.

Ghayal, M. R., and E. Curotto, 2000, J. Chem. Phys. **113**, 4298.

Gilb, S., P. Weis, F. Furche, R. Ahlrichs, and M. M. Kappes, 2002, J. Chem. Phys. **116**, 4094.

Girifalco, L. A., 1992, J. Phys. Chem. **96**, 858.

Girifalco, L. A., and V. G. Weizer, 1959, Phys. Rev. **114**, 687.

Grisenti, R. E., W. Schöllkopf, J. P. Toennies, G. C. Hegerfeldt, T. Köhler, and M. Stoll, 2000, Phys. Rev. Lett. **85**, 2284.

Grönbeck, H., and W. Andreoni, 2000, Chem. Phys. **262**, 1.

Grossman, J. C., and L. Mitás, 1995a, Phys. Rev. Lett. **74**, 1323.

Grossman, J. C., and L. Mitás, 1995b, Phys. Rev. B **52**, 16735.

Grygorian, V. G., and M. Springborg, 2003, Chem. Phys. Lett. **375**, 219.

Guardiola, R., 2000, Phys. Rev. B **62**, 3416.

Guardiola, R., and J. Navarro, 2000, Phys. Rev. Lett. **84**, 1144.

Guardiola, R., and J. Navarro, 2002, Phys. Rev. Lett. **89**, 193401.

Guillopé, M., and B. Legrand, 1989, Surf. Sci. **215**, 577.

Guirado-López, R., M. C. Desjonquères, and D. Spanjaard, 2000, Phys. Rev. B **62**, 13 188.

Gupta, R. P., 1981, Phys. Rev. B **23**, 6265.

Güvenc, Z. B., J. Jellinek, and A. F. Voter, 1992, in *Physics and Chemistry of Finite Systems: From Clusters to Crystals*, edited by P. Jena, S. N. Khanna, and B. K. Rao (Kluwer Academic, Dordrecht), p. 411.

Haberland, H., 1994, in *Clusters of Atoms and Molecules*, edited by H. Haberland (Springer, Berlin), p. 374.

Haberland, H., 2002, *Atomic Clusters and Nanoparticles: Les Houches Session LXXIII*, 2-28 July 2000 (Springer, Berlin), p. 31.

Häberlen, O. D., S.-C. Chung, M. Stener, and N. Rösch, 1996, J. Chem. Phys. **106**, 5189.

Hagen, M. H. J., E. J. Meijer, G. C. A. M. Mooij, D. Frenkel,

and H. N. W. Lekkerkerker, 1993, Nature (London) **365**, 425.
Häkkinen, H., and U. Landman, 2000, Phys. Rev. B **62**, R2287.
Häkkinen, H., M. Moseler, and U. Landman, 2002, Phys. Rev. Lett. **89**, 033401.
Hall, B. D., M. Flüeli, R. Monot, and J.-P. Borel, 1991, Phys. Rev. B **43**, 3906.
Hanszen, K. J., 1960, Z. Phys. **157**, 523.
Harris, I. A., R. S. Kidwell, and J. A. Northby, 1984, Phys. Rev. Lett. **53**, 2390.
Hartke, B., 1993, J. Phys. Chem. **97**, 9973.
Hartke, B., 1999, J. Comput. Chem. **20**, 1752.
Hartke, B., 2000, Z. Phys. Chem. (Munich) **214**, 1251.
Hartke, B., 2002, Angew. Chem., Int. Ed. **41**, 1468.
Hartke, B., 2003, Phys. Chem. Chem. Phys. **5**, 275.
Hendy, S., S. A. Brown, and B. D. Hall, 2003, Phys. Rev. B **68**, 241403.
Hendy, S. C., and B. D. Hall, 2001, Phys. Rev. B **64**, 085425.
Henry, C. R., 1998, Surf. Sci. Rep. **31**, 235.
Hill, T. L., 1964, *Thermodynamics of Small Systems*, Parts I and II (Benjamin, Amsterdam).
Ho, J., K. M. Ervin, and W. C. Lineberger, 1990, J. Chem. Phys. **93**, 6987.
Ho, J., K. M. Ervin, M. L. Polak, M. K. Gilles, and W. C. Lineberger, 1991, J. Chem. Phys. **95**, 4845.
Ho, K. M., A. A. Shvartsburg, B. G. Pan, Z. Y. Lu, C. Z. Wang, J. G. Wacker, J. L. Fye, and M. F. Jarrold, 1998, Nature (London) **392**, 582.
Hoare, M. R., and J. McInnes, 1976, Faraday Discuss. Chem. Soc. **61**, 12.
Hoare, M. R., and P. Pal, 1975, Adv. Phys. **24**, 645.
Hohenberg, P., and W. Kohn, 1964, Phys. Rev. **136**, B864.
Honeycutt, J. D., and H. C. Andersen, 1987, J. Phys. Chem. **91**, 4950.
Hovick, J. W., and L. S. Bartell, 1997, J. Mol. Struct. **413**, 615.
Huang, S. P., and P. B. Balbuena, 2002, J. Phys. Chem. B **106**, 7225.
Hudgins, R. R., M. Imai, M. F. Jarrold, and P. Dugourd, 1999, J. Chem. Phys. **111**, 7865.
Hyslop, M., A. Wurl, S. A. Brown, B. D. Hall, and R. Monot, 2001, Eur. Phys. J. D **16**, 233.
Ikeshoji, T., B. Hafskjold, Y. Hashi, and Y. Kawazoe, 1996, Phys. Rev. Lett. **76**, 1792.
Ikeshoji, T., G. Torchet, M.-F. de Feraudy, and K. Koga, 2001, Phys. Rev. E **63**, 031101.
Imry, Y., 1980, Phys. Rev. B **21**, 2042.
Ino, S., 1969, J. Phys. Soc. Jpn. **27**, 941.
Ishikawa, Y., Y. Sugita, T. Nishikawa, and Y. Okamoto, 2001, Phys. Lett. A **333**, 199.
Jackschath, C., I. Rabin, and W. Schulze, 1992, Z. Phys. D: At., Mol. Clusters **22**, 517.
Jacobsen, K. W., J. K. Nørskov, and M. J. Puska, 1987, Phys. Rev. B **35**, 7423.
Jarrold, M. F., and J. E. Bower, 1992, J. Chem. Phys. **96**, 9180.
Jarrold, M. F., and V. A. Constant, 1991, Phys. Rev. Lett. **67**, 2994.
Jarrold, M. F., and E. C. Honea, 1991, J. Phys. Chem. **95**, 9181.
Jellinek, J., 1999, *Theory of Atomic and Molecular Clusters* (Springer, Berlin).
Jellinek, J., T. L. Beck, and R. S. Berry, 1986, J. Chem. Phys. **84**, 2783.
Jellinek, J., V. Bonacić-Koutecký, P. Fantucci, and M. Wiechert, 1994, J. Chem. Phys. **101**, 10 092.
Jellinek, J., and I. L. Garzón, 1991, Z. Phys. D: At., Mol. Clusters **20**, 239.
Jennison, D. R., P. A. Schultz, and M. P. Sears, 1997, J. Chem. Phys. **106**, 1856.
Jensen, P., 1999, Rev. Mod. Phys. **71**, 1695.
Johnston, R. L., 2002, *Atomic and Molecular Clusters* (Taylor & Francis, London).
Johnston, R. L., 2003, J. Chem. Soc. Dalton Trans. **2003**, 4193.
Jones, R. O., 1991, Phys. Rev. Lett. **67**, 224.
Jones, R. O., 1993, J. Chem. Phys. **99**, 1194.
Jones, R. O., and G. Seifert, 1992, J. Chem. Phys. **96**, 7564.
Jortner, J., 1992, Z. Phys. D: At., Mol. Clusters **24**, 247.
Jortner, J., 2003, J. Chem. Phys. **119**, 11 335.
José-Yacamán, M., J. A. Ascencio, H. B. Liu, and J. Gardea-Torresdey, 2001, J. Vac. Sci. Technol. B **19**, 1091.
José-Yacamán, M., M. Marín-Almazo, and J. A. Ascencio, 2001, J. Mol. Catal. A: Chem. **173**, 61.
Joshi, K., D. G. Kanhere, and S. A. Blundell, 2002, Phys. Rev. B **66**, 155329.
Joshi, K., D. G. Kanhere, and S. A. Blundell, 2003, Phys. Rev. B **67**, 235413.
Jug, K., B. Zimmermann, P. Calaminici, and A. M. Köster, 2002, J. Chem. Phys. **116**, 4497.
Jug, K., B. Zimmermann, and A. M. Köster, 2002, Int. J. Quantum Chem. **90**, 594.
Kallinteris, G. C., N. I. Papanicolaou, G. A. Evangelakis, and D. A. Papaconstantopoulos, 1997, Phys. Rev. B **55**, 2150.
Kaxiras, E., and K. Jackson, 1993a, Phys. Rev. Lett. **71**, 727.
Kaxiras, E., and K. Jackson, 1993b, Z. Phys. D: At., Mol. Clusters **26**, 346.
Kirkpatrick, S., C. D. Gelatt, and M. P. Vecchi, 1983, Science **220**, 671.
Knight, W. D., K. Clemenger, W. A. de Heer, W. A. Saunders, M. Y. Chou, and M. L. Cohen, 1984, Phys. Rev. Lett. **52**, 2141.
Kofman, R., P. Cheyssac, A. Aouaj, Y. Lereah, G. Deutscher, T. Ben-David, J. M. Penisson, and A. Bourret, 1994, Surf. Sci. **303**, 231.
Koga, K., T. Ikeshoji, and K. Sugawara, 2004, Phys. Rev. Lett. **92**, 115507.
Koga, K., and K. Sugawara, 2003, Surf. Sci. **529**, 23.
Kohn, W., and L. J. Sham, 1965, Phys. Rev. **140**, A1133.
Krivov, S. V., 2002, Phys. Rev. E **66**, 025701.
Kruger, S., S. Vent, F. Nörtemann, M. Staufer, and N. Rösch, 2001, J. Chem. Phys. **115**, 2082.
Kumar, V., and R. Car, 1991, Phys. Rev. B **44**, 8243.
Kumar, V., and Y. Kawazoe, 2002, Phys. Rev. B **66**, 144413.
Kusche, R., T. Hippler, M. Schmidt, B. von Issendorff, and H. Haberland, 1999, Eur. Phys. J. D **9**, 1.
Labastie, P., and R. L. Whetten, 1990, Phys. Rev. Lett. **65**, 1567.
Lai, S. K., P. J. Hsu, K. L. Wu, W. K. Liu, and M. Iwamatsu, 2002, J. Chem. Phys. **117**, 10 715.
Lai, S. L., J. Y. Guo, V. Petrova, G. Ramanath, and L. H. Allen, 1996, Phys. Rev. Lett. **77**, 99.
Lathiotakis, N. N., A. N. Andriotis, M. Menon, and J. Connolly, 1996, J. Chem. Phys. **104**, 992.
Leary, R. H., and J. P. K. Doye, 1999, Phys. Rev. E **60**, R6320.
Ledoux, G., O. Guillois, D. Porterat, C. Reynaud, F. Huisken, B. Kohn, and V. Paillard, 2000, Phys. Rev. B **62**, 15 942.
Lee, J., I.-H. Lee, and J. Lee, 2003, Phys. Rev. Lett. **91**, 080201.
Lee, J. K., J. A. Barker, and F. F. Abraham, 1973, J. Chem. Phys. **58**, 3166.
Lee, Y. H., and B. J. Berne, 2000, J. Phys. Chem. A **104**, 86.
Lee, Y. J., R. M. Nieminen, E.-K. Lee, and S. Kim, 2001, Comput. Phys. Commun. **142**, 201.

Lermé, J., M. Pellarin, J. L. Vialle, B. Baguenard, and M. Broyer, 1992, Phys. Rev. Lett. **68**, 2818.

Levi, A. C., and R. Mazzarello, 2001, J. Low Temp. Phys. **122**, 75.

Lewerenz, M., 1996, J. Chem. Phys. **106**, 4596.

Lewis, L. J., P. Jensen, and J.-L. Barrat, 1997, Phys. Rev. B **56**, 2248.

Li, B. X., P. L. Cao, and M. Jiang, 2000, Phys. Status Solidi B **218**, 399.

Li, B. X., M. Qiu, and P. L. Cao, 1999, Phys. Lett. A **256**, 386.

Li, J., X. Li, H.-J. Zhai, and L.-S. Wang, 2003, Science **299**, 864.

Li, T. X., Y. J. Ji, S. W. Yu, and G. H. Wang, 2000, Solid State Commun. **116**, 547.

Li, T. X., S. M. Lee, S. J. Han, and G. H. Wang, 2002, Phys. Lett. A **300**, 86.

Li, T. X., S. Y. Yin, Y. L. Ji, B. L. Wang, G. H. Wang, and J. J. Zhao, 2000, Phys. Lett. A **267**, 403.

Li, Y., E. Blaisten-Barojas, and D. A. Papaconstantopoulos, 1998, Phys. Rev. B **57**, 15 519.

Li, Z., and H. A. Scheraga, 1987, Proc. Natl. Acad. Sci. U.S.A. **84**, 6611.

Lim, H. S., C. K. Ong, and F. Ercolessi, 1992, Surf. Sci. **270**, 1109.

Lim, H. S., C. K. Ong, and F. Ercolessi, 1994, Comput. Mater. Sci. **2**, 495.

Liu, H. B., J. A. Ascencio, M. Pérez-Alvarez, and M. José-Yacamán, 2001, Surf. Sci. **491**, 88.

Liu, H. B., R. Perez, G. Canizal, and J. A. Ascencio, 2002, Surf. Sci. **518**, 14.

Liu, P., and B. J. Berne, 2003, J. Chem. Phys. **118**, 2999.

Lloyd, L. D., R. L. Johnston, S. Sahli, and N. T. Wilson, 2004, J. Mater. Chem. **2004**, 1691.

Locatelli, M., and F. Schoen, 2003, Comput. Optim. Appl. **26**, 173.

López, M. J., and J. Jellinek, 1999, J. Chem. Phys. **110**, 8899.

Lowen, H., 1994, Phys. Rep. **237**, 249.

Luo, F., G. C. McBane, G. Kim, G. F. Giese, and W. R. Gentry, 1993, J. Chem. Phys. **98**, 3564.

Luo, J., U. Landman, and J. Jortner, 1987, in *Physics and Chemical of Small Clusters*, edited by P. Jena, B. K. Rao, and S. N. Khanna (Plenum, New York), p. 201.

Lynden-Bell, R. M., and D. J. Wales, 1994, J. Chem. Phys. **101**, 1460.

Ma, J. P., and J. E. Straub, 1994, J. Chem. Phys. **101**, 533.

Mackay, A. L., 1962, Acta Crystallogr. **15**, 916.

Manninen, K., J. Akola, and M. Manninen, 2003, Phys. Rev. B **68**, 235412.

Manninen, K., and M. Manninen, 2002, Eur. Phys. J. D **20**, 243.

Maranas, C. D., and C. A. Floudas, 1992, J. Chem. Phys. **97**, 7667.

Marks, L. D., 1984, Philos. Mag. A **49**, 81.

Marks, L. D., 1994, Rep. Prog. Phys. **57**, 603.

Martin, T. P., 1996, Phys. Rep. **273**, 199.

Martin, T. P., 2000, Solid State Ionics **131**, 3.

Martin, T. P., T. Bergmann, H. Gohlich, and T. Lange, 1991a, Z. Phys. D: At., Mol. Clusters **19**, 25.

Martin, T. P., T. Bergmann, H. Gohlich, and T. Lange, 1991b, J. Phys. Chem. **95**, 6421.

Martin, T. P., U. Näher, and H. Schaber, 1992, Chem. Phys. Lett. **199**, 470.

Martin, T. P., U. Näher, H. Schaber, and U. Zimmermann, 1993, Phys. Rev. Lett. **70**, 3079.

Martin, T. P., U. Näher, H. Schaber, and U. Zimmermann, 1994, J. Chem. Phys. **100**, 2322.

Massen, C., T. V. Mortimer-Jones, and R. L. Johnston, 2002, J. Chem. Soc. Dalton Trans. **2002**, 4375.

Massobrio, C., A. Pasquarello, and R. Car, 1995, Chem. Phys. Lett. **238**, 215.

Matsuoka, H., T. Hirokawa, M. Matsui, and M. Doyama, 1992, Phys. Rev. Lett. **69**, 297.

Matulis, V. E., O. A. Ivashkevich, and V. S. Gurin, 2003, J. Mol. Struct.: THEOCHEM **664-665**, 291.

Matveentsev, A., A. Lyalin, I. A. Solov'yov, A. V. Solov'yov, and W. Greiner, 2003, Int. J. Mod. Phys. E **12**, 81.

Mazzone, A. M., 2000, Philos. Mag. B **80**, 95.

Mélinon, P., P. Keghelian, B. Prével, V. Dupuis, A. Perez, B. Champagnon, Y. Guyot, M. Pellarin, J. Lermé, M. Broyer, J. L. Rousset, and P. Délichere, 1998, J. Chem. Phys. **108**, 4607.

Mélinon, P., P. Keghelian, B. Prével, A. Perez, G. Guiraud, J. LeBrusq, J. Lermé, M. Pellarin, and M. Broyer, 1997, J. Chem. Phys. **107**, 10 278.

Meunier, I., 2001, Ph.D. thesis (University of Aix-Marseille II).

Michaelian, K., 1998, Chem. Phys. Lett. **293**, 202.

Michaelian, K., N. Rendón, and I. L. Garzón, 1999, Phys. Rev. B **60**, 2000.

Milani, P., and S. Iannotta, 1999, *Cluster Beam Synthesis of Nanostructured Materials* (Springer, Berlin).

Mirkin, C. A., R. L. Letsinger, R. C. Mucic, and J. J. Storhoff, 1996, Nature (London) **382**, 607.

Mitás, L., J. C. Grossman, I. Stich, and J. Tobik, 2000, Phys. Rev. Lett. **84**, 1479.

Montalenti, F., and R. Ferrando, 1999a, Phys. Rev. B **59**, 5881.

Montalenti, F., and R. Ferrando, 1999b, Phys. Rev. Lett. **82**, 1498.

Morse, P. M., 1929, Phys. Rev. **34**, 57.

Moseler, M., H. Häkkinen, R. N. Barnett, and U. Landman, 2001, Phys. Rev. Lett. **86**, 2545.

Mottet, C., J. Goniakowski, F. Baletto, R. Ferrando, and G. Tréglia, 2004, Phase Transitions **77**, 101.

Mottet, C., G. Tréglia, and B. Legrand, 1997, Surf. Sci. **383**, L719.

Nalwa, H. S., 2004, Ed., *Encyclopedia of Nanoscience and Nanotechnology* (American Scientific, New York).

Nam, H.-S., N. M. Hwang, B. D. Yu, and J.-K. Yoon, 2002, Phys. Rev. Lett. **89**, 275502.

Natanson, G., F. Amar, and R. S. Berry, 1983, J. Chem. Phys. **78**, 399.

Nautchil, V. V., and A. J. Petsin, 1980, Mol. Phys. **40**, 1341.

Nava, P., M. Sierka, and R. Ahlrichs, 2003, Phys. Chem. Chem. Phys. **5**, 3372.

Nayak, S. K., B. Reddy, B. K. Rao, S. N. Khanna, and P. Jena, 1996, Chem. Phys. Lett. **253**, 390.

Neirotti, J. P., F. Calvo, D. L. Freeman, and J. D. Doll, 2000, J. Chem. Phys. **112**, 10 340.

Nelson, D. R., and F. Spaepen, 1989, Solid State Phys. **42**, 1.

Nichols, F. A., and W. W. Mullins, 1965, J. Appl. Phys. **36**, 1826.

Nishioka, H., K. Hansen, and B. R. Mottelson, 1990, Phys. Rev. B **42**, 9377.

Northby, J. A., 1987, J. Chem. Phys. **87**, 6166.

Northby, J. A., 2001, J. Chem. Phys. **115**, 10 065.

Northby, J. A., J. Xie, D. L. Freeman, and J. D. Doll, 1989, Z. Phys. D: At., Mol. Clusters **12**, 69.

Nygren, M. A., P. E. M. Siegbahn, U. Wahlgren, and H. Akeby, 1992, J. Phys. Chem. **96**, 3633.

Oviedo, J., and R. E. Palmer, 2002, J. Chem. Phys. **117**, 9548.

Pacheco, J. M., and J. P. Prates-Ramalho, 1997, Phys. Rev.

Lett. **79**, 3873.

Padeletti, G., and P. Fermo, 2003, Appl. Phys. A: Mater. Sci. Process. **76**, 515.

Parks, E. K., K. P. Kerns, and S. J. Riley, 1998, J. Chem. Phys. **109**, 10 207.

Parks, E. K., G. C. Nieman, K. P. Kerns, and S. J. Riley, 1997, J. Chem. Phys. **107**, 1861.

Parks, E. K., L. Zhu, J. Ho, and S. J. Riley, 1994, J. Chem. Phys. **100**, 7206.

Parks, E. K., L. Zhu, J. Ho, and S. J. Riley, 1995, J. Chem. Phys. **102**, 7377.

Parravicini, G. B., A. Stella, P. Tognini, P. G. Merli, A. Migliori, P. Cheyssac, and R. Kofman, 2003a, Appl. Phys. Lett. **82**, 1461.

Parravicini, G. B., A. Stella, M. C. Ungureanu, P. G. Merli, A. Migliori, and R. Kofman, 2003b, Phys. Status Solidi B **237**, 374.

Patil, A. N., D. Y. Paithankar, N. Otsuka, and R. P. Andres, 1993, Z. Phys. D: At., Mol. Clusters **26**, 135.

Pawlow, P., 1909, Z. Phys. Chem., Stoechiom. Verwandtschaftsl. **65**, 1.

Perdew, J. P., K. Burke, and Y. Wang, 1996, Phys. Rev. B **54**, 16 533.

Perdew, J. P., J. A. Chevary, S. H. Vosko, K. A. Jackson, M. R. Pederson, D. J. Singh, and C. Fiolhais, 1992, Phys. Rev. B **46**, 6671.

Perdew, J. P., and Y. Wang, 1986, Phys. Rev. B **33**, 8800.

Peters, K. F., J. B. Cohen, and Y.-W. Chung, 1998, Phys. Rev. B **57**, 13 430.

Pillardy, J., and L. Piela, 1995, J. Phys. Chem. **99**, 11 805.

Pimpinelli, A., and J. Villain, 1998, *Physics of Crystal Growth* (Cambridge University, Cambridge).

Polak, W., and A. Patrykiejew, 2003, Phys. Rev. B **67**, 115402.

Poteau, R., and F. Spiegelmann, 1993, J. Chem. Phys. **98**, 6540.

Qi, Y., T. Cagin, W. L. Johnson, and W. A. Goddard III, 2001, J. Chem. Phys. **115**, 385.

Quirke, N., and P. Sheng, 1984, Chem. Phys. Lett. **110**, 63.

Raghavachari, K., and V. Logovinsky, 1985, Phys. Rev. Lett. **55**, 2853.

Raghavachari, K., and C. McMichael-Rohlfing, 1988, J. Chem. Phys. **89**, 2219.

Ramakrishna, M. V., and A. Bahel, 1996, J. Chem. Phys. **104**, 9833.

Raoult, B., and J. Farges, 1973, Rev. Sci. Instrum. **44**, 430.

Raoult, B., J. Farges, M. F. de Feraudy, and G. Torchet, 1989a, Philos. Mag. B **60**, 5067.

Raoult, B., J. Farges, M. F. de Feraudy, and G. Torchet, 1989b, Z. Phys. D: At., Mol. Clusters **12**, 85.

Rata, I., A. A. Shvartsburg, M. Horoi, T. Frauenheim, K. W. M. Siu, and K. A. Jackson, 2000, Phys. Rev. Lett. **85**, 546.

Reddy, B. V., S. N. Khanna, and B. I. Dunlap, 1993, Phys. Rev. Lett. **70**, 3323.

Reinhard, D., B. D. Hall, P. Berthoud, S. Valkealahti, and R. Monot, 1997, Phys. Rev. Lett. **79**, 1459.

Reinhard, D., B. D. Hall, P. Berthoud, S. Valkealahti, and R. Monot, 1998, Phys. Rev. B **58**, 4917.

Reinhard, D., B. D. Hall, D. Ugarte, and R. Monot, 1997, Phys. Rev. B **55**, 7868.

Reiss, H., P. Mirabel, and R. L. Whetten, 1988, J. Phys. Chem. **92**, 7241.

Reiss, H., and I. B. Wilson, 1948, J. Colloid Sci. **3**, 551.

Reuse, F. A., and S. N. Khanna, 1995, Chem. Phys. Lett. **234**, 77.

Reuse, F. A., S. N. Khanna, and S. Bernel, 1995, Phys. Rev. B **52**, R11 650.

Rey, C., L. J. Gallego, and J. A. Alonso, 1994, Phys. Rev. B **49**, 8491.

Rey, C., G. García-Rodeja, and L. J. Gallego, 2004, Phys. Rev. B **69**, 073404.

Rey, C., J. García-Rodeja, and L. J. Gallego, 1997, Z. Phys. D: At., Mol. Clusters **40**, 395.

Reyes-Nava, J. A., I. L. Garzón, M. R. Beltrán, and K. Michaelian, 2002, Rev. Mex. Fis. **48**, 450.

Romero, G., C. Barrón, and S. Gómez, 1999, Comput. Phys. Commun. **123**, 87.

Roques, J., C. Lacaze-Dufaure, and C. Mijoule, 2001, Surf. Sci. **479**, 231.

Rosato, V., M. Guillopé, and B. Legrand, 1989, Philos. Mag. A **59**, 321.

Rossi, G., A. Rapallo, C. Mottet, A. Fortunelli, F. Baletto, and R. Ferrando, 2004, Phys. Rev. Lett. **93**, 105503.

Röthlisberger, U., and W. Andreoni, 1991, J. Chem. Phys. **94**, 8129.

Röthlisberger, U., W. Andreoni, and P. Giannozzi, 1992, J. Chem. Phys. **96**, 1248.

Rousset, J. L., A. M. Cadrot, F. S. Aires, A. Renouprez, P. Melinon, A. Pérez, M. Pellarin, J. L. Vialle, and M. Broyer, 1996, Surf. Rev. Lett. **3**, 1171.

Rytkönen, A., H. Häkkinen, and M. Manninen, 1998, Phys. Rev. Lett. **80**, 3940.

Rytkönen, A., H. Häkkinen, and M. Manninen, 1999, Eur. Phys. J. D **9**, 451.

Rytkönen, A., S. Valkealahti, and M. Manninen, 1997, J. Chem. Phys. **106**, 1888.

Rytkönen, A., S. Valkealahti, and M. Manninen, 1998, J. Chem. Phys. **108**, 5826.

Sachdev, A., R. I. Masel, and J. B. Adams, 1992, Catal. Lett. **15**, 57.

Saha, D. K., K. Koga, and H. Takeo, 1997, Nanostruct. Mater. **8**, 1139.

Saha, D. K., K. Koga, and H. Takeo, 1999, Eur. Phys. J. D **9**, 539.

Sambles, J. R., 1971, Proc. R. Soc. London, Ser. A **324**, 339.

Santamaria, R., I. G. Kaplan, and O. Novaro, 1994, Chem. Phys. Lett. **218**, 395.

Sattler, K., J. Mühlback, and E. Recknagel, 1980, Phys. Rev. Lett. **45**, 821.

Schaaff, T. G., and R. L. Whetten, 2000, J. Phys. Chem. B **104**, 2630.

Schmidt, M., J. Donges, T. Hippler, and H. Haberland, 2003, Phys. Rev. Lett. **90**, 103401.

Schmidt, M., R. Kusche, T. Hippler, J. Donges, W. Kronmüller, B. von Issendorff, and H. Haberland, 2001, Phys. Rev. Lett. **86**, 1191.

Schmidt, M., R. Kusche, W. Kronmüller, B. von Issendorff, and H. Haberland, 1997, Phys. Rev. Lett. **79**, 99.

Schmidt, M., R. Kusche, B. von Issendorff, and H. Haberland, 1998, Nature (London) **393**, 238.

Schmude, R. W., Q. Ran, and K. A. Gingerich, 1993, J. Chem. Phys. **99**, 7998.

Schmude, R. W., Q. Ran, K. A. Gingerich, and J. E. Kingcade, 1995, J. Chem. Phys. **102**, 2574.

Scoles, G., and K. K. Lehmann, 2000, Science **287**, 2429.

Sebetci, A., and Z. B. Güvenc, 2003, Surf. Sci. **525**, 66.

Shah, P., S. Roy, and C. Chakravarty, 2003, J. Chem. Phys. **118**, 10 671.

Shao, X., H. Jiang, and W. Cai, 2004, J. Chem. Inf. Comput. Sci. **44**, 193.

Shvartsburg, A. A., and M. F. Jarrold, 2000, Phys. Rev. Lett. **85**, 2530.

Soler, J. M., M. R. Beltrán, K. Michaelian, I. L. Garzón, P. Ordejón, D. Sánchez-Portal, and E. Artacho, 2000, Phys. Rev. B **61**, 5771.

Soler, J. M., I. L. Garzón, and J. D. Joannopoulos, 2001, Solid State Commun. **117**, 621.

Solov'yov, I. A., A. V. Solov'yov, and W. Greiner, 2002, Phys. Rev. A **65**, 053203.

Solov'yov, I. A., A. V. Solov'yov, and W. Greiner, 2004, Int. J. Mod. Phys. E **13**, 697.

Solov'yov, I. A., A. V. Solov'yov, W. Greiner, A. Koshelev, and A. Shutovich, 2003, Phys. Rev. Lett. **90**, 053401.

Spiegelman, F., R. Poteau, B. Montag, and P.-G. Reinhard, 1998, Phys. Lett. A **242**, 163.

Stave, M. S., and A. E. DePristo, 1992, J. Chem. Phys. **97**, 3386.

Steinhardt, P. J., D. R. Nelson, and M. Ronchetti, 1983, Phys. Rev. B **28**, 784.

Stillinger, F. H., and T. A. Weber, 1982, Phys. Rev. A **25**, 978.

Stillinger, F. H., and T. A. Weber, 1985, Phys. Rev. B **31**, 5262.

Sun, Q., Q. Wang, P. Jena, S. Waterman, and Y. Kawazoe, 2003, Phys. Rev. A **67**, 063201.

Sung, M.-W., R. Kawai, and J. H. Weare, 1994, Phys. Rev. Lett. **73**, 3552.

Sutton, A. P., and J. Chen, 1990, Philos. Mag. Lett. **61**, 139.

Swendsen, R. H., and J.-S. Wang, 1986, Phys. Rev. Lett. **57**, 2607.

Takagi, M., 1954, J. Phys. Soc. Jpn. **9**, 359.

Tchofo-Dinda, P., G. Vlastou-Tsinganos, N. Flyzanis, and A. D. Mistriotis, 1995, Phys. Rev. B **51**, 13 697.

Tekin, A., and B. Hartke, 2004, Phys. Chem. Chem. Phys. **6**, 503.

Toennies, J. P., and A. F. Vilesov, 1998, Annu. Rev. Phys. Chem. **49**, 1.

Tomanek, D., A. A. Aligia, and C. A. Balseiro, 1985, Phys. Rev. B **32**, 5051.

Tsai, C. J., and K. D. Jordan, 1993, J. Phys. Chem. **97**, 11 227.

Turner, G. W., R. L. Johnston, and N. T. Wilson, 2000, J. Chem. Phys. **112**, 4773.

Uppenbrink, J., and D. J. Wales, 1992, J. Chem. Phys. **96**, 8520.

Valerio, G., and H. Toulhoat, 1996, J. Phys. Chem. **100**, 10 827.

Valerio, G., and H. Toulhoat, 1997, J. Phys. Chem. A **101**, 1969.

Valkealahti, S., and M. Manninen, 1993, Z. Phys. D: At., Mol. Clusters **26**, 255.

Valkealahti, S., and M. Manninen, 1997, J. Phys.: Condens. Matter **9**, 4041.

Valkealahti, S., and M. Manninen, 1998, Phys. Rev. B **57**, 15 533.

Valkealahti, S., U. Näher, and M. Manninen, 1995, Phys. Rev. B **51**, 11 039.

van de Waal, B. W., 1989, J. Chem. Phys. **90**, 3407.

van de Waal, B. W., 1996, Phys. Rev. Lett. **76**, 1083.

van de Waal, B. W., G. Torchet, and M.-F. de Feraudy, 2000, Chem. Phys. Lett. **331**, 57.

Vanfleet, R. R., and J. M. Mochel, 1995, Surf. Sci. **341**, 40.

Vlachos, D. G., L. D. Schmidt, and R. Aris, 1992, J. Chem. Phys. **96**, 6880.

Voter, A. F., 1993, Los Alamos Unclassified Technical Report LA-UR 93, 3901.

Wales, D. J., 1994a, J. Chem. Soc., Faraday Trans. **90**, 1061.

Wales, D. J., 1994b, J. Chem. Phys. **101**, 3750.

Wales, D. J., 2003, *Energy Landscapes with Applications to Clusters, Biomolecules and Glasses* (Cambridge University, Cambridge, England).

Wales, D. J., and J. P. K. Doye, 1997, J. Phys. Chem. A **101**, 5111.

Wales, D. J., J. P. K. Doye, M. A. Miller, P. N. Mortenson, and T. R. Walsh, 2000, Adv. Chem. Phys. **111**, 1.

Wales, D. J., and M. P. Hodges, 1998, Chem. Phys. Lett. **286**, 65.

Wang, G. M., E. Blastein-Barojas, A. E. Roitberg, and T. P. Martin, 2001, J. Chem. Phys. **115**, 3640.

Wang, J., G. Wang, and J. Zhao, 2003, Chem. Phys. Lett. **380**, 716.

Wang, J. L., G. H. Wang, F. Ding, H. Lee, W. F. Shen, and J. J. Zhao, 2001, Chem. Phys. Lett. **341**, 529.

Wang, J. L., G. H. Wang, and J. J. Zhao, 2002, Phys. Rev. B **66**, 035418.

Wang, L., Y. Zhang, X. Bian, and Y. Chen, 2003, Phys. Lett. A **310**, 197.

Watari, N., and S. Ohnishi, 1998, Phys. Rev. B **58**, 1665.

Westergren, J., H. Grönbeck, A. Rosen, and S. Nordholm, 1998, J. Chem. Phys. **109**, 9848.

Westergren, J., and S. Nordholm, 2003, Chem. Phys. **290**, 189.

Westergren, J., S. Nordholm, and A. Rosen, 2003, Phys. Chem. Chem. Phys. **5**, 136.

Wetzel, T. L., and A. E. DePristo, 1996, J. Chem. Phys. **105**, 572.

Whaley, K. B., 1994, Int. Rev. Phys. Chem. **13**, 41.

Whetten, R. L., J. T. Khoury, M. M. Alvarez, S. Murthy, I. Vezmar, Z. L. Wang, P. W. Stephens, C. L. Cleveland, W. D. Luedtke, and U. Landman, 1996, Adv. Mater. (Weinheim, Ger.) **5**, 428.

Wille, L. T., 1987, Chem. Phys. Lett. **133**, 405.

Wille, L. T., and J. Vennik, 1985, J. Phys. A **18**, L419.

Wilson, N. T., and R. L. Johnston, 2000, Eur. Phys. J. D **12**, 161.

Xiao, Y., and D. E. Williams, 1993, Chem. Phys. Lett. **215**, 17.

Xie, J., J. A. Northby, D. L. Freeman, and J. D. Doll, 1989, J. Chem. Phys. **91**, 612.

Xue, G. L., 1994, J. Global Optim. **4**, 425.

Yang, S. H., D. A. Drabold, J. B. Adams, P. Ordejón, and K. Glassford, 1997, J. Phys.: Condens. Matter **9**, L39.

Yu, D. K., R. Q. Zhang, and S. T. Lee, 2002, Phys. Rev. B **65**, 245417.

Zacarias, A. G., M. Castro, J. M. Tour, and J. M. Seminario, 1999, J. Phys. Chem. A **103**, 7692.

Zanchet, D., B. D. Hall, and D. Ugarte, 2000, J. Phys. Chem. B **104**, 11 013.

Zeiri, Y., 1995, Phys. Rev. E **51**, R2769.

Zhang, W., Q. Ge, and L. Wang, 2003, J. Chem. Phys. **118**, 5793.

Zhao, J., Y. Luo, and G. Wang, 2001, Eur. Phys. J. D **14**, 309.

Zhao, J., J. L. Yang, and J. G. Hou, 2003, Phys. Rev. B **67**, 085404.

Zhou, Y., M. Karplus, K. D. Ball, and R. S. Berry, 2002, J. Chem. Phys. **116**, 2323.

Zhu, H., 1996, Philos. Mag. Lett. **73**, 27.

Zickfeld, K., M. E. García, and K. H. Bennemann, 1999, Phys. Rev. B **59**, 13 422.